ACTA Mineralogica Petrographica

ACTA MINERALOGICA-PETROGRAPHICA, FIELD GUIDE SERIES, VOL. 28, PP. 1–36.

Slovak Ore Mountains: Origin of hydrothermal mineralization and environmental impacts of mining

VRATISLAV HURAI[1*], MARTIN CHOVAN[2**], MONIKA HURAIOVÁ[2***], PETER KODĚRA[3], PATRIK KONEČNÝ[4] AND ONDREJ LEXA[5]

[1] Geological Institute, Slovak Academy of Sciences, Dúbravská cesta 9, Bratislava, Slovakia; vratislav.hurai@savba.sk, *corresponding author
[2] Department of Mineralogy and Petrology, Comenius University, Mlynská dolina G, 842 15 Bratislava, Slovakia; **chovan@fns.uniba.sk; ***huraiova@fns.uniba.sk
[3] Department of Economic Geology, Comenius University, Mlynská dolina G, 842 15 Bratislava, Slovakia; kodera@fns.uniba.sk
[4] Geological Survey of the Slovak Republic, Mlynská dolina 1, 817 04 Bratislava, Slovakia; patrik.konecny@geology.sk
[5] Czech Geological Survey, Klárov 3, 118 21 Praha, Czech Republic; ondrej.lexa@geology.cz

Table of contents

1. Geological introduction to study area

The Western Carpathians are located in the Alpine-Carpathian orogenic belt, which formed during Late Jurassic–Tertiary subduction-collision in the Tethyan mobile zone between the stable North European Platform and drifting continental fragments correlated with the Apulia/Adria (Plašienka *et al.*, 1997). Outer Carpathians extending northward from the Pieniny Klippen Belt are composed of flysch sequences of a Tertiary accretionary wedge. Central Carpathians south of the Pieniny Klippen Belt contain only relics of the Mesozoic accretionary wedge thrusted over the Tatric, Veporic and Gemeric basement (Fig. 1, inset) and covered by relics of unfolded fore-arc Eocene–Oligocene flysch sediments.

1.1 The Veporic unit

The crystalline basement of the Veporic unit is composed of high-grade, occasionally retrograded rocks (Proterozoic?–Early Palaeozoic?) of the lower structural level; low- to medium-grade, Silurian to Lower Carboniferous (Klinec *et al.*, 1975; Bezák & Planderová, 1981) rocks of the middle and upper structural levels; and Carboniferous to Permian S-type granitoids (Cambel *et al.*,1990). In comparison with neighbouring Gemeric and Tatric tectonic units, the Veporic basement underwent the most intense Alpine metamorphism. The complicated structure of the unit results from repeated activity during pre-Alpine (mainly Variscan), paleo- and neo-Alpine events. Distinguishing among them is ambiguous due to overlapping *P–T* conditions and overprint by superimposed postkinematic stages accompanied by formation of thermal domes and intrusions of granitoids. The highest metamorphic grade has been recorded in gneisses of the lowermost structural level (675–770 °C, 4–6 kbar). Retrogression took place at 590–650 °C and 3–4 kbar (Bezák, 1991; Vozárová, 1993). The synkinematic Variscan metamorphism reached conditions of amphibolite facies in some units and lower amphibolite-to-greenschist facies in others (Bezák *et al.*, 1993). The Variscan metamorphism was overprinted by low-pressure and medium-temperature Permian metamorphism (500–650 °C, ~3 kbar) triggered by an elevated heat flow during the post-Variscan crustal extension and continental rifting (Jeřábek *et al.*, 2008). Syn-kinematic Alpine recrystallization took place mostly under conditions of the chlorite zone, while post-kinematic stages attained conditions of biotite to garnet zones in places. *PT* estimates correspond to 530–550 °C and 5–6.5 kbar in northern (Jeřábek *et al.*, 2008), and 500–620 °C, 7–10 kbar in southern Veporic unit (Janák *et al.*, 2001). Overlying Mesozoic sedimentary cover and nappe sequences have been modified at temperatures between 180 and 200 °C (Plašienka *et al.*, 1989), but temperatures along thrust planes increased to 450 °C due to frictional heating incidental to the Silicic nappe movement (Milovský *et al.*, 2003).

1.2 The Gemeric unit

The Gemeric unit consists of Early Palaeozoic-to-Middle Triassic basement/cover sheet, Late-Palaeozoic-to-Mesozoic successions of the Meliata nappes, detachment cover nappes of the Silicicum and the overstepping Senonian–Tertiary post-nappe cover (Bajaník *et al.*, 1983; Plašienka *et al.*, 1997). The Gemeric unit differs from the underlying Veporic unit by a lower degree of metamorphic reworking of the basement rocks metamorphosed during Variscan and Alpine orogenic cycles mostly at greenschist facies conditions, and by the presence of blueschists in the lowermost nappe units preserved along the southern margin. The Early Palaeozoic basement is

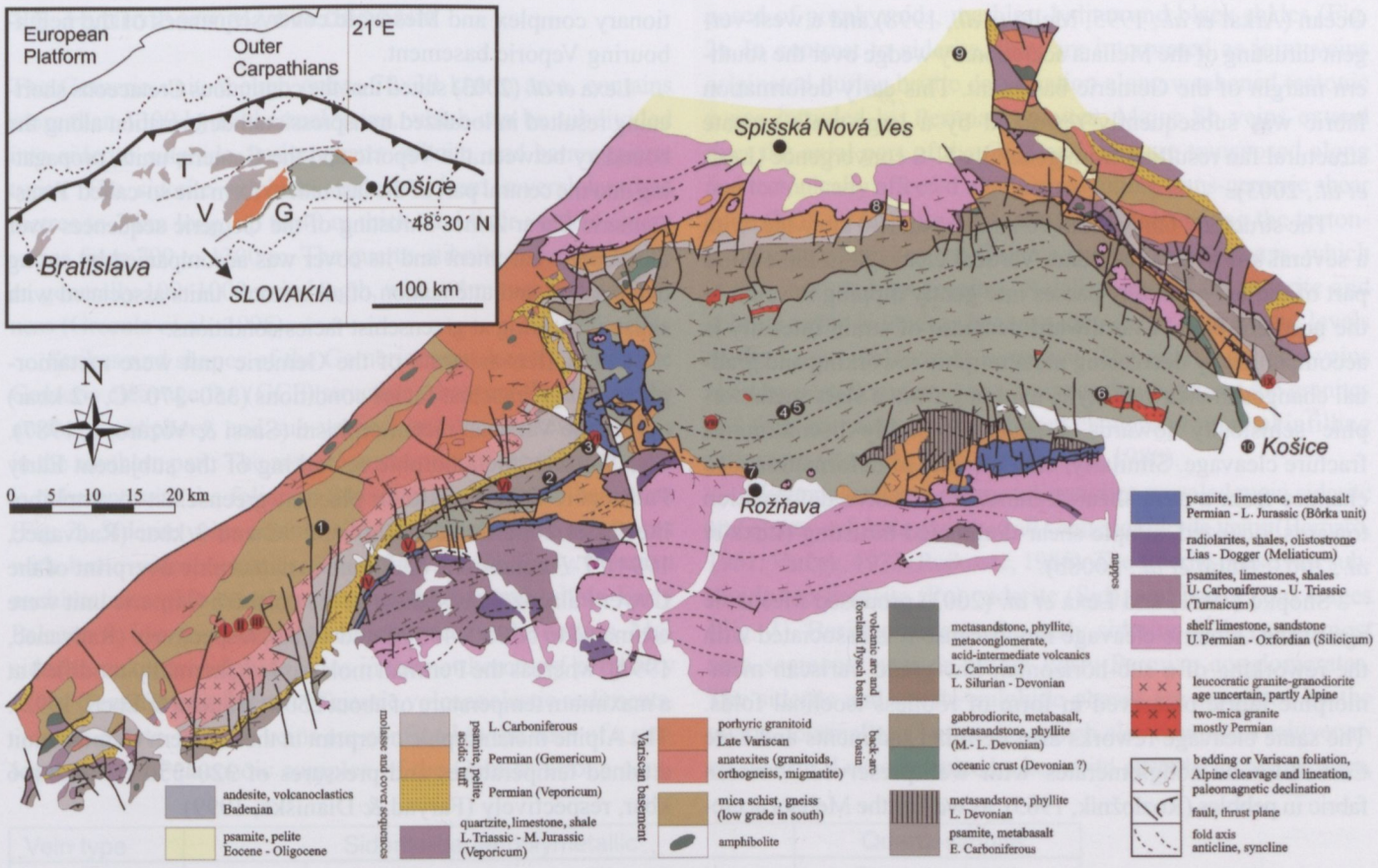

Fig. 1. Simplified geological map of the Gemeric unit and the adjoining southern part of the Veporic unit compiled after Lexa *et al.* (2000, 2003).

Inset shows locations of the Variscan basements of the Tatric (T), Veporic (V) and Gemeric (G) units in the territory of Slovakia. Numbers in black circles correspond to excursion stops (1 – magnesite-talc deposit Hnúšťa-Mútnik, 2 – magnesite deposit Jelšava, 3 – Ochtiná aragonite cave, 4 – Sb veins near Čučma, 5 – stratiform Mn-mineralization near Čučma, 6 – Sb veins near Poproč, 7 – siderite veins Rožňava-Nadabula, 8 – outcrops of barite-siderite vein Droždiak near Rudňany, 9 – travertine-precipitating springs near Sivá Brada, 10 – mineral collection of East-Slovakian Museum in Košice. Red circles designate other important magnesite-talc deposits: I – Kokava, II – Sinec, III – Samo, IV – Ploské, V – Burda, VI – Jelšava, Ochtiná, VIII – Gemerská Poloma, IX – Košice (Bankov, Medvedia)

subdivided into the Gelnica, Rakovec, and Klátov Groups (Bajaník *et al.*, 1981, 1983; Vozárová & Vozár, 1996), which are correlated with a geosynclinal stage of the Variscan orogeny. The Gelnica Group (Upper Cambrian? – Lower Devonian) contains conglomerates, sandstones, claystones, lydites and carbonates intercalated with acid volcanic rocks (porphyroids). The sandstones, claystones and basic volcanic rocks of the Rakovec Group correspond to Devonian ? – Lower Carboniferous (Vozárová & Vozár, 1988). The Klátov Group represents a pre-Westfalian complex of amphibolite-facies rocks with affinity to the oceanic crust. The Variscan basement is intruded by small "specialized" S-type granite bodies (tin-bearing, F- and P-rich) correlated with a Permian continental rifting (Broska & Uher, 2001; Finger *et al.*, 2003).

Syn- and post-orogenic Late Palaeozoic molasse sediments have been deposited discordantly on the Early Palaeozoic basement complexes. They can be subdivided in the Ochtiná, Dobšiná, Krompachy and Gočaltovo Groups (Bajaník *et al.*, 1981; Vozárová & Vozár, 1988). The Ochtiná Group represents a Lower Carboniferous, late geosynclinal, synorogenic remnant basin filled with metasediments and basic volcanoclastics. The Dobšiná Group corresponds to an Upper Carboniferous foreland basin with terrigeneous, volcanogenic and carbonatic lithofacies. Continental sub-aerial and aquatic sedimentations are typical of the Krompachy and Gočaltovo Groups composed of variegated Permian conglomerates, psammites, pelites, evaporites, and intermediate effusive and explosive volcanic rocks.

Remnants of the Late Palaeozoic–Mesozoic cover are rarely preserved below outliers of the Meliata nappes (Kozur & Mock, 1973) containing high-pressure blueschists formed at 350–460 °C and 10–12 kbars (Faryad, 1995a, 1995b). The Meliata nappes are overlain by the Turnaicum – a very low-grade metasedimentary complex of Middle Carboniferous flysch, Permian red-beds, Triassic carbonates and Jurassic flysch formations, representing a portion of the Meliata accretionary wedge (Vozárová & Vozár, 1992). The Silicic nappes in the northern and southern parts of the Gemericum unit are composed mainly of Triassic carbonates.

The complex tectonic structure of the Gemeric unit has been interpreted in terms of either Variscan (Grecula, 1982) or Alpine deformations (Tomek, 1993; Tréger *et al.*, 2004), the latter correlated with the Upper Jurassic (Faryad & Henjes-Kunst, 1997) obduction of the passive margin of the Meliata

Ocean (Árkai *et al.*, 1995; Mello *et al.*, 1998) and a west-vergent thrusting of the Meliata accretionary wedge over the southern margin of the Gemeric basement. This early deformation fabric was subsequently reworked by a large-scale arcuate structural fan resulting from generally N-S convergence (Lexa *et al.*, 2003).

The structural fan is about 70 km long and 30 km wide, with a several km wide axial zone. Vertical cleavage in the central part of the fan gradually passes into gently dipping to south in the northern part. A northward decrease of strain intensity is accompanied by decreasing metamorphic reworking and gradual changes in cleavage style, evolving from a slaty metamorphic schistosity towards a spaced-to-highly-discontinuous fracture cleavage. Similarly, the character of deformation also changes from a pure shear-dominated pervasive deformation towards localized, simple shear-dominated thrusting (Lexa *et al.*, 2003; Hurai *et al.*, 2008b).

Snopko (1971) and Lexa *et al.* (2003) proposed Mesozoic age of the Gemeric cleavage fan, because it is associated with the reworking of a sub-horizontal, low-grade Variscan metamorphic fabric preserved in form of rootless isoclinal folds. The same cleavage reworks also Permian sediments and Late Carboniferous conglomerates with well-preserved Variscan fabric in pebbles (Rozložník, 1965), as well as the Meliata accretionary complex and Mesozoic cover sequences of the neighbouring Veporic basement.

Lexa *et al.* (2003) stated that the continuous Cretaceous shortening resulted in localized transpressional deformation along the boundary between the Veporic and the Gemeric units, propagating into the central part of the last unit to form the so-called Trans-Gemeric Shear Zone. Thrusting of the Gemeric sequences over the Veporic basement and its cover was accompanied by strong deformation and attenuation of all tectonic units associated with sinistral shearing at greenschist facies conditions.

Carboniferous strata of the Gemeric unit were metamorphosed at greenschist facies conditions (350–370 °C, ~2 kbar) during the Variscan metamorphism (Sassi & Vozárová, 1987). The Variscan metamorphic reworking of the subjacent Early Palaeozoic complexes took place at greenschist-to-amphibolite facies conditions, at 460–650 °C and 3 kbar (Radvanec, 1994). *T-P* conditions of Alpine metamorphic overprint of the Lower Palaeozoic basement in the northern Gemeric unit were estimated to be 350–400 °C and 4 kbar, respectively (Radvanec, 1994), whereas the Permian molasse was thermally modified at a maximum temperature of about 250 °C (Šucha & Eberl, 1992). The Alpine metamorphic overprint in the southern Gemeric unit attained temperatures and pressures of 320–350 °C and 4–6 kbar, respectively (Faryad & Dianiška, 1999).

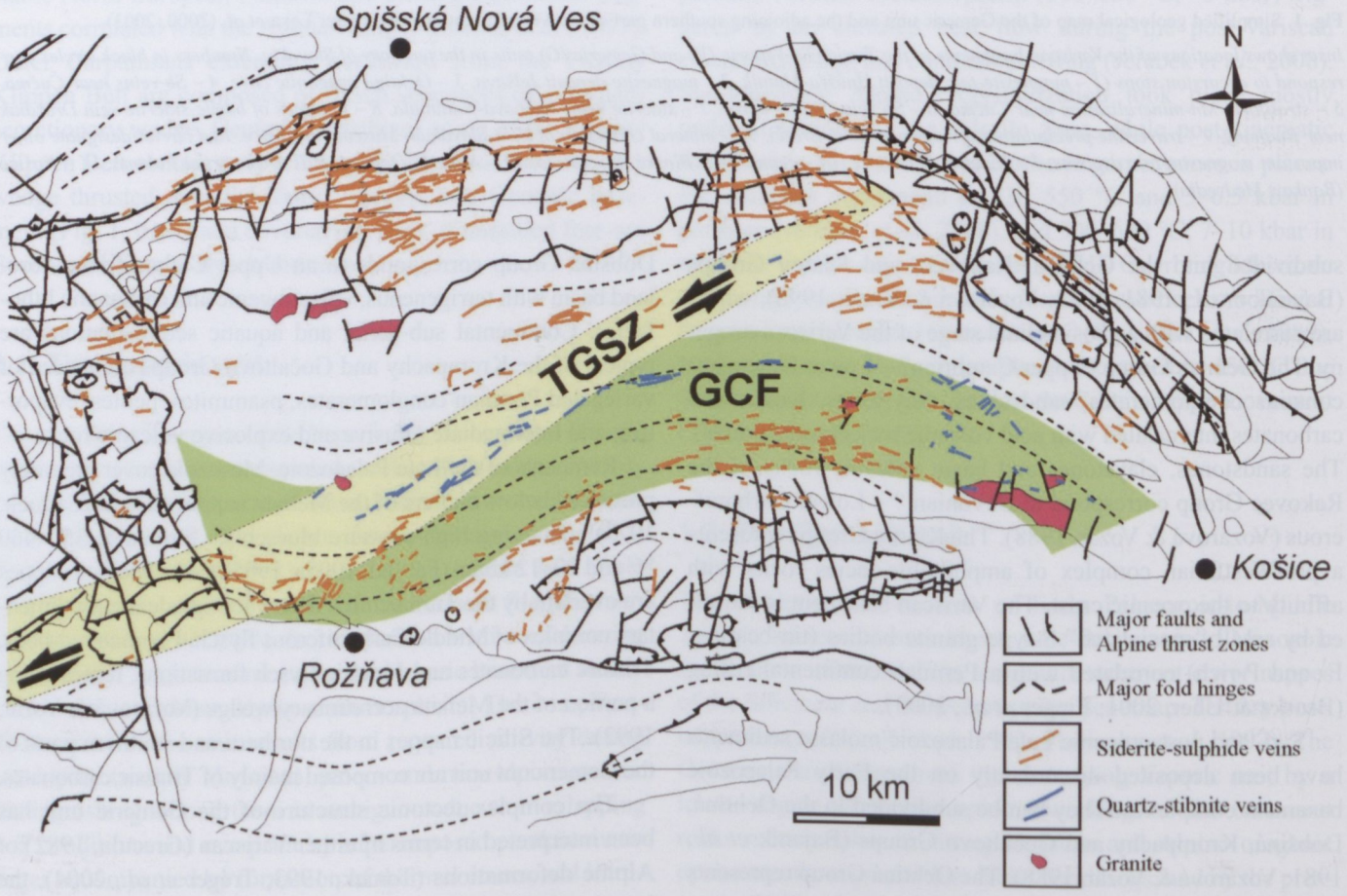

Fig. 2. Distribution of ore veins in the Gemeric unit redrawn from the metallogenetic map of Lexa *et al.* (2004), with the assumed position of the trans-Gemeric shear zone (TGSZ) superimposed onto the Gemeric cleavage fan – GCF (Hurai *et al.*, 2008b).

1.3 Hydrothermal vein deposits

The Gemeric unit, though only ~70×30 km in area, contains more than 1300 hydrothermal veins, which can be subdivided into siderite–sulphide, barite, quartz–stibnite, and barren quartz types. The siderite–sulphide veins are from several hundred metres to 7 km long, up to 40 m thick, and their vertical extent varies from 700 to 1300 m. The quartz–stibnite veins are smaller, generally 100–1000 m in length, with a 4 m maximum thickness (Grecula *et al.*, 1995).

Strikes and shapes of the Gemeric veins largely match the Gemeric cleavage fan (GCF) structure, showing flat dips in the northern periphery, and sub-vertical and locally reversal dips in the southern part. The arcuate orientation of the siderite veins is coherent with the foliation fabrics of the Gemeric basement (Fig. 2). Siderite veins occur mainly in Carboniferous sequences with basic volcanoclastics. They fade out in Early Permian anchimetamorphic conglomerates at the top and within Early Palaeozoic low-to-medium grade sequences at the bottom. Mg-siderite–ankerite–sulphide veins in the northernmost periphery of the Gemeric unit intersect Triassic volcanoclastic sediments.

The quartz–stibnite veins are confined to the base of a variegated early Palaeozoic complex of the Gelnica Group composed of porphyroids, marbles, lydites and black shales (Fig. 2). In contrast to siderite, they are interpreted as joint veins originated during brittle deformation along weakened tectonic zones intruded by Permian granites. Major Sb veins extend over the axial part of the GCF and they are transposed along and tectonically affected by the crosscutting trans-gemeric shear zone (TGSZ). Smaller veins are located also along the tectonic boundary between the Gelnica and Rakovec Groups, which is also intruded by granites. Relative age of the siderite and stibnite veins is unclear because they occur in different levels of the Lower Palaeozoic sequence. The quartz–stibnite veins must be post-Permian in age, because they intersect the granites and their contact aureoles without changes of mineral infilling or texture (Rozložník & Slavkovský, 1980).

Mineralogical and paragenetic studies revealed main siderite and quartz–sulphide phases in all Gemeric siderite veins (Bernard, 1961; Varček, 1973; Rojkovič, 1985). The siderite phase was subdivided to fuchsite (Fu), siderite (Sid), and barite (Ba) stages (Fig. 3). Barite postdates the early siderite in the uppermost vein segments near or within Early Permian conglomerates. The siderite and quartz–sulphide phases are separated by the quartz–tourmaline (Tm) stage, which also comprises rejuvenated siderite II accompanied by hematite-specularite, white mica,

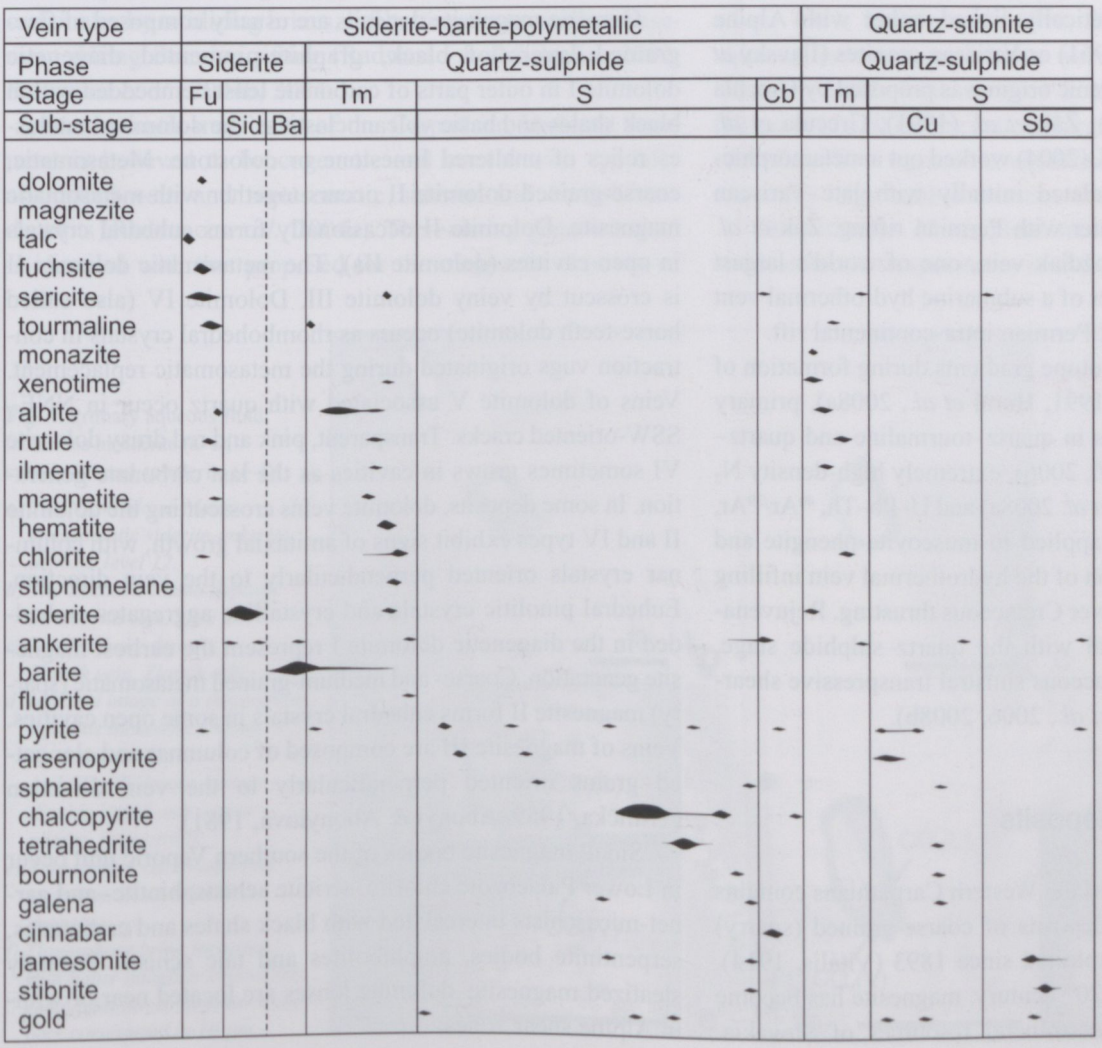

Fig. 3. Simplified succession scheme of hydrothermal vein mineralizations of the Gemeric unit (Varček, 1985; Hurai *et al.*, 2008b). Some rare minerals, mainly sulphides, were omitted.

monazite, xenotime, apatite, zircon, rutile and subordinate Fe-As sulphides (pyrite, arsenopyrite). The main sulphide stage (S) of the quartz–sulphide phase contains ankerite as the dominant gangue carbonate, and a plethora of sulphides and sulphosalts, with chalcopyrite, tetrahedrite and bournonite as the most common minerals. Cinnabar and native quicksilver are the most important minerals of the latest cinnabar stage (Cb).

The mineral succession of quartz–stibnite veins resembles that of the siderite veins, but fuchsite, siderite, barite, and cinnabar stages are missing (Beňka & Caňo, 1992). The succession scheme starts with the quartz–tourmaline stage (Tm) postdated by sulphides (S). Similar to siderite veins, Cu sulphides and sulphosalts (chalcopyrite, tetrahedrite, bournonite) associate with ankerite, but Sb sulphides and sulphosalts (berthierite, boulangerite, jamesonite, stibnite) postdate the Cu sulphides and sulphosalts. Muscovite-phengite, monazite, xenotime, apatite, rutile, arsenopyrite, pyrite, zircon, and titanite are common accessory minerals of the quartz–tourmaline stage of the quartz–stibnite veins (Urban *et al.*, 2006).

1.4 Review of genetic models of hydrothermal vein deposits

Gemeric veins were genetically linked either with Alpine (Varček, 1957; Bernard, 1961) or Variscan granites (Ilavský *et al.*, 1977). A metamorphogenic origin was proposed by Grecula (1982) and Varček (1985). Žák *et al.* (1991), Grecula *et al.* (1995), and Radvanec *et al.* (2004) worked out a metamorphic-hydrothermal model correlated initially with late Variscan orogenic processes, and later with Permian rifting. Žák *et al.* (2005) interpreted the Droždiak vein, one of world's largest carbonate veins, as a feeder of a submarine hydrothermal vent discharging in an incipient Permian intra-continental rift.

Low vertical oxygen isotope gradients during formation of early siderite (Žák *et al.*, 1991, Hurai *et al.*, 2008a), primary superdense CO_2 inclusions in quartz–tourmaline and quartz–stibnite stages (Urban *et al.*, 2006), extremely high-density N_2 inclusions in barite (Hurai *et al.* 2008a) and U–Pb–Th, $^{40}Ar/^{39}Ar$, and K/Ar geochronology applied to muscovite-phengite and monazite indicate formation of the hydrothermal vein infilling during Upper Jurassic–Lower Cretaceous thrusting. Rejuvenation, probably coincidental with the quartz–sulphide stage, occurred during Late Cretaceous sinistral transpressive shearing and extension (Hurai *et al.*, 2006, 2008b).

1.5 Magnesite–talc deposits

The Palaeozoic basement of the Western Carpathians contains numerous medium-sized deposits of coarse-grained (sparry) metasomatic magnesite exploited since 1893 (Vitális, 1914). During the second half of 20th century, magnesite has become one of the most important mineral resources of Slovakia. Average annual production of raw magnesite and concentrate in period 1991–2003 attained 1.2–1.6 and 0.8–0.9 million metric tones (Mt), respectively. Potential economic reserves are around 350 Mt and a total of 1600 Mt of raw magnesite was produced since the beginning of exploitation at the outset of 20th century (Grecula *et al.*, 2000; Csikósová *et al.*, 2000).

Structural characteristics and reserves of some important Carpathian magnesite deposits are summarised in Table 1 (Appendix). Largest magnesite deposits are aligned along the paleo-Alpine thrust boundary between Gemeric and Veporic units (Fig. 1), together with Fe carbonate (siderite–ankerite) replacement-type deposits. Most important Gemeric magnesite deposits occur in the Upper Turnaisian–Viséan (Planderová, 1982; Bajaník & Planderová, 1985) Hrádok Formation, and the Upper Viséan–Serpukhovian (Kozur *et al.*, 1976) Ľubeník Formation. Lower Palaeozoic rocks of the Gelnica Group contain the second productive horizon of the Gemeric unit, which hosts the Gemerská Poloma talc–magnesite deposit (also called Dlhá Dolina) and the occurrences near Henclová, Vlachovo and Mníšek nad Hnilcom villages. Mg carbonates occur here in volcanic-sedimentary complexes composed of black shales, chlorite–sericite schists, metarhyolites, basic pyroclastics and porphyroids belonging to the Bystrý Potok and Vlachovo Formations (Grecula *et al.*, 1995; Tréger *et al.*, 2004).

Gemeric magnesite deposits are usually composed of fine-grained layers of black, graphite-pigmented diagenetic dolomite I in outer parts of carbonate lenses embedded within black shales and basic volcanoclastics. The dolomite I encloses relics of unaltered limestone or dolostone. Metasomatic, coarse-grained dolomite II occurs together with metasomatic magnesite. Dolomite II occasionally forms euhedral crystals in open cavities (dolomite IIa). The metasomatic dolomite II is crosscut by veiny dolomite III. Dolomite IV (also called horse-teeth dolomite) occurs as rhombohedral crystals in contraction vugs originated during the metasomatic replacement. Veins of dolomite V associated with quartz occur in NNE–SSW-oriented cracks. Transparent, pink and red drusy dolomite VI sometimes grows in cavities as the last carbonate generation. In some deposits, dolomite veins crosscutting the dolomite II and IV types exhibit signs of antitaxial growth, with columnar crystals oriented perpendicularly to the vein direction. Euhedral pinolitic crystals and crystalline aggregates embedded in the diagenetic dolomite I represent the earliest magnesite generation. Coarse- and medium-grained metasomatic (sparry) magnesite II forms euhedral crystals in some open cavities. Veins of magnesite III are composed of columnar and elongated grains oriented perpendicularly to the vein direction (Trdlička, 1959, Abonyi & Abonyiová, 1981).

Small magnesite bodies of the southern Veporic unit occur in Lower Palaeozoic chlorite–sericite schists, biotite- and garnet-micaschists intercalated with black shales and carbonates, serpentinite bodies, amphibolites and talc schists. Strongly steatized magnesite–dolomite lenses are located near or within Alpine shear zones.

1.6 Review of genetic models of magnesite deposits

Origin of the Carpathian magnesite deposits remains unresolved. Kužvart (1954), Trdlička (1959), Varček (1968), Varga (1970), Abonyi (1971), Abonyi & Abonyiová (1981) favoured a hydrothermal-metasomatic origin. Most authors invoked metasomatic Mg-rich fluids associated with magmatic intrusions (Kužvart, 1954; Trdlička, 1959; Varček, 1967) or metamorphic processes (Ilavský, 1957; Varček, 1968). The Mg-metasomatism was correlated either with Variscan (Kužvart, 1954; Ilavský, 1957) or Alpine processes (Trdlička, 1959; Slávik, 1967; Varček, 1968; Abonyi, 1971).

Ilavský *et al.* (1975, 1991), Turan & Vančová (1976, 1979), Turanová *et al.* (1996) proposed a syn-sedimentary chemogenic precipitation of magnesite due to seawater evaporation. A sedimentary-exhalative deposition connected with submarine basic volcanism was also considered (Zorkovský, 1955; Ilavský, 1979). Some models assumed initially syn-sedimentary (chemogenic or sedimentary-exhalative) precipitation followed by reworking and metasomatism during superimposed metamorphism (Turan & Vančová, 1979; Ilavský *et al.*, 1991; Grecula *et al.*, 1995). Most recently, the Mg-metasomatism is attributed to hydrothermal-metasomatic replacement of marine reef carbonates by oxidizing brines, infiltrating the crystalline basement during Permian rifting (Radvanec & Prochaska, 2001, Radvanec *et al.*, 2004b, 2004c).

Metasomatic magnesite of the Carpathian Variscan basement is believed to be cogenetic and coeval with spatially associated vein and metasomatic siderite and Fe-dolomite deposits (Radvanec *et al.*, 2004a). The existing genetic model is identical with that proposed for the magnesite deposits of the Eastern Alps, where the influx of basinal brines is correlated with the Late Permian–Early Triassic rifting during initial stages of the Alpine orogenic cycle (Prochaska, 1999, 2001; Ebner *et al.*, 1999). Fluid inclusion and stable isotope data from the Carpathian deposits (Vozárová *et al.*, 1995; Huraiová *et al.*, 2002; Koděra & Radvanec, 2002; Radvanec *et al.*, 2004b, 2004c) indicate strong metamorphogenic affinity of the ore-forming fluids, presence of various fluid types, including high salinity brines and CO_2-rich low-salinity aqueous fluids.

2. Review of geochemical data on hydrothermal vein deposits

2.1 Fluid inclusions

Siderite sub-stage. Primary fluid inclusions have rhombohedral negative crystal shapes, are isolated and randomly distributed and occur rarely in coarse-grained early siderite (Fig. 9a-c). Secondary inclusions within healed cracks are more abundant. All the siderite-hosted inclusions contain aqueous liquid with a 5–15 vol% of vapour phase (Varček, 1968; Borisenko *et al.*, 1984; Hurai *et al.*, 1998, 2002, 2008b). Three-phase aqueous inclusions with halite were occasionally observed in siderite crystals from cavities in the coarse-grained siderite (Hurai *et al.*, 2002). Inclusions larger than 10–15 μm in diameter often show signs of re-equilibration (decrepitation cracks, unusually large bubble volumes, recrystallization of walls).

Temperatures of incipient melting were appropriate for stable eutectic temperatures in the aqueous solutions contain-

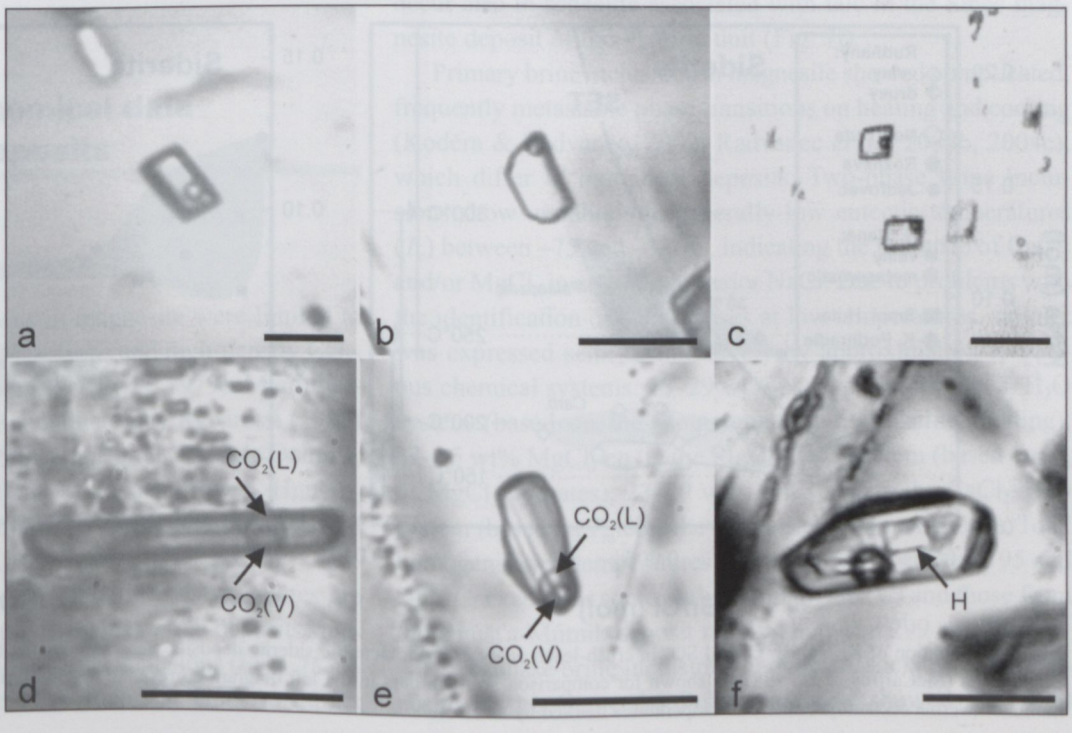

Fig. 4. Primary aqueous fluid inclusions in siderite (**a–c**), stibnite (**d**) and sphalerite (**e–f**).
a) The Nižná Slaná-Manó metasomatic siderite-ankerite deposit, level 12.
b) The Rožňava-Mária deposit, Striebornà vein, level 2.
c) The Rudňany deposit, Zlatník vein, Zlatník adit.
d) Infrared image of a three-phase aqueous inclusion, Čučma Sb-deposit. CO_2(L) and CO_2(V) denote carbon dioxide liquid and vapour phases, respectively.
e) Three-phase carbo-aqueous inclusion, Zlatá Idka Sb-Au deposit.
f) Three-phase brine inclusion with halite daughter crystal (H), Zlatá Idka Sb-Au deposit. Scale bars correspond to 10 μm.

ing NaCl, KCl, $CaCl_2$ and $MgCl_2$ as dominant dissolved species. Total salt concentrations varied between 18–26 wt% in vein-filling siderite and 14–35 wt% in siderite crystals from cavities. The presence of CO_2 was indicated by double freezing and crystallization of the gas hydrate on cooling.

Barite sub-stage. Barite contains primary brine inclusions with variable NaCl/$CaCl_2$ ratios and total salt concentrations. The brine inclusions are closely spatially associated with high density (0.548–0.745 g□cm^{-3}) N_2 inclusions containing 0–16 mol% CO_2 in the northern part of the Gemeric unit (Hurai *et al.*, 2008a). In contrast, barites from the south-Gemeric veins contain high-density (up to 1.02 g□cm^{-3}) $CO_2 \pm N_2$ inclusions with 0–52 mol% N_2. Other gas species were below detection limit, although some inclusions homogenizing to liquid plot above the critical curve of the N_2–CO_2 system, thus indicating some CH_4 admixture. Metastable high-density brines devoid of vapour bubble are diagnostic of a homogeneous fluid trapped at high pressure. Occurrence of carbonic-aqueous inclusions with variable phase ratios indicates entrapment from a heterogeneous parent fluid.

Quartz–tourmaline and quartz–sulphide stages precipitated from moderate-to-very-high-salinity NaCl–KCl–$CaCl_2$ brines (Varček, 1967; Borisenko *et al.*, 1984; Chovan *et al.*, 1996; Hurai *et al.*, 2002), coexisting locally with a CO_2-rich immiscible liquid (Hurai *et al.*, 1998). The brine inclusions homogenize either by vapour bubble disappearance or halite dissolution. Cinnabar contains two-phase brine inclusions (19–29 wt% NaCl eq.) with total homogenization temperatures between 110 and 125 °C (Borisenko *et al.*, 1984).

Immiscibility was documented in quartz–sulphide and quartz–tourmaline stages of quartz–stibnite veins, where high salinity brines (23–32 wt% NaCl eq.) are often accompanied by high-density-to-superdense CO_2 inclusions (0.75–1.197 g□cm^{-3}) with 0–7.3 mol% N_2 and 0–2.5 mol% CH_4. Stibnite from Čučma contains rare primary aqueous inclusions showing a small bubble filled with liquid and vapour CO_2 phases (Fig. 4d). Sphalerite and quartz from the Zlatá Idka stibnite deposit contain essentially pure CO_2 inclusions with a few mol% of additional gases (T_mCO_2 from –56.5 °C to –57.4 °C) and densities between 0.63 and 0.77 g□cm^{-3}, low-salinity (1.6–5.2 wt% NaCl eq.) carbo-aqueous inclusions with 30–95 vol% of the carbonic gas at room T, and brine inclusions (16–38 wt% NaCl + $CaCl_2$ eq.) devoid of the carbonic gas, which homogenize either by bubble disappearance or halite dissolution (Fig. 4e-f).

Bromine concentrations in fluid inclusion leachates normalized to total salt content expressed in wt% NaCl equivalents vary from 355 to 1930 ppm in various siderite deposits. Iodine concentrations are generally low, but constant (4–16 ppm), except for the Fe-dolomite-ankerite veins near Novoveská Huta, where up to 88 ppm was determined. Fluorine contents fluctuated from low (95 ppm) to extremely high values (21,300 ppm), and these local extremes are probably due to contamination with fluorite, although this mineral has never been optically identified.

Some extremely high SO_4 concentrations (*e.g.* 90,000 ppm at Novoveská Huta) must also reflect anhydrite or barite contaminants. However, values below ~15,000 ppm (1.5 wt%) are probably due to the sulphate dissolved in the ore-forming fluid.

Crush-leach analyses of siderite exhibit a negative correlation between bromine and sulphate contents. The antithetic Br–SO_4 behaviour in the siderites tends to propagate with the increasing K/Na ratio (Fig. 5). Fluorine and SO_4 concentrations in metasomatic siderites of the Nižná Slaná replacement-

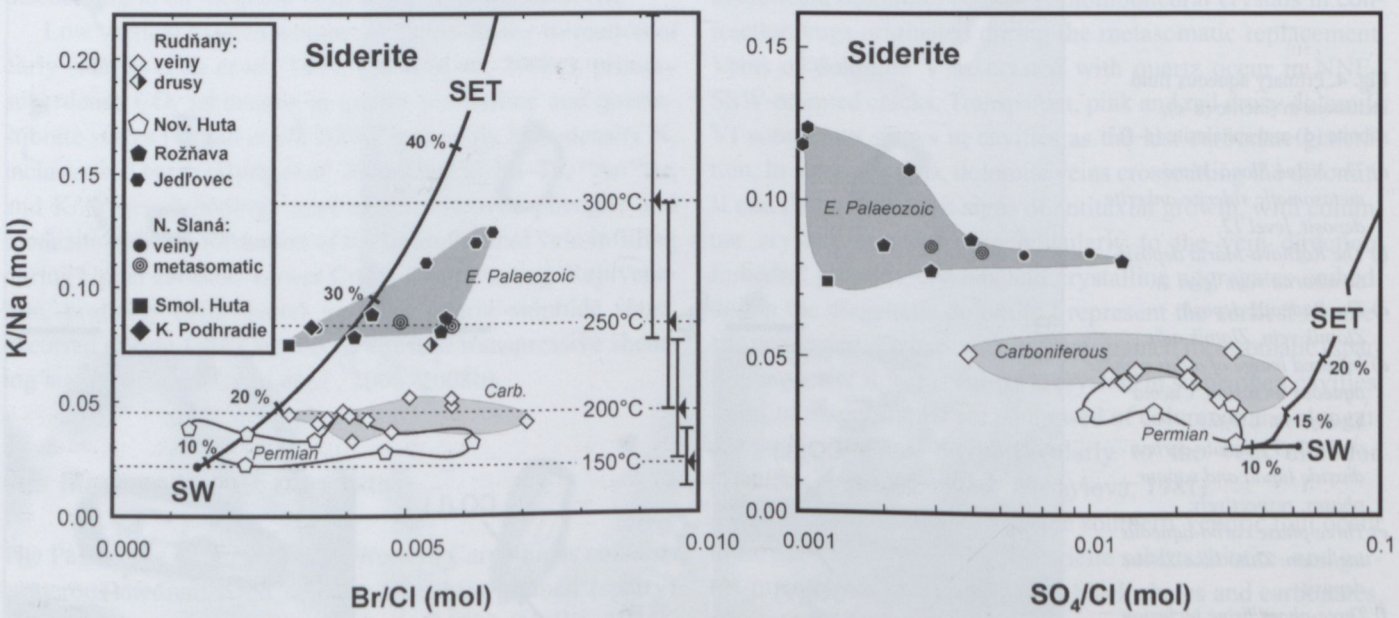

Fig. 5. Covariation of K, Na, Br, Cl and SO_4 in crush-leach analyses from Gemeric siderite deposits. Seawater evaporation trend (SET) with percentages of evaporation (McCaffrey *et al.*, 1987) is shown for comparison. Vertical bars in the left diagram correspond to total propagated error (1σ) of K/Na geothermometer (Verma & Santoyo, 1997) at temperatures marked by an arrow.

type stratabound deposit are significantly lower than those in the crosscutting siderite veins. In contrast, the vein-forming fluids are depleted in Br compared to the metasomatic siderite, but K/Na ratios are similar in both siderite types.

2.2 Stable isotopes

Oxygen and carbon isotope compositions of the Gemeric siderites were studied by Cambel *et al.* (1985), Žák *et al.* (1991), Iró & Radvanec (1997), Hurai *et al.* (1998, 2002, 2008a, 2008b). Siderite veins in the Lower Palaeozoic series of the south-Gemeric unit are significantly depleted in heavy isotopes compared to those intersecting the Upper Palaeozoic strata in the northern periphery of the Gemeric unit (Fig. 6). In some deposits (*e.g.* Rudňany, Rožňava – Nadabula), the almost constant $\delta^{13}C$ value is coupled with a wide variation in $\delta^{18}O$ values. The $\delta^{18}O$ values decreased during growth of siderite crystals from Rudňany – Poráč, thus reflecting a temperature increase (Hurai *et al.*, 2002).

The $\delta^{18}O$ values from the Rožňava – Nadabula ore field of the south-Gemeric unit decrease with depth at a rate of 0.9‰ km^{-1}, whilst the $\delta^{13}C$ values remain constant along the vertical extent of about 1000 m (Žák *et al.*, 1991). A similar trend was observed along the Droždiak vein in the northern part of Gemeric unit, where the oxygen isotopic gradient correspond to 1.8–2.3‰ km^{-1}, and the $\delta^{13}C$ values oscillate within a narrow range of 4.5 ± 0.5‰ (Hurai *et al.*, 2002, 2008a). Other siderite veins showed wider ranges of $\delta^{13}C$ values positively correlated with the $\delta^{18}O$ values (Fig. 6). Dispersed δ-values without any discernible trends are diagnostic of the Novoveská Huta deposit. Stable isotope ratios in the vein and metasomatic siderite types of the Nižná Slaná replacement-type deposit are similar.

3. Review of geochemical data on magnesite deposits

3.1 Fluid inclusions

First reports on fluid inclusions in magnesite were limited to description of various types of aqueous and high-density CO_2-rich inclusions at room temperature (Eliáš, 1979). Microthermometric measurements were conducted by Rybárová (1985) at Burda, Huraiová *et al.* (2002) at Burda, Ploské, Ochtiná, Koděra & Radvanec (2002) at Miková-Jedľovec, Hnúšťa-Mútnik, Radvanec *et al.* (2004b) at Gemerská Poloma, and Radvanec *et al.* (2004c) at Košice-Medvedia deposits.

Generally, primary fluid inclusions in Mg carbonates are rare and usually less than 10 μm in diameter. All deposits studied contain primary two-phase aqueous inclusions (Figs. 7a, e). Brine inclusions with halite were found at Hnúšťa-Mútnik

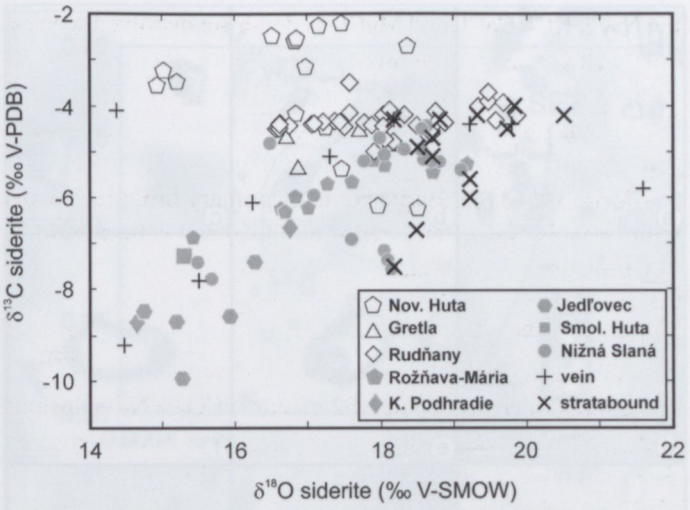

Fig. 6. Carbon and oxygen isotope covariation in Gemeric hydrothermal siderites. Open and shaded symbols correspond to prevailingly Upper and Lower Palaeozoic host rocks, respectively. Shown for comparison are also stable isotope compositions of vein (Schendleck, Wagrein, Mitterberg, Teltschen, Gollrad, Hirschwang, Altenberg) and stratabound (Erzberg, Radmer, Hirschwang, Bärenach, Hüttenberg) siderites of the Greywacke Zone of Eastern Alps compiled from Schroll *et al.* (1986), Laube *et al.* (1995) and Prochaska *et al.* (1996).

(Fig. 7h) and Košice-Medvedia. Three-phase CO_2-rich aqueous inclusions were described from all deposits studied (Figs. 7a-g), except for the Gemerská Poloma deposit. In some localities, the CO_2-rich aqueous inclusions seem to be coeval with two-phase aqueous inclusions (Burda), while in other localities they clearly postdate them (Miková-Jedľovec, Košice-Medvedia), or exhibit uncertain age relationship (Hnúšťa-Mútnik). At Košice-Medvedia, the CO_2-rich aqueous inclusions are coeval with the halite-bearing brine inclusions and appear to be primary in quartz with ore minerals, post-dating the Mg carbonates (Fig. 7b). Primary CO_2-rich aqueous inclusions occur also in scheelite associated with talc in the Sinec magnesite deposit of the Veporic unit (Fig. 7i).

Primary brine inclusions in magnesite showed complicated, frequently metastable phase transitions on heating and cooling (Koděra & Radvanec, 2002; Radvanec *et al.*, 2004b, 2004c), which differ in individual deposits. Two-phase brine inclusions show variable, but generally low eutectic temperatures (T_e) between –75 and –32 °C, indicating the presence of $CaCl_2$ and/or $MgCl_2$ in addition to major NaCl. Due to problems with the identification of solid phases at low temperatures, salinity was expressed semi-quantitatively by approximation to various chemical systems: 23–29 wt% NaCl eq. in the NaCl–H_2O system (based on the temperature of hydrohalite melting), 32–35 wt% $MgCl_2$ eq. in the $MgCl_2$–H_2O system (based on T_m of $MgCl_2$ hydrates), 23–29 wt% $CaCl_2$ eq. in the $CaCl_2$–H_2O system (based on $T_m$ice – the Gemerská Poloma deposit). Total homogenisation temperatures (T_h) are mostly between 195 and 248 °C, except for some outliers (up to 358 °C) and those from the Hnúšťa-Mútnik deposit ranging between 299 and 336 °C.

Two-phase brine inclusions in quartz associated with magnesite at the Gemerská Poloma deposit showed T_e values

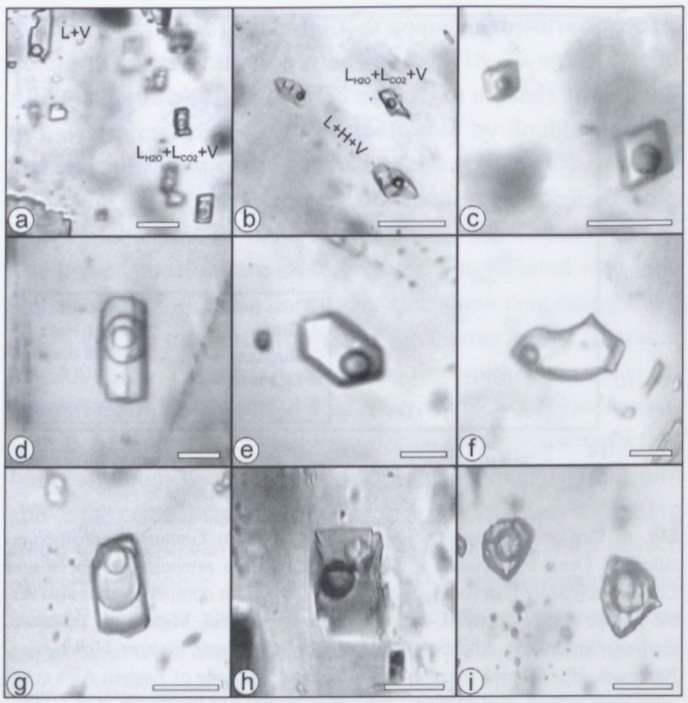

Fig. 7. Fluid inclusions in minerals of magnesite deposits. **a**) Primary, probably re-equilibrated, two-phase brine inclusion (L + V) and a trail of intact secondary three-phase CO_2-rich aqueous inclusions ($L_{H2O} + L_{CO2} + V$) in magnesite from Miková-Jedľovec deposit. Scale bar = 20 μm. **b**) Halite-bearing brine inclusions (L + H + V) and three-phase aqueous CO_2-rich inclusion ($L_{H2O} + L_{CO2} + V$) in quartz superimposed to magnesite. All inclusions appear to be primary, thus indicating a heterogeneous fluid system. Košice-Medvedia. Scale bar = 20 μm. **c**). Secondary CO_2-rich aqueous inclusions in magnesite from Košice-Medvedia deposit. Scale bar = 10 μm. **d**) Primary CO_2-rich aqueous inclusion in dolomite II from Burda deposit. Scale bar = 20 μm. **e**) Primary low salinity aqueous inclusions in dolomite II from Burda deposit. Scale bar - 20 μm. **f**) Primary two-phase aqueous inclusion in yellow veiny dolomite V from Podrečany-Točnica deposit. Scale bar = 20 μm. **g**) CO_2-rich aqueous inclusion (probably primary) in magnesite from Mútnik deposit. Scale bar = 10 μm. **h**) Primary brine inclusion with halite in magnesite from Mútnik deposit. Scale bar = 10 μm. **i**) Primary, partly re-equilibrated CO_2-rich aqueous inclusions in scheelite from talc-bearing soapstone rock from Sinec deposit. Scale bar = 10 μm.

between –29 and –25 °C, corresponding to the NaCl–KCl–H_2O or MgCl–H_2O systems. Salinity is around 26–29 wt% NaCl eq. based on T_m of hydrohalite in the NaCl–H_2O system, or 34–35 wt% $MgCl_2$ eq. based on T_m of $MgCl_2$ hydrate in the $MgCl_2$–H_2O system.

Primary and secondary halite-bearing brine inclusions in magnesite from Hnúšťa-Mútnik, and in magnesite and quartz from Košice-Medvedia show similar T_e values, ranging from –71 to –35 °C. Salinities based on T_m of halite in the NaCl–H_2O system correspond to 29–32 and 33–42 wt% NaCl eq., respectively. Increased T_h values of the halite-bearing brine inclusions from Hnúšťa-Mútnik (319–348 °C) probably result from re-equilibration. Variable T_h values at Košice-Medvedia (208–298 °C) reflect the trapping of a heterogeneous CO_2-rich aqueous fluid.

CO_2-solid in three-phase CO_2-rich aqueous inclusions melted between –57.5 and –56.6 °C, thus indicating essentially pure carbon dioxide compositions. The inclusions exhibited low total salinity (0–8 wt% NaCl eq.) and CO_2 densities between 0.53 and 0.69 g□cm^{-3}. In contrast, the CO_2-rich aqueous inclusions from the Košice-Medvedia deposit displayed broader ranges of the CO_2 densities (0.28–0.77 g□cm^{-3}) and salinities (1–22 wt% NaCl eq.). T_h values in the Miková-Jedľovec, Košice-Medvedia, Burda and Hnúšťa-Mútnik deposits ranged between 260 °C and 343 °C.

Two-phase aqueous inclusions in magnesite showed a broader range of T_e values (from –61 °C to –23 °C) and salinities (1–22 wt% NaCl eq.). Majority of the salinities were below 8 wt% NaCl eq. (Miková-Jedľovec, Burda, Ploské). T_h values were variable, but generally low (132–260 °C at Miková-Jedľovec, Košice-Medvedia, Gemerská Poloma, 100–130 °C at Burda, and Ploské).

Primary three- and two-phase CO_2-bearing aqueous inclusions in scheelite associated with talc in Sinec deposit (the Veporic unit) were strongly re-equilibrated, and their densities were thus not representative of the trapping conditions. Maximum density of the CO_2-rich phase attained 0.796 g□cm^{-3} (T_h = 17.8 °C to liquid). Melting of CO_2-solid occurred between –57.5 and –58 °C, indicating minor admixture of other gas species. Aqueous phase exhibited T_e values around –49 °C (a $CaCl_2$-dominated system), but T_h values could not be determined due to decrepitation prior to total homogenization.

Crush-leach analyses have been performed in order to reveal elemental ratios in fluid inclusions in metasomatic carbonates and associated minerals (Radvanec & Prochaska, 2001; Radvanec *et al.*, 2004b, 2004c, Hurai & Prochaska, unpublished data). Leachates from early metasomatic dolomites of the Gemeric unit exhibit a wide range of Br/Cl ratios and a narrow range of K/Na ratios. The Gemeric dolomites do not exhibit noticeable differences between Carboniferous and Early Palaeozoic productive horizons (Fig. 8). In contrast, metasomatic dolomites of the Veporic unit show variable, mostly extremely high K/Na and low Br/Cl ratios. This behaviour is probably erratic, owing to low yield of leachates. Leachate chemistry of horse-teeth dolomite IV of the Gemeric unit is indistinguishable from that of the earlier metasomatic Mg carbonates, but vein-filling dolomite V, postdating the metasomatic carbonates, differs significantly, showing the elemental signature similar to normal seawater.

Crush-leach analyses of metasomatic magnesite show similar elemental distribution in the Gemeric and Veporic units, projecting to the right side of seawater evaporation trend (Fig. 5). Compared to siderite vein deposits, Br/Cl ratios in magnesite leachates are substantially higher, reaching the maximum value of 0.021. The largest Br-enrichment (Br/Cl molal = 0.038) was recorded in scheelite from the Sinec magnesite–talc deposit of the Veporic unit. Generally, the Veporic magnesites exhibit higher K/Na ratio and larger Br-enrichment compared to those of the Gemeric unit.

A negative correlation exists between the bromine and sulphate contents in the Mg carbonate leachates. Contrary to the K–Na–Br–Cl correlation diagram, all but dolomite V crush-

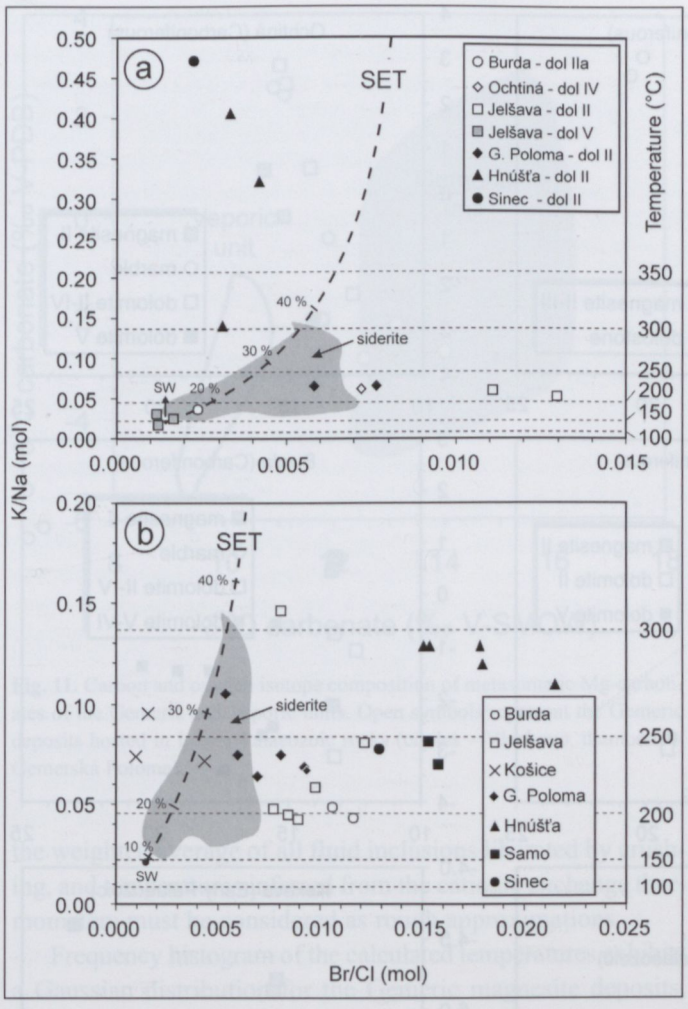

Fig. 8. K–Na–Br–Cl correlation diagram of crush-leach analyses from various types of dolomites (a) and metasomatic (sparry) magnesite (b) from Carpathian Mg-metasomatic deposits. Shaded fields correspond to crush-leach data on siderite deposits (Hurai *et al.*, 2008b). SET is the evaporation trend of modern seawater (McCaffrey *et al.*, 1987). Temperatures along the right vertical axis are calculated from the K/Na ratio according to Verma & Santoyo (1997). Data sources: Hurai & Prochaska, unpublished, Radvanec & Prochaska (2001), Radvanec *et al.* (2004b, 2004c), Németh *et al.* (2004).

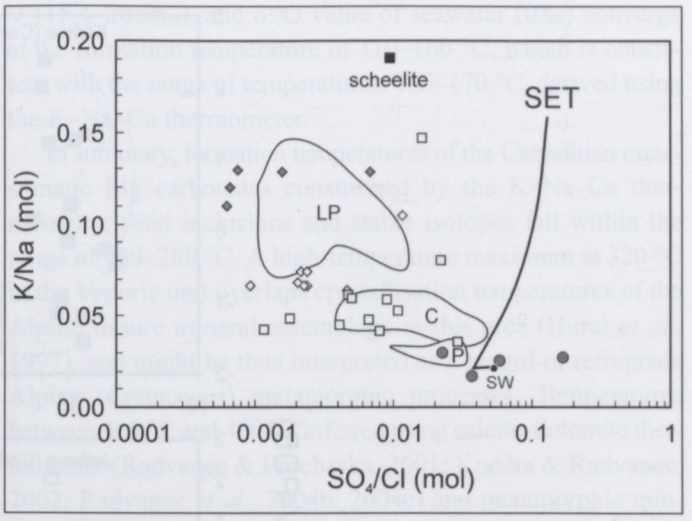

Fig. 9. K–Na–SO_4–Cl correlation diagram of crush-leach analyses from metasomatic magnesite and dolomite of the Gemeric unit hosted in Carboniferous (open squares) and Lower Palaeozoic rocks (open diamonds). Other symbols correspond to metasomatic magnesite of the Veporic unit (shaded diamonds), scheelite from soapstone of the Sinec magnesite deposit of the Veporic unit (solid squares). Shaded circles are projection points of dolomite V from the Gemeric unit. Data sources: Hurai & Prochaska, unpublished, Radvanec & Prochaska (2001), Radvanec *et al.* (2004b, 2004c), Németh *et al.* (2004). Contoured are also fields for siderite veins intersecting the Permian (P), Carboniferous (C), and Lower Palaeozoic (LP) rocks of the Gemeric unit (Hurai *et al.*, 2008b). SET is the seawater (SW) evaporation path (McCaffrey *et al.*, 1987).

leach analyses project to the left side of seawater evaporation trend, thus indicating depletion in SO_4 with the increasing K/Na ratio (Fig. 9). The contrasting behaviour of SO_4 and Br is qualitatively similar to that recorded in the Carpathian siderite deposits, but fluctuations of the SO_4 contents and extent of the sulphate depletion is somewhat larger.

The measured K/Na, Br/Cl and SO_4/Cl ratios are correlated with the metamorphic grade of the country rocks. The highest K/Na, Br/Cl and the lowest SO_4/Cl ratios occur in the magnesites from medium-grade metamorphic rocks in the Early Palaeozoic Veporic basement; the lowest ratios were recorded from the magnesites in greenschist-facies Carboniferous rocks of the Gemeric unit. Leachates from Mg carbonates of the Gemeric unit show roughly similar K–Na–Br–SO_4–Cl abundances as those of the spatially associated siderite veins intersecting the same host lithologies (Carboniferous and Lower Palaeozoic) with different degree of the Variscan metamorphic reworking.

Lithium concentrations are significantly lower in magnesite leachates compared to those in siderite. The Li/Na molar ratios do not exceed the value of 0.02, and are typically below 0.01, except for the Gemerská Poloma deposit located above Li- and F-rich granite. Here, the Li/Na ratio as high as 0.054 has been recorded in magnesite leachates.

3.2 Stable isotopes

Carbon and oxygen isotope data on metasomatic Mg carbonates from Western Carpathians have been published by Kralik *et al.* (1989), Ilavský *et al.* (1991), Vozárová *et al.* (1995), Turanová *et al.* (1996), Huraiová *et al.* (2002), Radvanec *et al.* (2004). The Carpathian Mg carbonates are typical of large variation of carbon isotopes compared to oxygen isotopes. Individual magnesite deposits (*e.g.* Burda, Mútnik, Kokava) exhibit almost constant $\delta^{18}O$ value in various generations of Mg carbonates, while the carbon isotope ratios vary within several ‰ (Fig. 10). This contrasts with siderites, where larger spread of $\delta^{18}O$ values is accompanied by minor changes in $\delta^{13}C$ (Hurai *et al.* 2008b). Veins of dolomite V – the latest Mg carbonate generation – display increased $\delta^{18}O$ values compared to the earlier carbonates. Mg carbonates (dolomite, magnesite) of the Gemeric unit are enriched in ^{18}O by at least ~2‰ compared to those of the Veporic unit, but significant differences have not been recorded among the Gemeric deposits hosted in the Carboniferous and the Early Palaeozoic strata (Fig. 11).

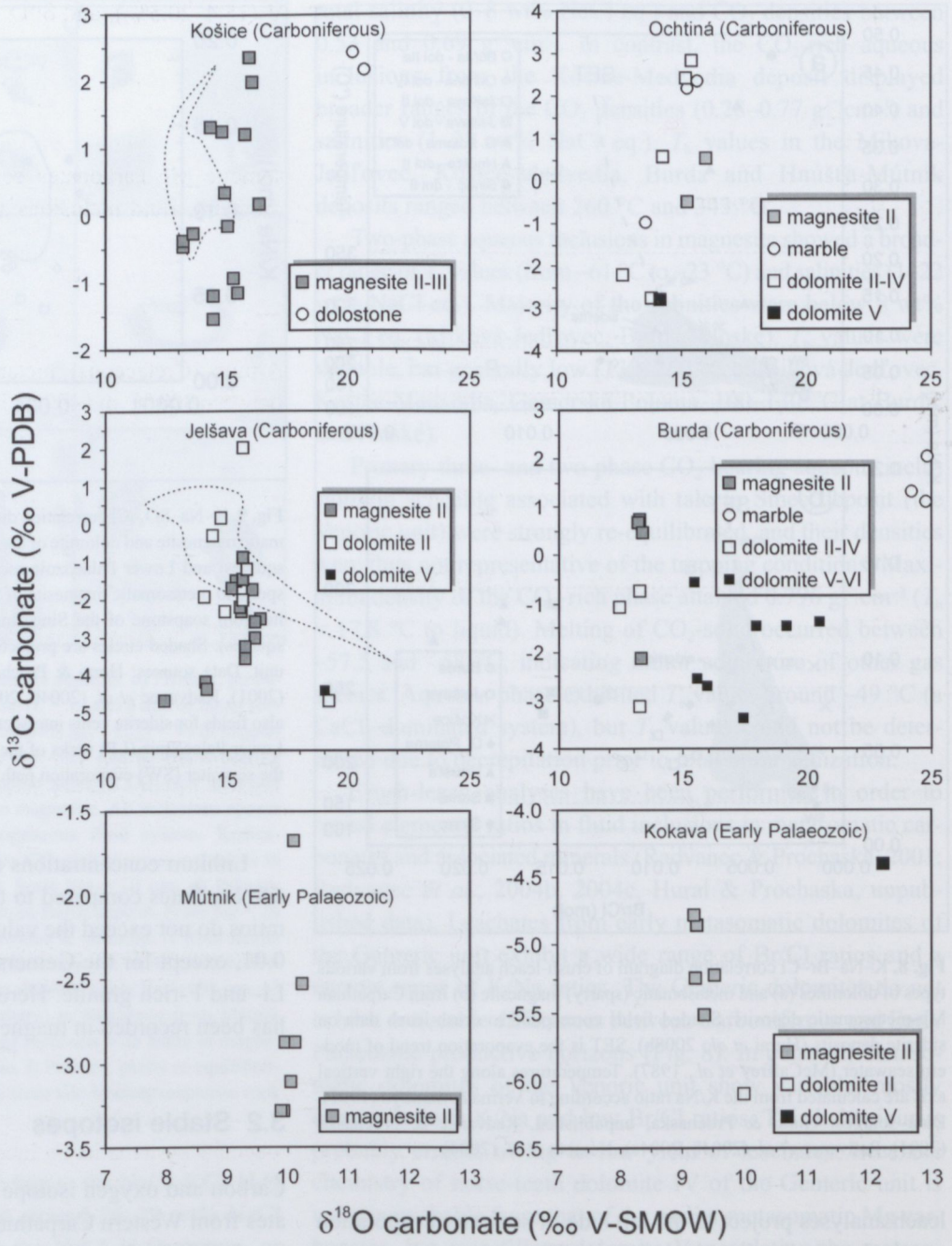

Fig. 10. Stable isotope covariation in various carbonates from magnesite deposits of the Gemeric (Košice-Bankov, Ochtiná, Jelšava, Burda) and the Veporic (Hnúšťa-Mútnik, Kokava) units. Open fields in the Jelšava and Košice deposits correspond to stable isotope data on magnesite taken from Turanová *et al.* (1996).

4. Interpretation of geochemical data

4.1 Temperature of magnesium metasomatism

Quantitative interpretation of stable isotopes from the Carpathian magnesite deposits was ambiguous due to a lack of reliable temperature determinations. For instance, acoustic and thermovacuometric decrepitation methods (Trdlička & Kupka, 1964; Eliáš, 1979) applied to magnesite yielded temperatures between 175 and 320 °C. The temperature of around 235 °C was obtained using the method of intersecting isochores of CO_2-rich aqueous inclusions with contrasting density at the Burda deposit (Huraiová *et al.*, 2002). The Mg-in-calcite/Fe-in-dolomite thermometry in the magnesite deposits yielded the temperatures between 300 and 490 °C (Radvanec & Prochaska, 2001; Koděra & Radvanec 2002; Radvanec *et al.* 2004b, 2004c).

Independent temperature estimates can be obtained also from Na/K, Na/Li, and Na/K/Ca ratios in leachates using empirical cationic exchange thermometers (Fournier & Truesdell, 1973; Verma & Santoyo, 1997; Michard & Fouillac, 1981). The K/Na/Ca ratios in leachates from Gemeric siderite deposits yield temperatures compatible with those derived from fluid inclusions and stable isotopes (Hurai *et al.*, 2002, 2008a, 2008b). However, due to variable composition of fluid inclusions in the metasomatic Mg carbonates, the leachate chemistry reflects

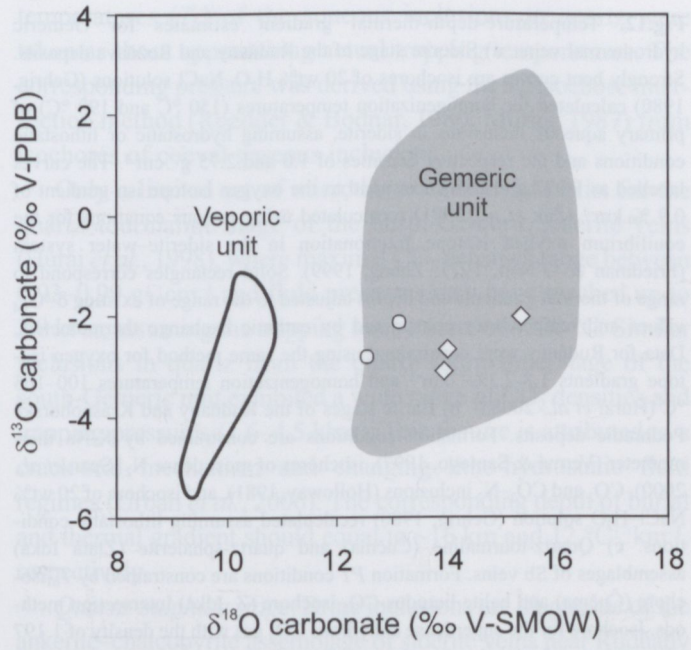

Fig. 11. Carbon and oxygen isotope composition of metasomatic Mg-carbonates of the Gemeric and Veporic units. Open symbols represent the Gemeric deposits hosted in Lower Palaeozoic rocks (circles – Vlachovo, diamonds – Gemerská Poloma).

the weighted average of all fluid inclusions liberated by crushing, and temperatures inferred from the cationic exchange thermometers must be considered as rough approximations.

Frequency histogram of the calculated temperatures exhibits a Gaussian distribution for the Gemeric magnesite deposits, with an average value of 210 °C (± 20, 1σ) and the overall extent from 180 to 260 °C. Temperatures between 135 and 170 °C were inferred for the veins of dolomite V from the Jelšava and Burda deposits.

Metasomatic magnesites and dolomites of the Veporic unit probably crystallised at increased temperatures compared to those of the Gemeric unit, as indicated by the increased $\delta^{18}O$ values and K/Na ratios. The K–Na ± Ca geothermometry yielded the temperatures between 225 and 340 °C, and frequency histogram shows two maxima at 250 ± 30 and 320 ± 20 °C. The temperatures over 400 °C indicated for some metasomatic dolomites from the Mútnik and Sinec deposits must be considered with caution due to low yield of the crush-leach analyses.

An independent temperature was estimated for the dolomite IIa of the Burda deposit of the Gemeric unit, where isochores of primary CO_2-rich aqueous inclusions with contrasting densities and various CO_2-contents intersected at 232–242 °C and 0.5 kbar (Huraiová *et al.*, 2002). The fluid-inclusion-derived temperatures are somewhat higher than that of 182 °C indicated by the Na-K-Ca geothermometer in this deposit.

Halogen, sulphate and alkali metal ratios in crush-leach analyses of vein-filling dolomite V from the Gemeric unit project close to the field of unmodified seawater (Figs. 8, 9). Oxygen isotope fractionation factor in the dolomite-water system (Friedman & O'Neil, 1977), the $\delta^{18}O$ value of the dolomite V (15.4–20.5‰), and $\delta^{18}O$ value of seawater (0‰) converge at the formation temperature of 110–160 °C, which is consistent with the range of temperatures, 135–170 °C, derived using the K–Na–Ca thermometer.

In summary, formation temperatures of the Carpathian metasomatic Mg carbonates constrained by the K–Na–Ca thermometry, fluid inclusions and stable isotopes fall within the range of 180–280 °C. A high-temperature maximum at 320 °C in the Veporic unit overlaps crystallisation temperatures of the Alpine fissure mineral assemblage in this area (Hurai *et al.*, 1997), and might be thus interpreted as a record of retrograde Alpine (Cretaceous) metamorphic processes. Temperatures between 300 °C and 490 °C inferred using calcite–dolomite thermometer (Radvanec & Prochaska, 2001; Koděra & Radvanec, 2002; Radvanec *et al.*, 2004b, 2004c) and metamorphic mineral assemblages in country rocks (Radvanec *et al.* 2004a) have not been corroborated.

4.2 Temperature–pressure–depth estimates

4.2.1 Hydrothermal vein deposits

Siderite sub-stage. Lack of critical minerals precludes reliable temperature determinations and the existing estimates are controversial. For instance, Iró & Radvanec (1997) and Žák *et al.* (2005) determined temperatures of 300–400 °C in the Nižná Slaná metasomatic siderite–ankerite deposit using the calcite–dolomite thermometer (Powell *et al.*, 1987), and admitted temperatures down to 200 °C for the latest siderite generations. Hurai *et al.* (2002, 2008a) calculated temperatures of 175–230 °C in the Rudňany ore field using phase transitions in halite-oversaturated brines, $\delta^{18}O$ values of siderite, and K/Na thermometers (Fournier & Truesdell, 1974; Verma & Santoyo, 1997).

K/Na ratios in crush-leach analyses of the Gemeric siderite deposits systematically increase from north to south. This can be explained in terms of increase in the formation temperature from ~140 °C in north to ~300 °C in south (Fig. 5). The estimated temperature difference is corroborated also by oxygen isotope ratios in siderites, which decrease in the same manner. The calculated $\delta^{18}O$ values for the equilibrium fluid increase from 4–5‰ in the north-Gemeric veins to 10‰ in the veins from the southern part of the Gemeric unit. The strong ^{18}O-enrichment of all siderite-forming fluids together with the rather uniform fluid composition yield compelling evidence for a rock-buffered hydrothermal system, and rule out infiltration of depleted meteoric and/or marine waters. Hence, it is reasonable to calculate paleodepths using oxygen isotope gradients and isochores of fluid inclusions.

The oxygen isotope gradient of 0.9‰ km^{-1} in the Rožňava-Nadabula ore field in the southern part of the Gemeric unit (Žák *et al.*, 1991) and isochores of 20 wt% NaCl aqueous inclusions with homogenization temperatures between 150 °C and 195 °C from the neighbouring Nižná Slaná deposit con-

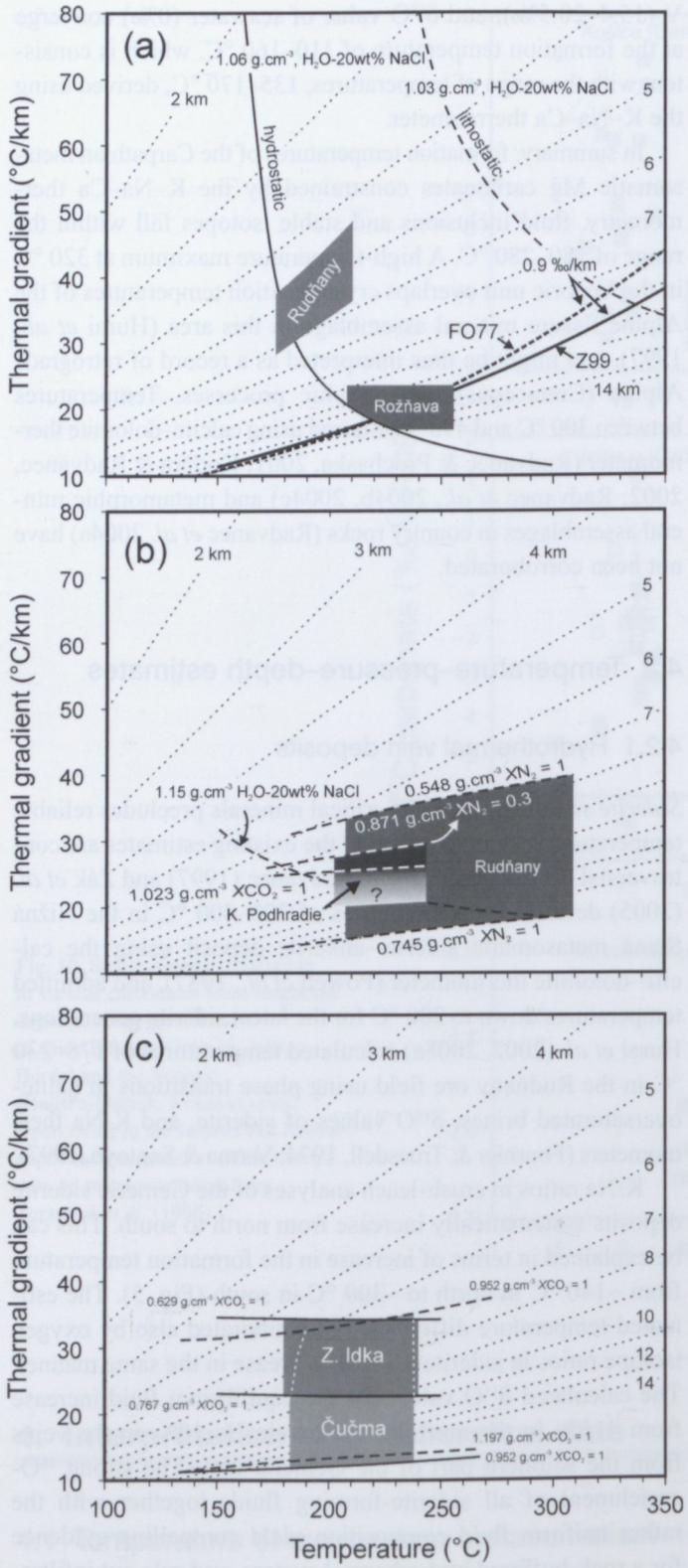

Fig.12. Temperature-depth-thermal gradient estimates for Gemeric hydrothermal veins. **a**) Siderite stage of the Rudňany and Rožňava deposits. Strongly bent curves are isochores of 20 wt% H_2O–NaCl solutions (Gehrig, 1980) calculated for homogenization temperatures (150 °C and 190 °C) of primary aqueous inclusions in siderite, assuming hydrostatic or lithostatic conditions and the respective densities of 1.0 and 2.75 g□cm^{-3}. The curves labelled as FO77 and Z99 correspond to the oxygen isotope iso-gradient of 0.9 ‰.km^{-1} (Žák *et al.*, 1991) recalculated using various equations for the equilibrium oxygen isotope fractionation in the siderite–water system (Friedman & O´Neil, 1977; Zheng, 1999). Solid rectangles correspond to range of thermal gradients and depths adjusted to the range of existing $\delta^{18}O_{sid}$ values and temperatures constrained by cationic exchange thermometers. Data for Rudňany were constrained using the same method for oxygen isotope gradients 1.8-2.3‰□km^{-1} and homogenization temperatures 100–165 °C (Hurai *et al.*, 2008a). **b**) Barite stages of the Rudňany and Krásnohorské Podhradie deposits. Formation conditions are constrained by K/Na thermometer (Verma & Santoyo, 1997), isochores of most dense N_2 (Span *et al.*, 2000), CO_2 and CO_2–N_2 inclusions (Holloway, 1981), and isochore of 20 wt% NaCl–H_2O solution (Gehrig, 1980) recalculated assuming lithostatic conditions. **c**) Quartz-tourmaline (Čučma) and quartz-sphalerite (Zlatá Idka) assemblages of Sb veins. Formation *PT* conditions are constrained by T_h-isochore (Čučma) and halite liquidus-CO_2 isochore (Z. Idka) intersection methods. Isochore for the superdense anhydrous CO_2 gas with the density of 1.197 g□cm^{-3} was calculated using the equation of state proposed by Sterner & Pitzer (1994), other isochores were calculated according to Span & Wagner (1996). Solid curves – hydrostatic load, dashed curves – lithostatic load.

verge at depths between 8.6–12 km (Fig. 12). Formation temperatures 207–255 °C, thermal gradients 19–24 °C□km^{-1} and 11.2 ± 0.6 km paleodepth are the best estimates corresponding to the existing fluid inclusion, leachate chemistry and stable isotope data. Oxygen isotope gradients 1.8–2.3‰□km^{-1}, and homogenization temperatures between 100 and 165 °C converge at a 5.3 ± 1 km depth of burial, formation temperatures 175–210 °C and thermal gradients 38 ± 10 °C□km^{-1} in the Rudňany deposit of the north-Gemeric unit (Fig. 12).

Barite sub-stage. Immiscible gaseous-aqueous fluids provide the opportunity for calculating crystallization *PT* parameters from microthermometric data only. This method is, however, hampered by the impossibility of measuring the temperature of total homogenization due to decrepitation and/or stretching of the inclusions in barite on moderate heating. Moreover, most gaseous inclusions in barite show signs of natural re-equilibration due to internal overpressure. For this reason, only isochores of the densest gaseous inclusions were combined with the K/Na exchange thermometer in order to roughly evaluate formation *PT* conditions. Another *PT* constraint was provided by the existence of primary metastable monophase aqueous inclusions with densities greater than ~1.15 g□cm^{-3} (Hurai *et al.*, 2008a).

Combination of the isochores with cation exchange thermometer yielded temperatures 200–300 °C and pressures 1.7–4.4 kbar for barite from Rudňany, and 200–240 °C, 2–2.4 kbar for that from the Krásnohorské Podhradie-Drnava region. Fluid pressures above 2.4 kbar are needed here to stabilize metastable monophase aqueous inclusions in barite. Minimum depths and maximum thermal gradients defined by the lithostatic load and the average crust density (2.75 g□cm^{-3}) correspond either to 6–14 km and 15–40 °C□km^{-1}, respectively, in north, or 7–12 km and 20–30 °C□km^{-1}, respectively, in the southern part of the Gemeric unit.

Quartz–tourmaline stage. Typical fluid inclusions comprise immiscible carbonic-aqueous mixtures with variable phase ratios at room temperature. High-salinity brines were also occasionally observed. Minimum total homogenization

temperatures (T_h) of the aqueous inclusions in quartz were taken as those approaching actual trapping temperatures. The corresponding pressure was derived using the T_h-isochore intersection method (Roedder & Bodnar, 1980; Mullis, 1987) from isochores of coeval gaseous inclusions.

Only a limited set of microthermometric data exist for the quartz–tourmaline stage of the north-Gemeric siderite veins (Hurai *et al.*, 1998), where maximal CO_2 densities range between 0.93–0.99 g□cm^{-3} and fluid pressures may have reached up to 2.8 kbar, assuming the trapping temperature of ~200 °C. Similar inclusions in quartz from the quartz–tourmaline stage of the south-Gemeric unit exhibited a wide range of CO_2 densities and trapping pressures (1.6–4.5 kbar). This feature is attributed to a crack-seal mechanism and changing litho-hydrostatic fluid regimes (Urban *et al.*, 2006). The corresponding depth of burial and thermal gradient should equal to ~16 km and 12 °C□km^{-1}, respectively.

Quartz–sulphide stage. Brine inclusions are diagnostic of the ankerite–chalcopyrite assemblage of siderite veins near Rudňany (Chovan *et al.*, 1996; Hurai *et al.*, 2002). Prevailing homogeneous trapping is deduced from consistent phase ratios, but the domination of halite in some inclusions was interpreted in terms of episodic entrapment of halite-oversaturated brine. Using a halite liquidus-isochore intersection method, maximal crystallization *PT* conditions of the quartz–ankerite–chalcopyrite assemblage of the Rudňany deposit was estimated to 180 °C and 1–2 kbar (Hurai *et al.*, 2002)

Sphalerite and quartz from the Zlatá Idka stibnite deposit of the eastern part of the Gemeric unit contain heterogeneous carbonic-aqueous inclusions closely spatially associated with brine inclusions with variable salinities and densities. Most brine inclusions homogenize by halite dissolution. Intersection of halite liquidi (31–34 wt% NaCl) with isochores of essentially pure CO_2 inclusions yields trapping *PT* conditions corresponding to 0.6–0.75 kbar and 183–210 °C. Compared to the Čučma stibnite deposit, temperatures at Zlatá Idka are similar, but pressures differ significantly, possibly due to prevailing near-hydrostatic conditions. Assuming the hydrostatic load and the fluid density defined by inclusions, a 5.5–10.5 km paleodepth, and thermal gradients 22–34 °C□km^{-1} can be deduced.

4.2.2 Magnesite deposits

PT conditions and paleodepths pertaining to Mg-metasomatism can only roughly be estimated from fluid inclusions, crush-leach data and geological constraints. Intersections of isochoric envelopes for primary brine inclusions with the temperatures obtained from Na-K-Ca thermometer indicate formation pressures of ~0.2–0.5 kbar at Miková-Jedľovec and Burda deposits in the western Gemeric unit, and ~0.5–1.5 kbar in the central (Gemerská Poloma) and eastern parts (Košice-Medvedia). Pressures cannot be estimated for magnesite deposits of the Veporic unit, because density of primary brine inclusions was modified during post-entrapment re-equilibration.

Homogenization temperatures of CO_2-rich aqueous inclusions that often occur as primary inclusions in Mg carbonates exceed those of the associated brine inclusions and the temperatures derived from the K–Na–Ca geothermometry. This indicates that the closely spatially associated brine and CO_2-rich aqueous inclusions cannot represent coexisting immiscible phases trapped at same *PT* conditions, unless they would be modified after trapping. The CO_2-rich inclusions are interpreted as generally postdating the Mg-metasomatism: this is also supported by fluid inclusion petrography. In some deposits (Burda), the primary CO_2-rich aqueous inclusions in coarse-grained dolomite II are coeval with the apatite-rutile assemblage resembling that in the quartz–tourmaline stage of the Gemeric veins.

The 320–400 °C peak temperature for Alpine metamorphism (Radvanec, 1994; Faryad & Dianiška, 1999) defines maximum possible trapping pressures of the CO_2-rich aqueous fluids, corresponding to 1.6 kbar at Miková-Jedľovec, 2.7 kbar at Košice-Medvedia, and 3.2 kbar at Hnúšťa-Mútnik deposits. It must be noted, however, that the CO_2-rich aqueous inclusions from the Burda deposit show signs of heterogeneous trapping, thus reflecting much lower fluid pressure at around 0.5 kbar (Huraiová *et al.*, 2002). Generally, the variable fluid densities, signs of heterogeneous and homogeneous trapping are compatible with an open hydrothermal system and fluctuating pressures resulting from recurrent hydro- and lithostatic fluid regimes.

4.3 Interpretation of stable isotope data

In spite of large $\delta^{18}O$ difference in the metasomatic Mg carbonates of the Gemeric and Veporic units, isotope compositions of parental fluids remain similar due to the counterbalancing effect of temperature (Fig. 13). The $\delta^{18}O_{fluid}$ values calculated

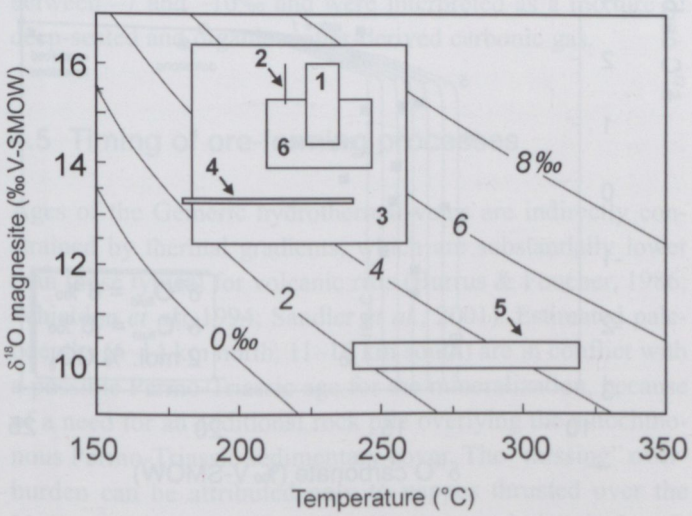

Fig. 13. Oxygen isotope composition of magnesite-precipitating fluids calculated from the fractionation factors in the magnesite–water system (Zheng, 1999) and temperatures derived from the K–Na–Ca geothermometry and stable isotopes (Burda deposit). Numbers correspond to Košice (1), Ochtiná (2), Jelšava (3), Burda (4), Mútnik (5), and Gemerská Poloma (6) deposits.

from the equation for oxygen isotope fractionation in the magnesite–water system (Zheng, 1999) vary between 2 and 8‰, and are about 2‰ lower than those in the siderite-precipitating fluids (Hurai *et al.*, 2008b). Significant differences have not been recorded between the oxygen isotope compositions of fluids precipitating the Mg carbonates in the Carboniferous and Lower Palaeozoic strata of the Gemeric unit.

Qualitatively different stable isotope patterns in the siderite and magnesite deposits were interpreted in different ways. Large variation of oxygen isotopes and almost fixed carbon isotope ratios in the Gemeric siderite veins result from a devolatilization-absent precipitation induced by the increasing temperature. Uniform composition of fluid inclusions and $\delta^{18}O$ values of the siderite-forming fluid controlled by metamorphic grade of country rocks are consistent with a closed, rock-buffered system and a low fluid-rock ratio (Hurai *et al.*, 2002, 2008b).

Stable isotope patterns of Mg carbonates either show larger spread of both $\delta^{18}O$ and $\delta^{13}C$ values, or a restricted range of $\delta^{18}O$ accompanied by variable $\delta^{13}C$, which indicates precipitation due to degassing CO_2-rich fluid. Fixed $\delta^{18}O$ values accompanied with variable $\delta^{13}C$ (*e.g.*, Burda, Košice-Bankov, Lubeník-Turčok, Ochtiná, Kokava, and Hnúšťa-Mútnik) is diagnostic of a low CO_2 content (few mol%) in the aqueous fluid (Fig. 14), which does not match the composition of primary CO_2-rich aqueous inclusions containing up to 30 mol% CO_2.

This discrepancy can be explained either in terms of fluid immiscibility, which produces CO_2- and H_2O-rich conjugate fluid phases at intermediate bulk CO_2 content. Alternatively, a successive replacement of the CO_2-poor brine precipitating the earlier Mg carbonates by the CO_2-rich aqueous fluid during later stages could also occur. The synergic effect of the CO_2-devolatilization, gradually increasing CO_2 contents and variable fluid/rock ratios, potentially accompanied also by influx of isotopically contrasting external fluid, could produce the dispersed C-O isotope patterns typical for the Jelšava deposit. In general, variable salinities and fluid compositions, together with the observed isotopic patterns are compatible with an open hydrothermal system with fluid-rock ratio mostly >5 and possibly various sources of the metasomatising fluids.

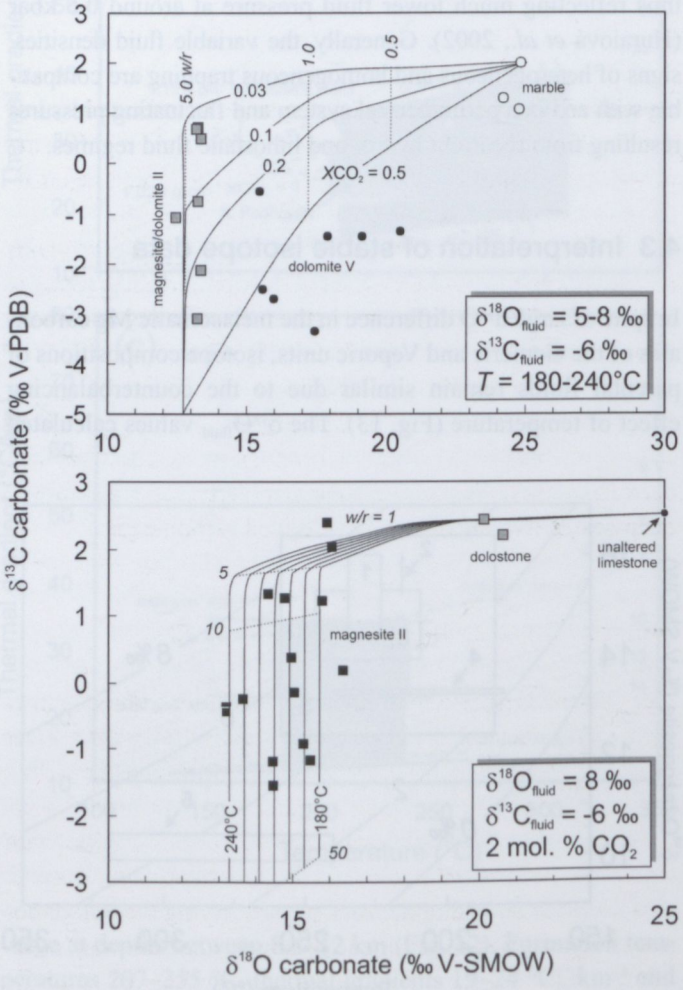

Fig. 14. Alteration model (Zheng & Hoefs, 1993) applied to Burda (top) and Košice-Bankov (bottom) deposits hosted in the Carboniferous rocks of the Gemeric unit. Isotope composition of parent fluid and fluid/rock (*w/r*) ratios were calculated from equations for oxygen isotope fractionation in the H_2O–calcite (O'Neil *et al.*, 1969) and carbon isotope fractionation in the CO_2–calcite (Ohmoto & Rye, 1979) systems.

4.4 Sources of magnesite- and siderite-forming fluids

Halogens and alkali metals are indicators of fluid provenance and nature of the fluid/rock exchange reactions (*e.g.* Fontes & Matray, 1993; Kesler *et al.*, 1996; Chi & Savard, 1997; Gleeson *et al.*, 2001; Heijlen *et al.*, 2001; Banks *et al.*, 2002; Germann *et al.*, 2003 and others). Evaporation of seawater leads to large enrichment of bromine in residual brines (McCaffrey *et al.*, 1987; Fontes & Matray, 1993), and significant Br-enrichment of the Gemeric siderite- and magnesite-forming brines was one of the main arguments for their Permian age.

If projected onto the K/Na–Cl/Br and K/Na–SO_4/Br diagrams, crush-leach data on the Gemeric siderites depart from the recent seawater evaporation trend (SET), exhibiting much greater Br-enrichment than that corresponding to a given K/Na ratio (Fig. 5). The maximum enrichment (Br/Cl molal = 0.007) is equivalent to a 50% water evaporation, and substantially exceeds the saturation limit of ~11% defined by anhydrite precipitation in the Permian–Triassic rift of the Gemeric unit.

Sulphate exhibits large depletions compared to the SET, thus behaving opposite to bromine. The veins hosted in Permian rocks project near the SET, indicating ~15% water evaporation, which is similar to the expected maximum limit in the Gemeric Permo-Triassic basin. Crush-leach data from south-Gemeric siderite veins project close to the SET at 20–40% water evaporation, but strong sulphate depletion rules out a higher degree of the evaporation compared to that in the north-Gemeric basement.

Crush-leach analyses from magnesite and dolomite deviate from the seawater evaporation trend, exhibiting Br-enrichment and SO_4-depletion larger than those in the siderite veins

from the same stratigraphic horizons (Figs. 8, 9). The largest Br-enrichment (Br/Cl molal = 0.038) was detected in scheelite associated with talc. Steatization of the Carpathian magnesite deposits is unequivocally correlated with the Alpine metamorphic overprint (Radvanec *et al.*, 2004b, 2004c), and hence the circulation of the extremely Br-rich brine must be also correlated with Alpine processes.

The maximum Br/Cl molal ratio of 0.018 determined in magnesite leachates substantially exceeds the limit of ~0.01 attained at ~80% seawater evaporation (McCaffrey *et al.*, 1987), when a density-driven gravitational separation of the residual brine from the evaporated salts is no longer possible. Consequently, an additional Br-enrichment process must be superimposed on the Permo-Triassic seawater evaporation.

Large and variable Br-enrichment observed in low-temperature (150–180 °C) siderite veins hosted by anchimetamorphic Permian sediments of the Gemeric unit reveals a low-temperature leaching of organic matter as a significant source of Br enrichment (Hurai *et al.*, 2008b). However, higher temperature crustal processes must be also admitted to account for the additional Br-enrichment observed in the Mg carbonates:

1. Halite separation at crustal PT conditions. Halite may precipitate also in deep crust at elevated temperature. Cationic exchange reactions leading to Ca-increase (*e.g.* dedolomitization, albitisation, anhydrite and calcite dissolution) can enhance this process, because of inhibiting the NaCl solubility in the aqueous solution, and finally causing the halite to precipitate and fractionate. However, entrapment of the NaCl-oversaturated brine has not been proven in fluid inclusions hosted in the Mg carbonates. Accordingly, the hydrothermal halite fractionation is thought to contribute insignificantly to the Br-enrichment of the magnesite-forming fluids only.

2. Dechlorination due to hydration. Brines with high Br/Cl mass ratio (up to 0.03) may originate by hydration reactions at eclogite facies conditions. Relics of seawater stored in subducting slab of oceanic crust can be depleted in chlorine and H_2O during high-temperature, amphibole- and mica-forming hydration reactions (Svensen *et al.*, 1999). It should be noted, however, that the Br/Cl mass ratios in our samples are locally higher, reaching the extreme values as much as 0.048 and 0.085, respectively, in magnesite and scheelite from the Veporic unit.

3. Dechlorination due to HCl degassing. Crustal brines can liberate HCl by $CaCl_2$ hydrolysis in liquid + vapour region (Bischoff *et al.*, 1996). The HCl is preferably partitioned into the vapour phase, thus resulting in Cl-depletion of the conjugate aqueous liquid, if the HCl-rich gaseous phase is continually removed from the system. Addition of CO_2 expands the two-phase immiscibility region of the H_2O–$CaCl_2$ fluids towards higher pressures (Plyasunova & Shmulovich, 1993). Hence, the CO_2 ingression could initiate the $CaCl_2$ hydrolysis, and dechlorination occurs after outgassing the CO_2–HCl–H_2O phase. Although experimental data do not exist to support this mechanism, the magnesite- and scheelite-hosted CO_2-rich aqueous inclusions with variable CO_2 contents, possibly indicating a heterogeneous parent fluid, and stable isotope patterns of Mg carbonates indicating a precipitation assisted by CO_2-degassing, could favour this mechanism.

Several lines of indirect evidences indicate a downward migration of brines infiltrating the Gemeric basement during crystallisation of hydrothermal vein infillling: 1) decreasing $\delta^{18}O_{fluid}$ values towards the centre of the Gemeric cleavage fan during crystallisation of siderite, probably as a consequence of a decreasing fluid/rock ratio with depth; 2) crystallisation of barite in the vein segments subjacent to evaporite-bearing Permo-Triassic series. The infiltrating brines may originally represent the connate water of Permo-Triassic age derived from Gemeric autochthonous cover, or the high-salinity fluid liberated by friction-induced dedolomitisation at the base of Mesozoic nappes (Milovský *et al.*, 2003). Increase in salinity from 17–25 wt% in the early siderite-percipitating brines up to 35 wt% in those crystallising the superimposed mineralizations could reflect the water uptake in metamorphic OH-bearing minerals (*e.g.* Kenis *et al.*, 2005), although the increased salinity reflects a sedimentary precursor – diagenetically modified, anhydrite-fractionated seawater (*cf.* Yardley & Graham, 2002). The modified basinal brine mixed with a low-salinity, CO_2-rich aqueous fluid during episodic vein opening. Sulphides probably crystallized in a permanently open system, as indicated by low density, low-salinity CO_2-rich aqueous inclusions in sphalerite and stibnite. Input of ore elements from deep-seated magmatic intrusions cannot be ruled out at this stage.

CO_2 content in the ore fluids revealed in siderite veins increased with time at the expense of nitrogen, which is assumed to have been derived from ammonium fixed in organic matter of platform sediments and in K-bearing silicates (biotite, plagioclases) of the subjacent Variscan basement (Hurai *et al.*, 2008b). The origin of the carbon dioxide is ambiguous. $\delta^{13}C$ values calculated from isotope composition of siderite varied between –7 and –10‰ and were interpreted as a mixture of deep-seated and organic matter-derived carbonic gas.

4.5 Timing of ore-forming processes

Ages of the Gemeric hydrothermal veins are indirectly constrained by thermal gradients, which are substantially lower than those typical for volcanic rifts (Burrus & Foucher, 1986; Whieldon *et al.*, 1994; Sandler *et al.*, 2001). Estimated paleodepths (6–14 km north, 11–16 km south) are in conflict with a possible Permo-Triassic age for the mineralization, because of a need for an additional rock pile overlying the autochthonous Permo-Triassic sedimentary cover. The "missing" overburden can be attributed only to nappes thrusted over the Variscan basement and its sedimentary cover during the Lower Cretaceous collision.

An Alpine age for the Gemeric hydrothermal mineralization is further indicated by small Fe-carbonate–sulphide veins intersecting Lower Triassic (Werfenian) sediments in the

south-Gemeric unit (Varček & Regásek, 1962). Similar veins penetrate Lower-Middle Triassic limestones (Ivanov, 1953; Halahyjová-Andrusovová, 1964; Antal, 2004) and Jurassic dolomites (Ďuďa, 1976) in the northern part. Fe-carbonate–sulphide veins near Novoveská Huta intersect not only an early Triassic gypsum–anhydrite horizon, but also a remobilized U–Mo mineralization dated at 70–130 Ma using radiogenic isotopes (Rojkovič *et al.*, 1993).

Previous geochronologic studies also corroborated the Alpine age of Gemeric hydrothermal veins. Potassium feldspar from a quartz–stibnite vein near Čučma (Kantor, 1957; Bagdasaryan *et al.*, 1977) and stilpnomelane from the Rožňava siderite deposit (Bagdasaryan *et al.*, 1977) yielded Upper Cretaceous K/Ar ages (68–97 Ma). In contrast, K/Ar ages of fuchsite from siderite veins near Rudňany ranged between 141 and 205 Ma (Bagdasaryan *et al.*, 1977; Cambel *et al.*, 1990). Monazite ages from the Čučma Sb deposit overlap with the 97 Ma K/Ar age for the hydrothermal K-feldspar (Kantor, 1957; Bagdasaryan *et al.*, 1977).

Electron probe chemical U–Pb–Th dating of monazites from Rožňava-Nadabula revealed two maxima, corresponding to 151 ± 3 and 119 ± 3.5 Ma (Hurai & Konečný, in prep.). These data coincide excellently with $^{40}Ar/^{39}Ar$ ages of phengite-muscovite from other siderite veins near Rožňava, as well as with the U–Pb–Th ages of hydrothermal monazites from Čučma. The determined ages cover the whole time interval of orogenic crustal thickening in the southern part of the Gemeric unit. Absence of the Late Jurassic peak in monazite from Čučma and Betliar – Bystrý Potok Sb deposits (Hurai *et al.*, 2008b) supports the hypothesis that the quartz–stibnite veins postdated siderite I – the dominant gangue mineral of siderite–polymetallic ± barite veins.

Distinct geometry, fluid inclusions and stable isotope signature of siderite veins are consistent with the vein opening during the advancing north-vergent thrusting of the Mesozoic nappes accompanied with the formation of arcuate deformation front in the subjacent Gemeric basement (Lexa *et al.*, 2003). Accelerated pressure increase accompanied by attenuated temperature due to low thermal conductivity of rocks resulted in the depression of thermal gradients with time along the prograde *PT* path. This model accounts for the ^{18}O-depletion during growth of siderite crystals (Hurai *et al.*, 2002) and increasing pressures and temperatures during crystallization of early siderite and the superimposed barite in the north-Gemeric unit (Hurai *et al.*, 2008a). The crystallization temperature of barite corresponds to the Alpine metamorphic thermal overprint of Permian molasse (Šucha & Eberl, 1992). Maximum depth of burial (14 km) determined from fluid inclusions in barite near the base of the Permian molasse can be explained by an integrated thicknesses of the autochthonous sedimentary cover and the imbricated Mesozoic accretionary wedge. Decreased fluid pressures and the existence of immiscible carbonic-aqueous fluids during the superimposed quartz–tourmaline and quartz–sulphidic stages reflect opening of the rock-buffered hydrothermal system and reduction of the overburden due to uplift or unroofing.

Crystallization temperatures of the early siderite and barite in the south-Gemeric veins are lower than the temperature of Alpine metamorphic overprint derived from the phengite–chlorite–albite–microcline–grossular assemblage in the subjacent Permian granites (Faryad & Dianiška, 1999). The temperature lag results partly from siderite crystallization during the prograde trajectory prior to peak metamorphic temperature, and partly from the position of the siderite–barite veins at the top, and the granites at the base of the Lower Palaeozoic sequence.

There is also a discrepancy between the formation *PT* conditions of phengite from the quartz–tourmaline stage of stibnite veins (180–240 °C, up to 4.5 kbar), and that derived from the Alpine metamorphic assemblage of the adjacent Permian granites where temperatures 320–350 °C and pressures 4–6 kbar were determined (Faryad & Dianiška, 1999). The relatively narrow range of densities of gaseous inclusions in barite compared to the much larger range in the quartz–tourmaline stage of quartz–stibnite veins probably also reflects different hydrothermal systems, which were possibly closed during the siderite–barite precipitation and open at the onset of quartz–stibnite stage. In this case, the estimated paleodepth (~11 km) during the siderite and barite crystallization reflects the burial along prograde path, and the depth of ~16 km during the quartz–tourmaline stage of the Sb veins corresponds to the retrograde *PT* trajectory. The maximum pressure of ~6 kbar recorded in the Alpine metamorphic assemblage of the Permian granites would correspond to the lithostatic load of ~5 km thick Variscan basement, ~1–2 km thick autochthonous sedimentary cover, and ~15 km thick stack of Mesozoic nappes. Hence, the estimated maximum thickness of the Mesozoic nappe units thrusted over the southern part of the Gemeric basement was quite similar to that in the northern part.

Incompatible *PT* conditions and the different character of the fluids reported from initial stages of the siderite and quartz–stibnite veins reflect vein opening at different depths of a crustal-scale deformation front associated with the rapid elevation of the core of the GCF during the Cretaceous convergence. The syn-tectonic model of hydrothermal vein formation coupled to the Cretaceous deformation requires particular stress conditions, reflecting vertical stress related to thick overburden that acted simultaneously with horizontal compression. In theory, the compressive stress should generate tensional failure parallel to σ_1, *i.e.* perpendicular to cleavage, assuming that the cleavage represents XY plane of instantaneous and finite strain ellipsoids, respectively. Therefore, according to classical stress considerations, one would predict vertical N-S-trending veins perpendicular to the main Cretaceous foliation structure (Price & Cosgrove, 1990). The fact that most Gemeric veins are sub-parallel to the tectonic fabrics along the whole arcuate trend of the Cretaceous deformation front indicates fluid pressure greater than the sum of the tensional strength of the rock and the plane-perpendicular

stress σ_n (Cosgrove, 1997). Consequently, the opening of tensile fractures parallel to the main anisotropy (*i.e.*, the Cretaceous foliation) can be explained in terms of a low differential stress (σ_1–σ_3), corresponding to a small difference between the horizontal tectonic stress and the vertical overburden pressure, and a large difference between tensional strengths T_p–T_n, where T_p is tensional strength parallel to main anisotropy and T_n perpendicular to it. Cosgrove (1997) showed that the tensional failure occurs parallel to main anisotropy in the direction perpendicular to the main compressive stress, if $(T_p–T_n) > (\sigma_1–\sigma_3)$. Therefore, we assume that the veining event in the Gemeric unit occurred within a restricted time interval, with specific stress conditions marked by building of high overburden pressure (vertical load due to thrusting) and strong horizontal stress (horizontal push related to the formation of Cretaceous fabrics). At these conditions, both vertical and horizontal stress components may have achieved similar magnitudes and the high fluid pressure associated with the large difference between tensional strengths may have generated veins parallel to the main compressive cleavage.

The large time span of Cretaceous tectonic activity indicated by radiometric age determinations fits well with fluid inclusion data indicating transition from an open to a closed system in siderite veins, and post-peak formation of quartz–stibnite veins. This indicates that the vein opening was possibly a cyclic process, perhaps related to pore pressure variations rather than due to one massive rupture. Cyclic vein opening is commonly reported from a range of fractured sedimentary basins and basement terrains (*e.g.*, Bahat & Engelder, 1984) indicating pulsed variations of fluid pressure (Hubbert & Rubey, 1959).

One of the two dated hydrothermal micas from siderite veins in the central part of the GCF, as well as the monazite U–Pb–Th ages from Nadabula indicate a Late Jurassic age which cannot be reconciled within the scope of existing tectonic models, because the onset age of the Cretaceous deformation is based on stratigraphic arguments. Additional data on hydrothermal zircon, monazite, and xenotime would be needed to refine the model of Alpine evolution of the Gemeric unit in time and space.

Radiometric age determinations are not available for minerals of magnesite deposits, and traditional succession schemes place crystallisation of magnesite prior to siderite. Varček (1962, 1985) admitted an overlap of the magnesite stage with the earliest siderite in the Gemeric hydrothermal veins. Small siderite veinlets intersect the magnesite lens at Burda, but their stable isotope signature differs from that of the major vein and replacement-type siderite deposits of the Gemeric unit. Isotope composition of the siderite veinlets at Burda show affinity to siderite–fluorite veins found within the Upper Permian–Early Triassic granite at Gemerská Poloma in the Gemeric unit. These veinlets can be correlated with siderite II of the quartz–tourmaline stage. There is no doubt that all Carpathian magnesite deposits have undergone strong Alpine metamorphic overprint (Radvanec *et al.* 2004b, 2004c), which locally resulted in the formation of talc. Therefore, the Mg-metasomatism must have occurred within the time interval between the Lower Carboniferous sedimentation and the onset of Late Jurassic (?) orogenic convergence.

Gravitational infiltration of bittern brines into the Variscan basement from Permo-Triassic riftogeneous marine basins was proposed to explain the origin of metasomatic sparry magnesite in the Eastern Alps and the Western Carpathians (Ebner *et al.*, 1999; Prochaska, 2001). Relatively low fluid pressure estimated from densities of fluid inclusions and crush-leach data in the Carpathian deposits are not in conflict with possible depths of burial (~ 3 km for Lower Carboniferous strata) and the increased thermal gradients (~100 °C/km) during the Permo-Triassic rifting. Stable isotope signatures of the Mg carbonates are also in accord, indicating the high fluid-rock ratio and open-system behaviour (Fig. 14) typical of an extensional tectonic setting.

Homogeneous oxygen isotope composition of the Gemeric Mg carbonates hosted in the Carboniferous and Lower Palaeozoic strata, and the contrasting oxygen isotope composition of the Veporic and Gemeric Mg carbonates, is controversial with the Late Palaeozoic age of the Mg-metasomatism, providing the Lower Palaeozoic sequences in both tectonic units have been emplaced approximately at the same level at these times. On the other hand, in the case of a rift-related origin, the magnesite-forming fluids in the Gemerská Poloma and Henclová deposits must have been largely thermally influenced by the subjacent Upper Permian–Lower Triassic granites either located at a distance of several metres, or directly underlying the Mg carbonate lenses.

The dolomite II from Burda deposit contains primary CO_2-rich aqueous inclusions closely associated with rutile-apatite crystals similar to those revealed in the quartz–tourmaline stage of siderite veins dated at Upper Jurassic times. Stable isotope composition of the dolomite II from Burda overlaps that of magnesites. Hence, it can be hypothesized that the stable isotope pattern (fixed $\delta^{13}C$, variable $\delta^{18}O$) typical of many Carpathian magnesite deposits reflects the Alpine metamorphic-hydrothermal processes. However, it cannot be reconcilled whether the stable isotopes pertain primarily to the Mg-metasomatism, or they just represent an overprint imposed by extensive Late Jurassic–Middle Cretaceous recrystallization. At any rate, the siderite and magnesite deposits of the Western Carpathians cannot be coeval, but they may be partly co-sanguineous in that sense that basinal brines isotopically and chemically modified to various extents during high-temperature interaction with Variscan basement rocks played important role during their formation.

5. Summary

1. Hydrothermal siderite–polymetallic veins of the Western Carpathians have precipitated at temperatures between 150–300 °C from high salinity brines (typically between 15–35 wt% NaCl eq.), and variable admixture of metamorphogenic gaseous components (CO_2, N_2, CH_4).
2. Variable formation temperature of early siderite reflects different position of the veins within the Gemeric cleavage fan – the large tectonic structure created during Alpine orogenic convergence.
3. High Br content and proportions of major ions (Ca, Na, K, Cl, SO_4) in the ore-forming brines suggest marine water modified by evaporation and interactions with crustal rocks at increased temperatures and low fluid/rock ratios.
4. Origin of early hydrothermal stages (siderite, barite, tourmaline) is linked with compressional tectonics and crustal thickenning during the Upper Jurassic–Early Cretaceous compression.
5. Superimposed sulphide stages originated during post-orogenic decompression and transtension taking place during Middle Cretaceous times.
6. Fluid inclusions in metasomatic magnesites also contain high salinity brines with increased Br contents. In addition, low salinity aqueous and carbonic-aqueous fluids are also frequently present.
7. The Br enrichment in magnesite leachates, much larger that that observed in the siderite deposits, cannot be explained in terms of seawater evaporation, and additional mechanisms responsible for the Br enrichment were proposed.
8. Stable isotope signature of the metasomatic magnesite indicates an open hydrothermal system and high fluid/rock ratios, i.e. it is qualitatively different from that preserved in the associated siderite deposits.

Acknowledgements: *Constructive review of F. Molnár and financial support from the VEGA grant 2/0040/08 are gratefully acknowledged.*

6. Field stops

6.1 Field stop 1: Mútnik magnesite–talc deposit, Hnúšťa

(GPS: 48°36'15.87N, 19°57'49.81E, Fig. 1)

The Mútnik magnesite–talc deposit near Hnúšťa discovered in 1870–1872 during the reconstruction of the Tisovec–Hnúšťa railway (Fig. 15) is the oldest magnesite deposit exploited in the Western Carpathians. The deposit belongs to the "northern magnesite belt" extending over the southern margin of the Veporic tectonic unit. Country rocks are represented by Lower Palaeozoic chlorite–sericite schist, biotite- and garnet-mica-schist intercalated with black shale and carbonate, serpentinite bodies, amphibolite and talc schist. Strongly steatized magnesite–dolomite lenses are located near or within Alpine mylonitic shear zones. Fine-grained diagenetic and medium-grained dolomite and magnesite are the most abundant Mg carbonate types. The coarse-grained (sparry) magnesite contains negligible graphite pigmentation and CaO contents are typically below 5 wt% (Kužvart, 1955; Trdlička, 1959; Abonyi, 1971). The association of sulphide minerals comprises chalcopyrite, tetrahedrite, cobaltite, and other accessory sulphides and sulphosalts. Pyrite metacrystals with hexahedral and pentagonal-dodecahedral habits, up to 20 cm in diameter, occurring in talc–magnesite matrix as well as in the surrounding chloritic schists are famous from this locality (Koděra *et al.*, 1986).

The environment in the vicinity of Hnúšťa town has been primarily polluted by mining activity at the Mútnik, Polom and Hačava magnesite deposits, and secondarily by emissions from local chemical factory, magnesite processing and talc grinding plants. Absence of dust-capturing collectors in the processing plants caused extensive devastation of landscape (Fig. 16). In the vicinity of the Mútnik deposit, a coherent vegetation-free crust, several cm thick, extends over the area of several km^2. The crust is composed mainly of highly reactive caustic MgO and periclase. Secondary minerals are represented by brucite, hydromagnesite, nesquehonite and hydrocalcite, which recrystallize to calcite and dolomite causing the stony and resistant properties of the crust (Bobro & Hančuľák, 2001). Recently, after ceasing the mining activity, the crust gradually disintegrates and the environment slowly recovers.

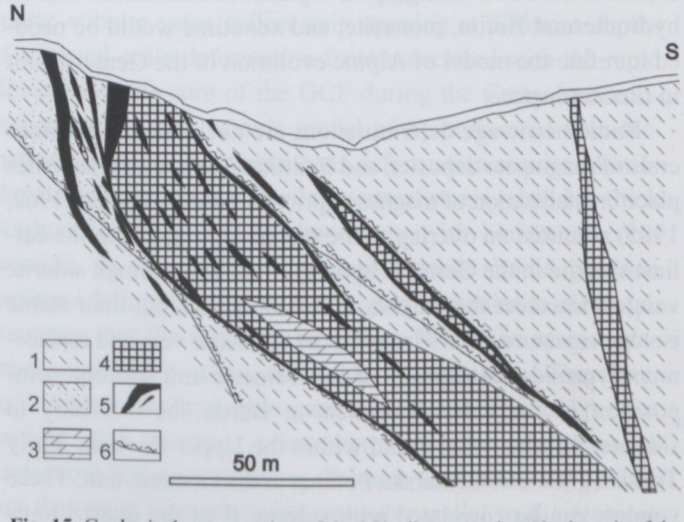

Fig. 15. Geological cross-section of the Mútnik magnesite-talc deposit of the Veporic unit (Suchár, 1960).

Legend: 1 – sericite and chlorite schists, 2 – talc schists, 3 – dolomite, 4 – magnesite, 5 – talc, 6 – mylonitic shear zone.

Fig. 16. Recent landscape in the vicinity of the Mútnik magnesite-talc deposit with dumps at frontside and vegetation-free encrusted hill at horizon.

6.2 Field stop 2: The largest magnesite deposit of Slovakia, Jelšava

(GPS: 48°38'39.05N, 20°13'30.01E, Fig. 1)

The largest magnesite deposit of Slovakia occurs north-east of Jelšava town. According to calculated reserves, the deposit ranks among the largest magnesite deposits in the world with lifetime of about 100 years at present level of exploitation (Cicmanová, 2002). The deposit crops out in three different parts – Dúbrava Massif (Fig. 17), Miková, Jedľovec – which merge at depth to one coherent body. The deposit belongs to the so-called "southern magnesite belt" extending from Podrečany in the east to Bankov near Košice in the west (Koděra *et al.*, 1986). The southern magnesite belt is arranged along the paleo-Alpine thrust boundary of the Gemeric over the Veporic units. Most important deposits are hosted in the Upper Turnaisian–Viséan (Planderová, 1982; Bajaník & Planderová, 1985) Hrádok Formation, and the Upper Viséan–Serpukhovian (Kozur *et al.*, 1976)

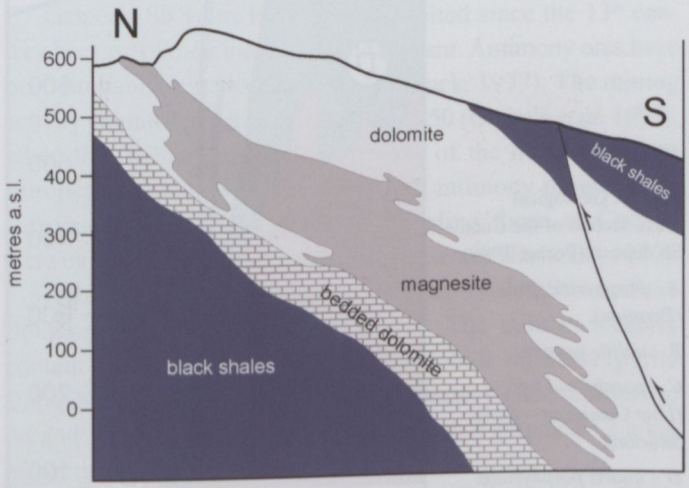

Fig. 17. Geological cross-section of the Jelšava – Dúbrava Massif magnesite deposit (Čapo *et al.*, 1992).

Ľubeník Formation. The deposits are lens-shaped or form layers interlaced with relics of metasomatic dolomite and emplaced in fine-grained dolomite. Country rocks are composed mostly of black shale, sericite–graphite- and talc–chlorite schists (Abonyi & Abonyiová, 1981).

Mining started in open pit operations, and later continued by underground mining using initially the rooming and later the flat-back methods. At present, active mining occurs at the 10th horizon (320 m altitude). Undermining has caused large inbreaks and accidental falls of terrain, some with catastrophic character (in 1992). Large abandoned open rooms are still present at Miková. The recently preferred flat-back mining is expected to cause only minimum deformation of the hanging wall units (Cicmanová, 2002).

Magnesite has been continuously exploited and processed here since 1895 (Bobro & Hančulák, 2001) and this area belongs to the most polluted and damaged regions of Slovakia. In 1970s, the extent of the polluted area was 32 km^2 (Leško & Bobro, 1987). Installed dust-capturing filters were ineffective, and this caused devastation of vegetation and formation of crust deposited on strongly alkalised (pH 8–9.5) soils. Forest stand was totally removed or petrified due to crystallisation of calcite and dolomite from Ca-Mg hydrates. A crust composed of Mg-salts from dust outlets has formed in close vicinity of two magnesite processing plants, now operating a total of 10 rotary and shaft furnaces. It is assumed that the Mg-rich crust forms during the annual dust fall-out exceeding 600 tkm^{-2} (Bobro & Hančuľák, 2001). Recently, the formation of crust is stopped thanks to the implementation of more effective dust collectors. The average annual emission of solid dust particles in the Jelšava – Lubeník area declined from 4800 t in 1970s to recent values corresponding to 85–170 t (Hančuľák, 2000).

All groundwaters and mine drainage waters were used for magnesite processing in the neighbouring plants. Waste waters are discharged into setting pit, existing since 1968. Surface waters are polluted by NO_2, NO_3, NH_4 and metals (Pb, Zn, Hg, Sb, Fe, Mn), but a significant groundwater pollution directly related to magnesite mining has not been proved (Cicmanová, 2002).

6.3 Field stop 3: Aragonite cave, Ochtiná

(GPS: 48°39'52.15N, 20°18'32.40E, Fig. 1)

A unique cave (UNESCO world heritage site) was discovered 2-km northwest of Ochtiná in 1954, when driving a geologic exploratory gallery. The Ochtiná Aragonite Cave is a 300-m long cryptokarstic irregular labyrinth controlled by three parallel NNE–SSW-oriented faults. The cave is hosted by Early Palaeozoic (Early Devonian–Upper Silurian) metalimestone, partly metasomatically altered to ankerite and siderite. Oxygen-enriched meteoric water seeping along the faults caused siderite/ankerite weathering and transformation to ochres that were later removed by mechanical erosion. Corrosion was enhanced by sulphide weathering and by carbon dioxide released from

Fig. 18. Acicular aragonite crystals, about 10 cm long, grown on Palaeozoic limestones in the Ochtiná Aragonite cave (courtesy of M. Orvošová).

decomposition of siderite/ankerite. The initial phreatic speleogens, older than 780 ka, were created by dissolution in density-derived convectional circulation conditions of very slow flow. Thermohaline convection cells operating in the flooded cave probably also influenced its morphology. Later vadose corrosional events have altered the original form. Water levels have fluctuated many times as the cave was filled up during wet periods and then it was slowly drained. Mn-rich loams with Ni-bearing asbolane and birnessite formed by microbial precipitation in the ponds remaining after the floods. Allophane was produced in the acidic environment of sulphide weathering. A La-Nd phosphate and a REE-enriched Mn oxide precipitated along geochemical barriers in the asbolane layers. The oldest aragonite generation is preserved as corroded relics in ceiling niches truncated by corrosional bevels. TIMS and α-counting U-series dating have yielded ages of about 500–450 and 138–121 ka, indicating several episodes of deposition coincidental with Quaternary warm periods (Elsterian 1/2, Eemian). Spiral and acicular aragonite (Fig. 18) representing second generation began to have been deposited in Late Glacial (14 ka – Alleröd) times. Deposition of the youngest frostwork aragonite still continues nowadays. Both younger aragonite generations have similar isotopic compositions, thus indicating formation conditions very similar, or identical, to those found at present days (Bosák *et al.*, 2002).

6.4 Field stop 4: Abandoned stibnite deposits, Čučma

(GPS: 48°42'58.15N, 20°33'27.24E, Fig. 1)

The stibnite-bearing veins near Čučma are hosted in mylonitic shear zones and overthrust faults of NW-SE direction. They have been developed in porphyroids and quartz porphyry tuffs of the Gelnica Group metamorphosed at greenschist facies (Fig. 19). A total of four mineralization stages have been distinguished here: 1) quartz (± pyrite, tourmaline), 2) Fe-dolomite, 3) quartz–sulphide (with the sub-stages: a – chalcopyrite, tetrahedrite, bournonite, b – galena, boulangerite, c – stibnite, jamesonite, berthierite), 4) calcite (Beňka & Caňo, 1992). An example of the vein infilling (Fig. 20a) shows brecciaed texture with the quartz–stibnite assemblage superimposed on a quartz–tourmaline–muscovite assemblage. Isolated grains of accessory monazite, xenotime, titanite, apatite, zircon and rutile occur either in the muscovite nests, or as individual inclusions in dravite tourmaline (Fig. 20b).

CO_2 inclusions with density of up to 1197 kg□m^{-3} occur in the quartz associated with stibnite and tourmaline. Such high-density gases have been previously known only in upper mantle xenoliths and granulites. Raman microanalysis corroborated CO_2 as dominant gas species accompanied by small amounts of nitrogen (< 7.3 mol%), and methane (< 2.5 mol%). The superdense CO_2 phase exsolved from an aqueous bulk fluid at temperatures of 183–237 °C and pressures between 1.6 and 3.5 kbar, possibly up to 4.5 kbar. Low thermal gradients (~12–13 °C/km) and the CO_2–CH_4–N_2 fluid composition rule out a genetic link with the subjacent Permian granites, as proposed by previous metallogenetic models. The quartz–tourmaline stage and the associated Ti-Zr-Y-REE-P-bearing minerals should be regarded as an Alpine-type metamorphogenic assemblage, rather than representing high temperature magmatogenic phases genetically linked with granitic intrusions. Apparently immobile Zr and REE were transported in high salinity basinal brines (Hurai *et al.* 2002) infiltrating and leaching the Variscan basement and the F-, B-, and P-rich Permian granites. Vein opening, pressure release and influx of externally derived CO_2 have caused destabilization of the halogen complexes and crystallization of zircon, Y-REE phosphates and (U)Ti oxides/silicates.

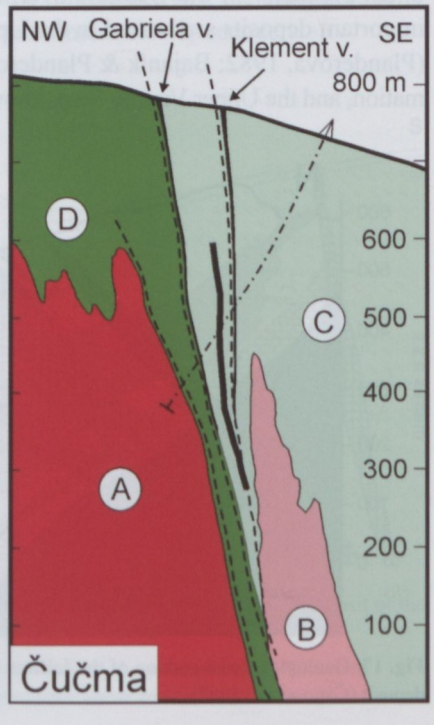

Fig. 19. Geological cross-section of the Čučma Sb deposit (Pecho, 1980):
A – porphyritic granite (Permian),
B – aplitic granite,
C – porphyroid tuffs (Late Cambrian – Early Silurian),
D – quartz porphyroids (Late Cambrian–Early Silurian).

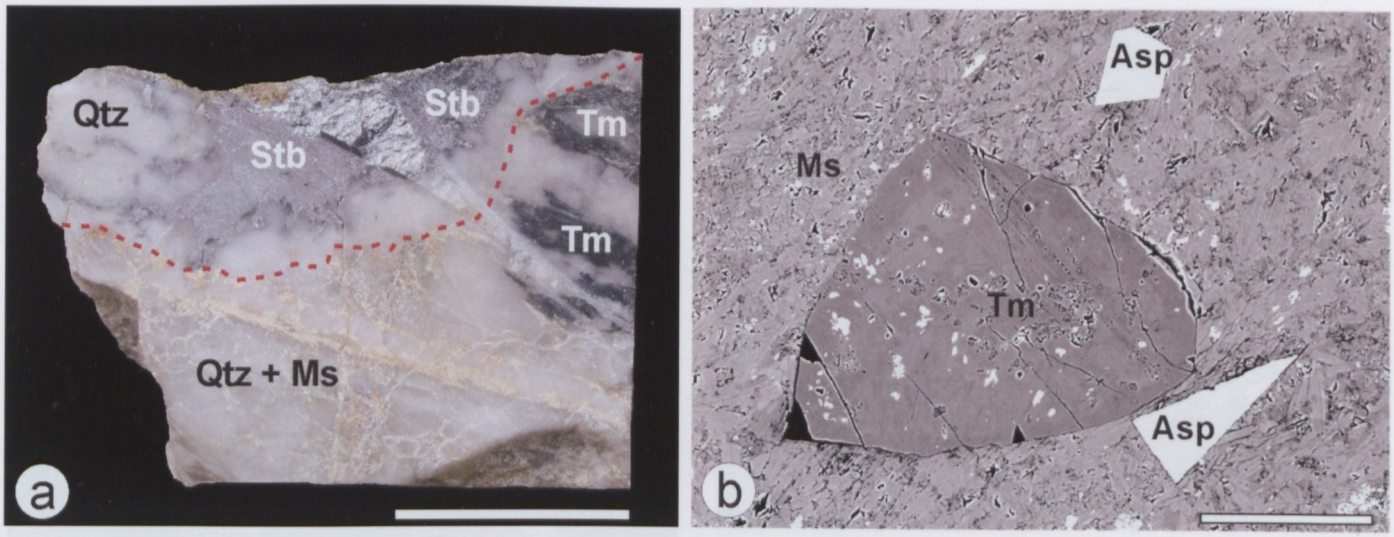

Fig. 20. Example of mineral infilling of the Klement vein near Čučma. a) Quartz–stibnite assemblage is in upper part, and quartz–tourmaline (Tm)–muscovite (Ms) assemblage in the lower portion of the sample. White bar corresponds to 5 cm. b) Back-scattered electron image of muscovite nest from the lower portion of the sample displayed in a). Shown are euhedral crystals of tourmaline (Tm) and arsenopyrite (Asp) enclosed in the muscovite (Ms) matrix. Bright dots in the tourmaline crystal and the muscovite matrix are accessory monazite, xenotime, rutile and titanite. White bar corresponds to 100 μm.

U–Pb–Th age of monazite from the quartz–tourmaline assemblage (Fig. 21) overlaps final stages of the compression coincidental with the thrusting of the Gemeric unit over the Veporic unit, which probably occurred during Lower Cretaceous (Plašienka, 2002; Lexa *et al.*, 2003; Schulmann *et al.*, 2005). The younger age overlaps the formation of transpressional trans-Gemeric shear zone dated at 85–75 Ma (Schulmann *et al.*, 2005). Our data indicate a near-isobaric cooling of the southern Gemeric unit from the peak Alpine metamorphic conditions (320–350 °C and 4–6 kbar) estimated from the newly-formed K-feldspar-muscovite-garnet-plagioclase assemblage in the Permian granites (Faryad & Dianiška, 1999) to ~240 °C and 4.5 kbar during the onset of the stibnite vein opening. The estimated depth of burial (15–18 km) reflects the integrative thicknesses of the Gemeric basement (~5 km), autochthonous Permo-Triassic cover (~2 km), and a 8–11 km thick pile of Permian–Jurassic nappes of the Meliatic accretionary complex, whose remnants are now preserved in the southern periphery of the Gemeric unit.

Gemeric Sb veins have been exploited since the 13th century because of their increased gold content. Antimony ores have been probably mined since 1696 (Beránek, 1977). The mining activity culminated between 1830 and 1850 (Grecula *et al.* 1995), when the Čučma deposit became one of the most important European producers of antimony. The antimony mines in the surroundings of Rožňava town, including those at Čučma, were closed in 1952 due to exhausted reserves (Beránek, 1977).

Antimony ore at Čučma was dressed by flotation and the flotation waste was stored in tailings. The tailings recently contain a relatively large amount of sulphide minerals (pyrite and stibnite) and their weathering products. Concentrations of As and Sb in the tailings material are up to 1 g/kg and 12 g/kg, respectively.

Oxidation zone of the tailings with the secondary Fe/Sb oxides and oxihydroxides reaches the depth of 2–3 meters.

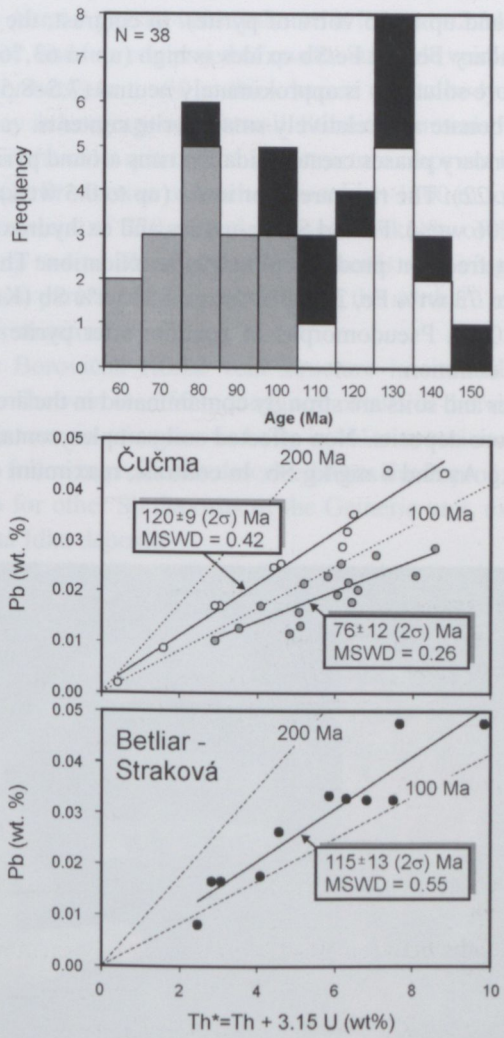

Fig. 21. Histogram of U-Th-Pb ages and monazite isochrons for the quartz–tourmaline–muscovite–phosphate–zircon–rutile–U(Th)oxide–titanite assemblage of the quartz–stibnite veins of the Čučma and Betliar-Straková deposits. Bar shadings in the frequency histogram correspond to those of symbols in the accompanied isochron diagrams (Hurai *et al.*, 2008b).

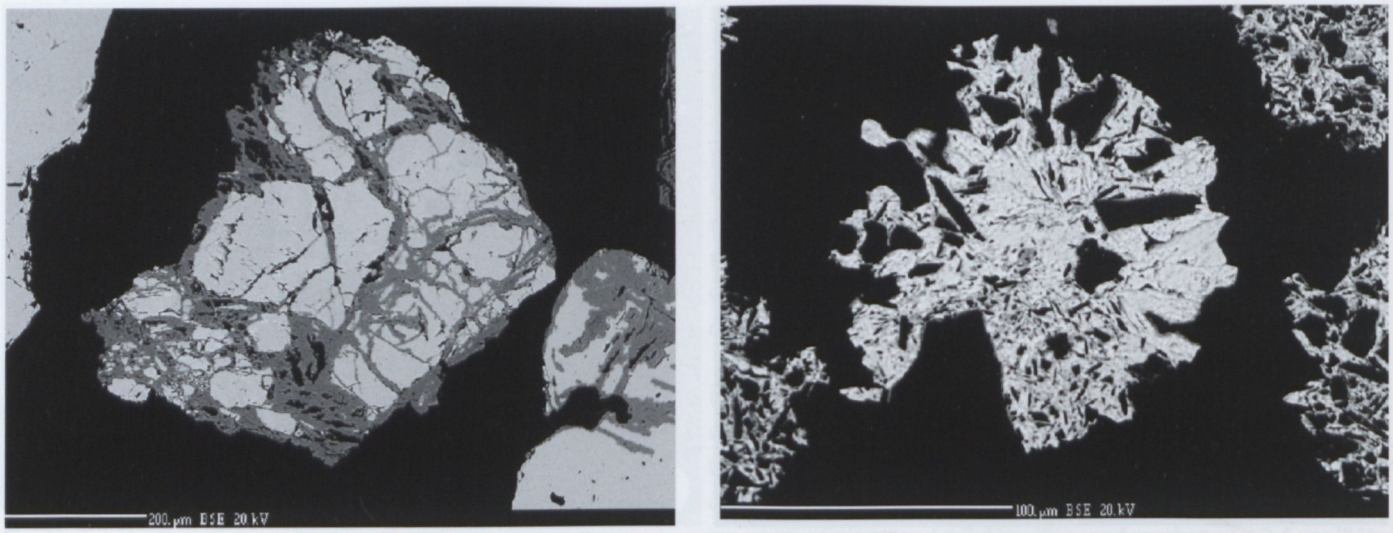

Fig. 22. Back-scattered electron images of minerals from tailing materials at Čučma. *Left*: Oxidation rim around pyrite crystal. *Right*: Secondary Sb oxide.

Content of primary sulphide minerals in heavy fraction of tailing's material (from oxidation zone) is low (up to 0.5 vol% of stibnite and up to 36 vol% of pyrite). In contrast, the content of secondary Fe and Fe/Sb oxides is high (up to 63.76 vol%). *p*H of pore solutions is approximately neutral (7.5–8.5) due to high carbonate and relatively small pyrite contents.

Secondary phases create oxidation rims around pyrite crystals (Fig. 22). The rims are poor in As (up to 0.5 wt%) and Sb (up to 0.06 wt%). Fe and Sb/Fe-oxides and oxihydroxides are the most frequent products of sulphide oxidation. They contain up to 73 wt% Fe, 2.5 wt% As, and 83 wt% Sb (Kučerová *et al.*, 2009). Pseudomorphs of goethite after pyrite crystals are also common.

Water and soils are strongly contaminated in the area of the Čučma ore deposits. Non-affected soil samples contain up to 30 mg/kg As and 6 mg/kg Sb. In contrast, maximum concentrations of these elements in contaminated soils attain 190 and 512 mg/kg, respectively. Fe-ochres are precipitating from water outflows from tailing impoundments (Fig. 23). These sediments contain up to 34 g/kg As and 8 g/kg Sb bound mainly in ferrihydrite (Lalinská *et al.*, 2009).

Fig. 23. Iron ochre (mainly ferrihydrite) precipitating from water outflows from tailing impoundment near Čučma.

6.5 Field stop 5: Stratiform manganese carbonate mineralization, Čučma

(GPS: 48°42'38.94N, 20°33'15.49E, Fig. 1)

A stratiform manganese deposit occurs 2 km NNE of Čučma village as small lenses embedded within Early Paleozoic black shale and lydite enriched in organic matter. Lenses of the manganese ore are 50–100 m long and up to 4 m thick (Fig. 24). The deposit was opened in 19th century by a small quarry and two short adits, and abandoned at the beginning of 20th century.

Several thousands metric tons of oxidized manganese ores with around 55% Mn, 11% Fe, 2.5% SiO_2 and 1% CaO were exploited from the deposit. Primary carbonate-silicate ores contain 34% Mn, 6% Fe, 39% SiO_2 and 5% CaO (Maderspach, 1880; Papp, 1919).

Based on detailed mineralogical study, the following mineral assemblages were distinguished (Rojkovič, 2001):

1) Rhodonite, rhodochrosite, tephroite, spessartite, anthophyllite, pyroxmangite, magnetite, pyrophanite, muscovite, manganpyrosmalite, albite, rutile, allanite-(Ce), and quartz are metamorphic minerals formed during reworking of sedimentary-diagenetic Mn-rich carbonate and oxide ores.
2) Hydrothermal minerals are represented by Mn-calcite, disseminated pyrite, pentlandite, sphalerite, chalcopyrite, pyrrhotite, cobaltite, ullmannite, galena, chamosite, bementite, and quartz.
3) Supergene assemblage consists of todorokite, pyrolusite, cryptomelane, goethite and "limonite".

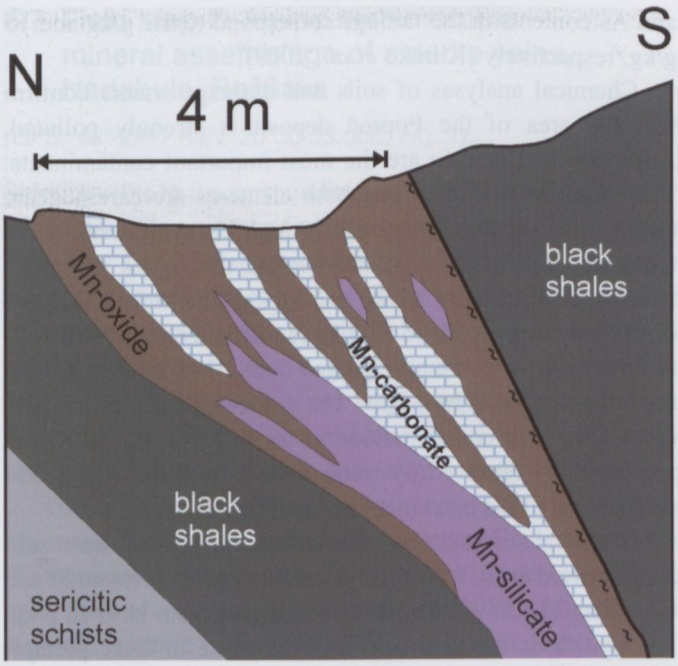

Fig. 24. Geological cross-section of the Čučma Mn-deposit (Slávik, 1967).

The Mn-rich carbonate-silicate ores from Čučma belong to queluzite – a metamorphic rock typical of Mn carbonates and presence of tephroite, and devoid of Mn oxides (Roy, 1992). During sedimentation, Mn was transported from deep anoxic parts of ocean to margins of black shale facies, where mixing with shallower oxygen-bearing water occurred. As a consequence, Mn oxides/hydroxides precipitated as primary Mn-rich minerals. Mn carbonates formed from pore water by MnO_2 reduction during the diagenetic stage. Primary calcite was replaced by rhodochrosite in the same way as described from Eocene Mn-deposits of Black Sea (Öztürk & Frakes, 1995). Mn silicates (rhodonite, pyroxmangite, anthophyllite), pyrophanite and magnetite originated during Variscan and Alpine regional metamorphism. Rhodonite-pyroxmangite geothermometer yielded 375 °C (Faryad, 1991) and 390 °C (Rojkovič *et al.*, 1995). PTX_{CO2} parameters, 400–420 °C at 3.5 kbar and X_{CO2} = 0.05–0.06, were attributed to regional metamorphism (Faryad, 1994).

The metamorphic minerals are enclosed and cut by hydrothermal veinlets with pyrite, chalcopyrite and pyrrhotite. Presence of these minerals may reflect adsorption of Ni and Cu in the former sedimentary-diagenetic mineral assemblages, and their later hydrothermal mobilization at favourable conditions. Metamorphosed silicate-carbonate rocks were later replaced by Mn oxides and hydroxides (mainly todorokite and pyrolusite) during supergene processes in the oxidation zone.

6.6 Field stop 6: Abandoned stibnite deposit, Poproč

(GPS: 48°43'51.40N, 20°58'59.67E, Fig. 1)

Quartz–stibnite veins near Poproč form the western continuation of the stibnite-ore productive belt extending from the surroundings of Rožňava. Underground mining activity ceased here in 1965 due to exhausted reserves (Beránek, 1977).

The Anna-Agneška vein structure is located ~2.5 km north of Poproč, and it is composed of quartz–sulphide veinlets along boundary between a ~30 m thick barren quartz body and tectonic clay in hanging and footwall. Stibnite forms also impregnations in the older quartz. The vein structure crops out in a 2 km long zone. Productive ore-rich segment is ~1300 m long, with vertical extent of 220 m and average thickness of 1.5–2 m, locally up to 4 m. The distribution of ores is very irregular and the richest parts are concentrated along the northern margin of the vein structure.

The Borovičná Hôrka vein structure is situated east of Poproč. The vein is ~250 m long, and occurs in the vicinity of southern margin of a granitic body in chlorite-sericite schist.

The following minerals described from the Poproč are typical also for other Sb deposits of the Gemeric unit, except for the Zlatá Idka deposit:

Fig. 25. Collar of Anna-Agnes adit at Poproč prior to and after remediation.

Stibnite (Sb_2S_3) is the dominant ore mineral, which almost alwas occurs together with quartz. Stibnite is older than the associated berthierite.

Berthierite ($FeSb_2S_4$) is the most common sulphosalt. It forms tiny veinlets in quartz and associates with stibnite and jamesonite.

Jamesonite ($Pb_4FeSb_6S_{14}$) is ubiquitous, but does not occur in large quantities. Most commonly it forms tiny, up to 2 μm large inclusions in berthierite and stibnite, and larger aggregates in quartz.

Zinckenite ($Pb_9Sb_{22}S_{42}$) and *fülöppite* ($Pb_3Sb_8S_{15}$) occur in quartz together with chalcostibite.

Chalcostibite ($CuSbS_2$) forms tiny needles and aggregates together with zinckenite and fülöppite, which are somewhat younger.

Unidentified Sb oxide forms very rare subhedral grains in berthierite and quartz.

Sphalerite (ZnS) is a very rare mineral creating tiny grains in quartz, pyrite and stibnite.

Pyrite (FeS_2) forms relatively rare inclusions in quartz and stibnite, and it is more frequent in massive aggregates and intergrowths with arsenopyrite.

The following mineral parageneses and successions can be deduced from spatial relationships: quartz–pyrite–arsenopyrite → sphalerite → quartz, stibnite, berthierite, Sb oxide, jamesonite → chalcostibite, zinckenite, fülöppite.

The Sb ores from Poproč were processed using flotation. A total of 31,500 m^3 of waste sediments was stored in three tailings (Kaličiaková *et al.*, 1996). Ore minerals in the tailings are rare due to massive oxidation, resulting in highly acidic drainage waters with pH ~3. Sb is preferentially incorporated in Fe oxides/oxihydroxides containing up to 69 wt% Sb and 2.1 wt% As. "Pure" Sb and Sb/Fe minerals similar to stibiconite and tripuhyite are subordinately formed. Maximum Sb and As contents in the tailings correspond to 4.7 g/kg and 15 g/kg, respectively (Klimko *et al.*, 2009).

Chemical analyses of soils and drainage waters confirm that the area of the Poproč deposit is strongly polluted. Antimony and arsenic are the most important contaminants. Their toxicity is similar and both elements are carcinogenic (Uexküll *et al.*, 2005). Extremely high concentrations of Sb were recorded in the area surrounding the Agnes adit, with values ranging from 4.7 g/kg to 10 g/kg. The highest As concentration corresponds to 57 g/kg (Jankulár *et al.*, 2008). A 2-m thick layer of ochre precipitated over a 200-m^2 area around the collar of the Agnes adit. The ochre deposits, potentially containing high concentrations of toxic elements, have been mechanically removed by water outlets from the Agnes adit discharging in the catchment of the Olšava River.

Chemical analyses of ochres collected from the Agnes adit and dissolved in HCl show increased As contents between 52 and 60.4 g/kg. The Sb content is lower, ranging from 11 to 12 g/kg. Ferrihydrite is the dominant mineral phase in these precipitates, whereas more stable goethite is present in minor amount (Lalinská *et al.*, 2009).

Stream sediments of the Olšava River also contain high concentrations of toxic elements due to constant influx of the ochreous sediments from the Agnes adit. Sb contents vary from 215 to 1360 mg/kg. Average As content corresponds to 1.1 g/kg, with a maximum at 5.5 g/kg (Šottník & Jurkovič, 2009).

Analogously to arsenic, antimony has an ability to create bonds with plant tissues, thus being a phytotoxic element (Foy *et al.*, 1978). Considering that the often described mobility of these elements is likely controlled by Fe, Mn oxides and pH, their biosorption or biovolatilization in organisms is important. High concentrations of As and Sb (46 and 2 mg□kg^{-1}, respectively) were detected in some plants (e.g. *Equisetum palustre*) near Agnes adit (Jankulár *et al.*, 2008).

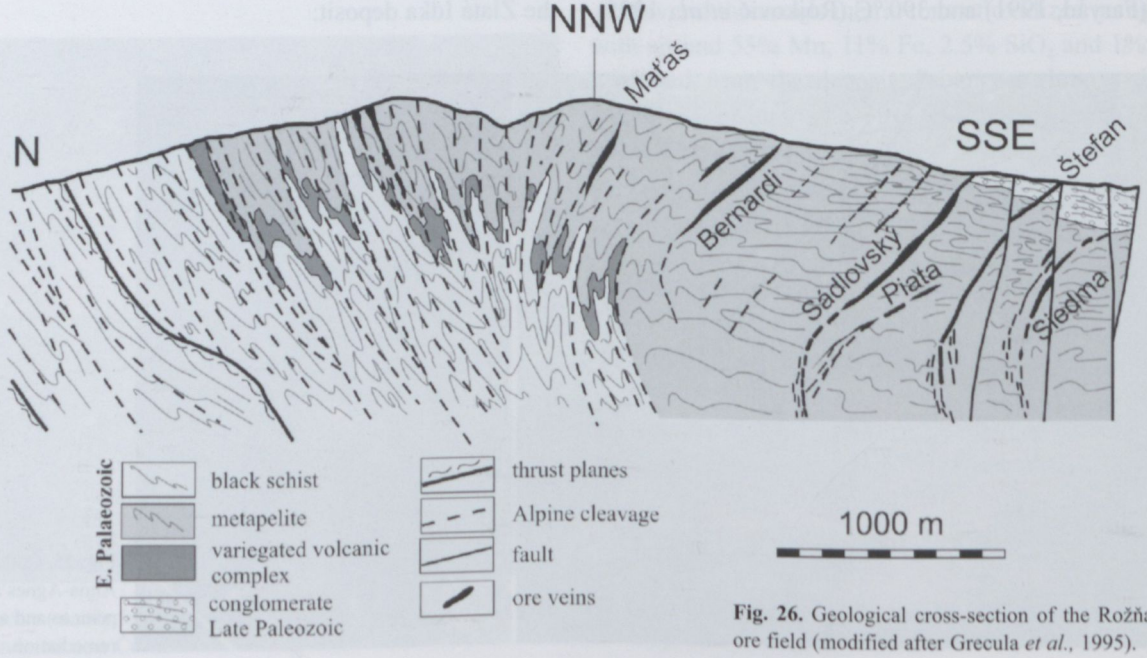

Fig. 26. Geological cross-section of the Rožňava-Nadabula ore field (modified after Grecula *et al.*, 1995).

6.7 Field stop 7: Alpine metamorphic mineral assemblage of siderite veins, Nadabula, Rožňava

(GPS: 48°40'17.84N, 20°30'53.56E, Fig. 1)

Siderite veins in the surroundings of Rožňava town are located in the axial part of the Gemeric cleavage fan. The veins are hosted by Early Palaeozoic variegated volcanic-sedimentary complex of the Gelnica Group, and their upper parts terminate in Permian conglomerates (Fig. 26). Some vein segments penetrating porphyroids contain large volumes of albite, which is locally together with siderite major gangue mineral (*e.g.* Bernardi vein). Occurrence of albite in the veins is directly correlated with extensive albitisation of country rocks.

The albite was interpreted as aplite vein (Ulrich, 1928), as magmatic differentiate genetically related to Gemeric granites (Kamenický & Kamenický, 1955) or as a regular member of hydrothermal vein paragenesis (Varček, 1955). Microscopic view of the albite gangue (Fig. 27) reveals variegated association of accompanying minerals: zircon, xenotime, schorl-dravite, apatite, rutile, monazite, and siderite II, all postdating siderite I. The mineral association resembles that demonstrated in the stibnite veins near Čučma.

Low thermal gradient typical of a thick continental crust was inferred from isotope composition of early siderite of the Nadabula deposit and densities of fluid inclusions in the Nižná Slaná metasomatic (replacement-type) siderite deposit. A vertical oxygen isotope gradient of 0.9‰ km^{-1} at Nadabula (Žák *et al.*, 1991) and isochores of 20 wt% NaCl aqueous inclusions converge at depths between 8.6–12 km. Formation temperatures 210–260 °C, thermal gradients 19–24 °C□km^{-1} and an 11.2 ± 0.6 km paleodepth are the best parameters adjusted to the existing fluid inclusion and stable isotope data from the vein and metasomatic siderite deposits near Rožňava (Hurai *et al.*, 2008b). The obtained data are consistent with the models suggesting vein formation during crustal thickening triggered by Late Jurassic–Early Cretaceous orogenic convergence.

6.8 Field stop 8: Open pit exploitation of the largest hydrothermal vein of Slovakia, Poráč, Rudňany

(GPS: 48°52'49.27N, 20°43'02.85E, Fig. 1)

The Rudňany ore field is located in the northern part of the Gemeric unit. A total of 10 siderite veins were recognized here. The thickest vein segments occur in Carboniferous black schist and metabasalt, and they fade out at depths of 900–1100 m within Early Paleozoic chlorite-sericite schist. The upper vein segments terminate within anchimetamorphic Early Permian conglomerates. The Droždiak vein, with a length of 7 km and a maximum thickness of 40 m, is the largest of the hydrothermal veins of the Western Carpathians, and one of the largest carbonate veins worldwide (Fig. 28). A 1 km long E–W-oriented exposure of the Droždiak vein is discernible south of the Poráč village on satellite images. One of abandoned open pits along the vein is displayed in Fig. 29.

Mineral succession in the Rudňany ore field, comprising fuchsite, siderite–barite, quartz–tourmaline, quartz–Cu sulphide and cinnabar stages, is similar to that in other siderite veins deposits of the Gemeric unit. Up to 15 m-thick monomineralic barite accumulations with unique up to 1 m long and 25 cm wide barite megacrystals embedded in siderite matrix occur in the uppermost parts of the Droždiak vein. Nice samples with up to 10-cm long barite megacrystals can be still found in abandoned open pits south of the Poráč village.

Various fluid inclusions were observed in the siderite–barite intergrowths. Primary two-phase aqueous inclusions in siderite

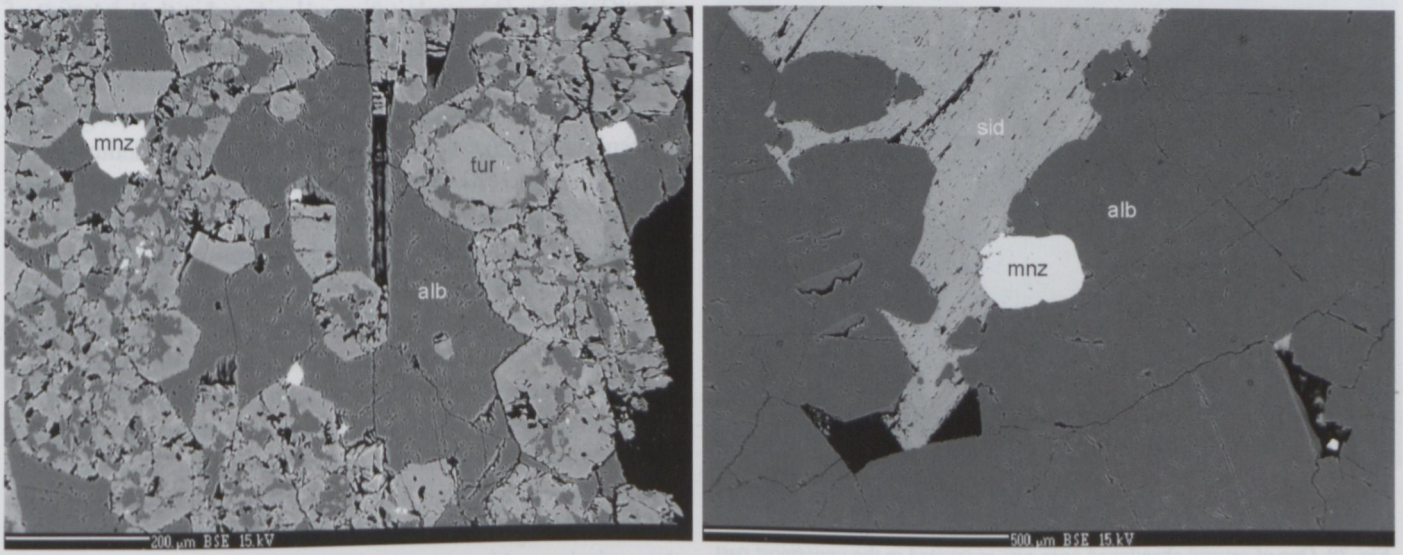

Fig. 27. Back-scattered electron images of albite-siderite vein infilling from Nadabula, showing (left photo) euhedral schorl–dravite (tur) with tiny rutile inclusions (bright) and larger monazite grains (mnz) in albite (alb) matrix. Right photomicrograph documents a large monazite crystal attached to siderite I metasomatically replaced by albite.

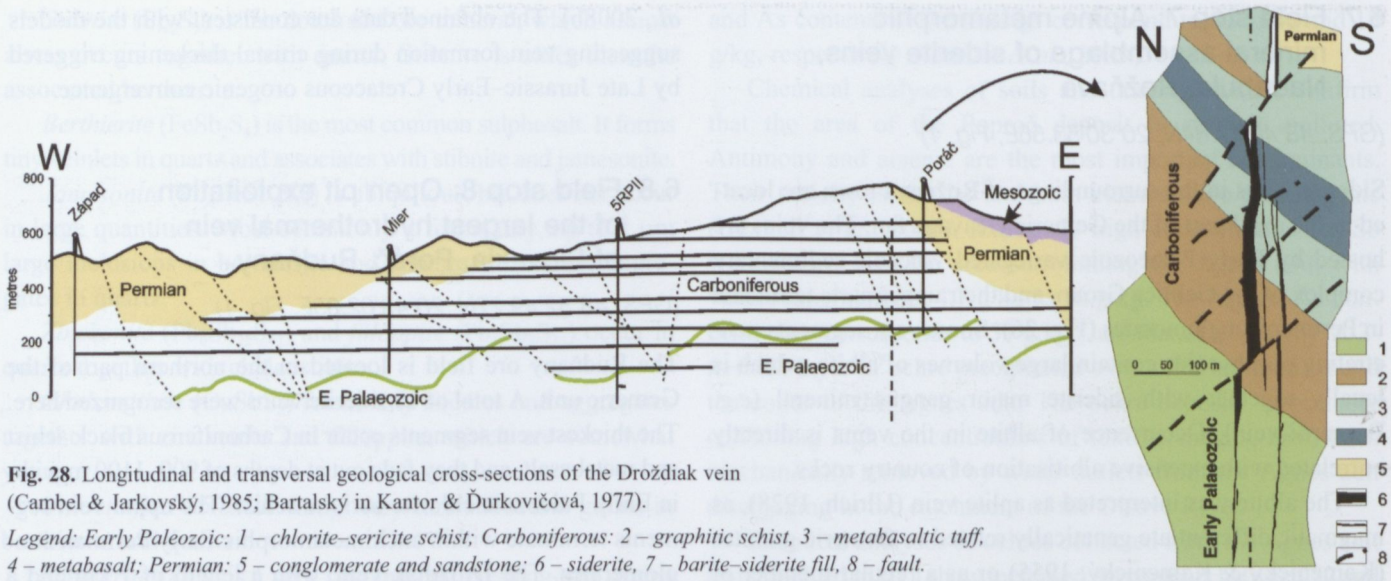

Fig. 28. Longitudinal and transversal geological cross-sections of the Droždiak vein (Cambel & Jarkovský, 1985; Bartalský in Kantor & Ďurkovičová, 1977).

Legend: Early Paleozoic: 1 – chlorite–sericite schist; Carboniferous: 2 – graphitic schist, 3 – metabasaltic tuff, 4 – metabasalt; Permian: 5 – conglomerate and sandstone; 6 – siderite, 7 – barite–siderite fill, 8 – fault.

homogenized between 101–165 °C, and total salinity ranged between 18 and 27 wt%, and $CaCl_2$/(NaCl + $CaCl_2$) weight ratios were fixed at 0.1–0.3. In contrast, mono- and two-phase aqueous inclusions in barite exhibited total salinities between 2 and 22 wt%, and the $CaCl_2$/NaCl ratios ranging from NaCl- to $CaCl_2$-dominated compositions. Aqueous inclusions in barite were closely associated with unique, very high density (0.55–0.75 g□cm^{-3}) nitrogen inclusions, in some cases containing up to 16 mol% CO_2 (Fig. 30).

Crystallization *PT* conditions of siderite (175–210 °C, 1.2–1.7 kbar) constrained by the vertical oxygen isotope gradient along the Droždiak vein (1.8–2.3‰ km^{-1}), isochores of fluid inclusions and K/Na exchange thermometry corresponded to minimal palaeodepths between 4.3 and 6.3 km, assuming lithostatic load and average crust density of 2.75 g□cm^{-3}. A higher fluid pressure, 3.6–4.4 kbar at 200–300 °C, was recorded during barite crystallization. The contrasting fluid compositions, increasing depths of burial (~4–14 km) and decreasing thermal gradients (~50–15 °C km^{-1}) during early evolutionary stages of the Droždiak vein are interpreted to reflect increasing overburden during Alpine crustal thickening induced by orogenic convergence. Variable salinities of the barite-hosted inclusions reflect transition to an open hydrothermal system. Lengths of decrepitation cracks proportional to fluid inclusion sizes (Fig. 30) indicate decompression during retrograde crystallization trajectory. Maximum pressures recorded by the fluid inclusions indicate ~12 km thick pile of imbricated nappe units accumulated over the northern Gemeric basement during the Early Cretaceous collision (Hurai *et al.*, 2008a).

Fig. 29. One of several abandoned open pits excavated in the uppermost part of the Droždiak siderite-barite vein, south of Poráč village. The documented quarry is 50 m wide and 230 m long, but the Droždiak vein crops out here in the total length of 1 km.

Mining around Rudňany had been focussed on exploitation of Cu-Ag ores until the seventies of the 19th century. New processing and roasting plants were built at the end of 19th century. Native quicksilver has been obtained by condensation of outlet gases. Ore exploitation culminated in the seventies of the 20th century with exploitation of siderite and barite ores. Mining of siderite ceased in 1992 and only barite has been exploited until recently. A total of 25–30 Mt of siderite, barite and sulphide (Cu, Ag, Hg) ores were recovered during the whole mining history. More than 3000 tons of quicksilver was obtained in the period between 1858 and 1945.

Setting pit for storage of tailings from processing plants was built in 1960. Weight of the waste deposited reaches 12 Mt. Average composition of the waste material is as follows (in wt%): 40–50 SiO_2, 8–12 $BaSO_4$, 6–8 Al_2O_3, 10–14 Fe. Flotation mud with pH ≈ 8 contains the following metal concentrations (in ppm): 456 Cu, 335 As, 23 ppm Hg, 6 ppm Pb.

The processing plants near Rudňany emitted around 2600 tons of dust each year, *i.e.* 63% of all dust outlets in the middle Spiš region. Hg, Cl, Fe, Sb and Ba were major elements of the emissions. About 142 tons of Hg was released in air during last 30 years of operations. Recently, after ceasing mining activity, additional 0.6 tons of Hg per year is blown out from

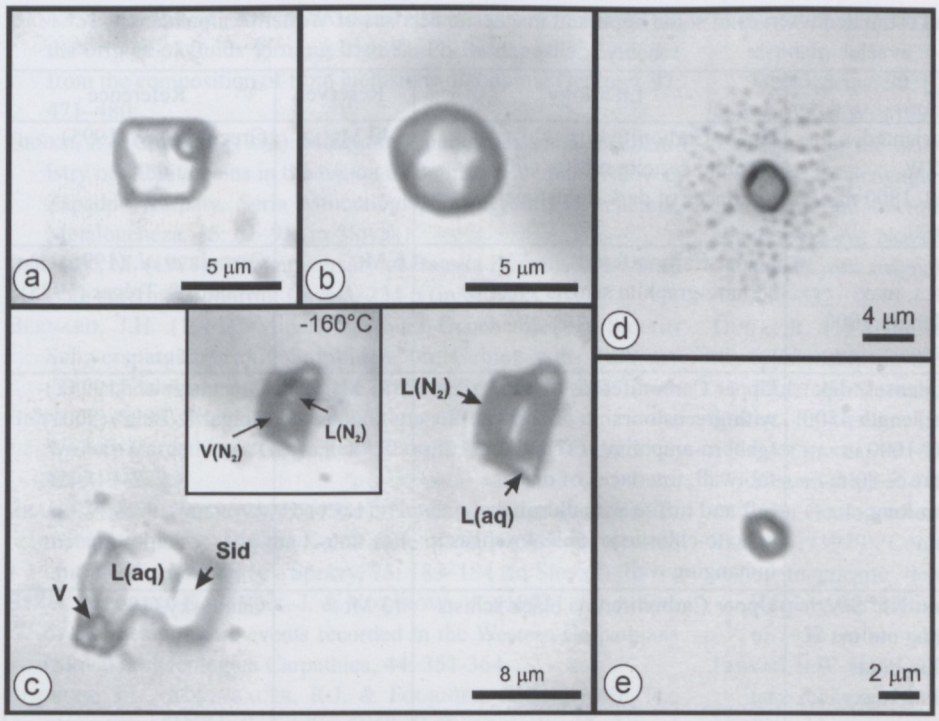

Fig. 30. Primary fluid inclusions in barite from the Drožďiak vein. **a**) Two-phase aqueous inclusion. **b**) Negative crystal-shaped inclusion containing aqueous liquid. **c**) Fluid inclusions with variable phase ratios. The irregular inclusion in the lower left corner contains aqueous solution – L(aq), small vapour bubble (V) and a carbonate daughter phase, probably siderite (Sid). The upper right inclusion consists of immiscible aqueous – L(aq), and nitrogen – $L(N_2)$ liquids. Nitrogen vapor – $V(N_2)$ – nucleates after cooling below –151 °C (inset). The aqueous liquid-dominated inclusion decrepitated at 60 °C, prior to the vapor bubble disappearance, thus indicating high internal pressure caused by dissolved gas. Variable phase ratios at room temperature indicate entrapment of a heterogeneous fluid. **d**) Perpendicular view of a decrepitation crack around primary gaseous inclusion, 4 μm in diameter, which homogenized to liquid by bubble disappearance at –164.2 °C. **e**) Smaller monophase negative crystal-shaped gaseous inclusion without optically discernible decrepitation cracks homogenizes to liquid at –175.5 °C and maintains an internal overpressure of ~1800 bar at room temperature.

dumps and setting pits by wind. Soils are contaminated up to the distance of 5 km from former processing plants and dumps. Measured concentrations of toxic metals fluctuate widely, but they all significantly exceed the allowed limits.

6.9 Field stop 9: Recent travertine precipitation and cultural monuments, Sivá Brada, Spišské Podhradie

(GPS: 49°00'26.01N, 21°15'11.80E, Fig. 1)

Spišské Podhradie is a well-preserved historical town. Its part – Spišská Kapitula – has been the seat of the Spiš Diocese since the 18th century and a center of church administration since the 12th century. Spišská Kapitula together with the overlooking Spiš Castle – the largest medieval castle in Central Europe – and with the late-Roman church of St. Spirit in Žehra village were registered as UNESCO World Heritage sites.

Numerous travertine heaps occur near Spišské Podhradie. These are aligned along tectonic lines with NW–SE, N–S and NE–SW directions. The travertine has been precipitating here from Pliocene–Pleistocene times up to recently. Most travertine occurrences were destroyed or mined out for decorative purposes. Karstic pockets filled with *terra rossa* contain remnants of interglacial fauna. Artefacts of Mousterian culture have been found at Sobotisko – the easternmost travertine occurrence in the region. The Sivá Brada locality is an active travertine heap discharging mineral waters (Fig. 31).

Fig. 31. Recent precipitation of travertine at Sivá Brada near Spišské Podhradie.

Table 1. Structural, lithological parameters and estimated reserves of some important magnesite deposits of Western Carpathians.

Deposit	Unit	Structure	Lithology	Reserves	Reference
Košice	Gemeric	Two irregular lenses oriented NW–SE, dip 40–70° SW, directional length 1600–1800 m, max. thickness 280 m	Upper Carboniferous graphite-sericite schists with interlaces of dark dolostones	540 Mt	Grecula *et al.* (1995)
Ochtiná	Gemeric	Several sub-horizontal NW–SE-oriented lenses, max. thickness 55–230 m, length 1000 m, width 400 m	Upper Carboniferous sericite-graphite schists	6 Mt	Grecula *et al.* (1995) Mihalík & Tréger (1995)
Jelšava	Gemeric	Several E–W-oriented lenses, dip 45–85° SE, directional length 4500 m, max. thickness 600–1000 m. Magnesite-rich parts are 5–80 m thick and up to 1500 m long	Upper Carboniferous black shales with greenstones (gabbro-amphibolites?) in footwall, interlaces of diabase tuff and tuffite with chlorite-, sericite-chlorite and black schists in hanging wall	535 Mt	Grecula *et al.* (1995) Tréger & Baláž (2001)
Lubeník	Gemeric	Lense-shaped, direction NE–SW, dip 55–60° SE, cropping out in directional length 300 m, total directional length 880 m, max. thickness 200 m	Upper Carboniferous black schists	13 Mt	Gánovský (1995)
Ploské	Gemeric	One major and 4 small lenses oriented NE–SW, dip 60° SE, directional length 180 m, max. thickness 18–25 m	Footwall: upper Carboniferous graphitic schists, slaty dolomites and metabasalts. Hanging wall: metapsammites, sericite-graphite schists	0.2 Mt	Varga (1992)
Burda	Gemeric	One lens oriented NE–SW, dip 25–55° SE, directional length 1500 m, thickness 200 m	Footwall: upper Carboniferous chlorite-sericite schists. Hanging wall: black shales, quartz phyllites with slaty crystalline limestones	51 Mt	Grecula *et al.* (1995) Varga (1992)
Mútnik	Veporic	Several irregular lenses 20–100 m thick, dip 45° S, W–E-oriented	Footwall: sericite-chlorite schists, talc schists, garnet mica schists and amphibolites. Hanging wall: sericite and chlorite schists	2.3 Mt magnesite 0.7 Mt talc	Varga (1992) Lisý (1971)
Kokava	Veporic	Several mylonitized lenses oriented NE–SW, dip 55° SE	Chlorite-sericite schists	0.25 Mt talc	Lisý (1971)

7. References

Abonyi, A. (1971): Magnesite deposits of Slovakia. Mineralia Slovaca, **3**: 319–342 (in Slovak).

Abonyi, A. & Abonyiová, M. (1981): Magnesite deposits of Slovakia. Bratislava: Alfa, 98 p (in Slovak).

Antal, B. (2004): Ore mineralization in Mesozoic carbonates of the Slovinky-Hŕbok locality (Spišsko-gemerské rudohorie Mts.). Mineralia Slovaca, **36**: 23–38 (in Slovak).

Árkai, P., Balogh, K. & Dunkl, I. (1995): Timing of low-temperature metamorphism and cooling of the Palaeozoic and Mesozoic formations of the Bükkium, innermost Western Carpathians, Hungary. Geologische Rundschau, **84**: 334–344.

Bagdasaryan, G.P., Cambel, B., Veselský, J. & Gukasyan, R.Ch. (1977): K-Ar age determinations of the rocks from crystalline complexes of the Western Carpathians and preliminary interpretation of results. Geologický Zborník Geologica Carpathica, **37**: 365–374 (in Russian).

Bahat, D. & Engelder, T. (1984): Surface morphology of joints of the Appalachian Plateau, New York and Pennsylvania. Tectonophysics, **104**: 299–313.

Bajaník, Š. & Planderová, E. (1985): Stratigraphic position of the lower part of the Ochtiná Fm. (between Magnezitovce and Magura). Geologické Práce – Správy, **82**: 67–76 (in Slovak).

Bajaník, Š., Vozárová, A. & Reichwalder, P. (1981): Lithostratigraphic classification of the Rakovec Group and the Upper Palaeozoic in the Spiš-Gemer Ore Mountains. Geologické Práce – Správy, **75**: 27–56 (in Slovak).

Bajaník, Š., Hanzel, V., Ivanička, J., Mello, J., Pristaš, J., Reichwalder, P., Snopko, L., Vozár, J. & Vozárová, A. (1983): Explanations to geological map of the Slovak Ore Mountains – eastern part 1:50 000. Bratislava: GÚDŠ, 223 p (in Slovak).

Banks, D.A., Boyce, A.J. & Samson, I.M. (2002): Constraints on the origins of fluids forming Irish Zn-Pb-Ba deposits: Evidence from the composition of fluid inclusions. Economic Geology, **97**: 471–480.

Beňka, J. & Caňo, F. (1992): Mineralogy, paragenesis and geochemistry of stibnite veins in the region of Betliar – Čučma – Volovec. Západné Karpaty, Séria Mineralógia, Petrografia, Geochémia, Metalogenéza, **15**: 61–91 (in Slovak).

Beránek, M. (1977): 30th anniversary of Banska Bystrica Ore Mines state enterprise. Martin: Osveta, 234 p (in Slovak).

Bernard, J.H. (1961): Mineralogie und Geochemie der Sideri-Schwerspatgänge mit Sulphiden im Gebiet von Rudňany (Tschechoslowakei). Geologické Práce – Zošit, **58**: 5–222.

Bezák, V. (1991): Metamorphic conditions of the Veporic unit in the Western Carpathians. Geologický Zborník Geologica Carpathica, **42**: 219–222.

Bezák, V. & Planderová, E. (1981): New knowledge about age of metamorphic rocks in the Kohút zone of the Veporicum tectonic unit. Geologické Práce - Správy, **75**: 183–184 (in Slovak).

Bezák, V., Sassi, F., Spišiak. J. & Vozárová, A. (1993): An outline of the metamorphic events recorded in the Western Carpathians (Slovakia). Geologica Carpathica, **44**: 351-364.

Bischoff, J.L., Rosenbauer, R.J. & Fournier, R.O. (1996): The generation of HCl in the system $CaCl_2$-H_2O: vapour-liquid relations from 380-500°C. Geochimica et Cosmochimica Acta, **60**: 7–16.

Bobro, M. & Hančuľák, J. (2001): Influence of Slovak magnesite processing on the environment. Mineralia Slovaca, **33**: 535–538.

Borisenko, A.S., Lebedev, V.I. & Tyulkin, V.G, (1984): Formation conditions of hydrothermal cobalt-bearing deposits. Novosibirsk: Nauka, 170 p (in Russian).

Bosák, P., Bella, P., Cílek, V., Ford, D.C., Hercman, H., Kadlec, J., Osborne, A. & Pruner, P. (2002): Ochtiná aragonite cave (Western Carpathians, Slovakia): Morphology, mineralogy of the fill and genesis. Geologica Carpathica, **6**: 399–410.

Broska, I. & Uher, P. (2001): Whole-rock chemistry and genetic typology of the West-Carpathian Variscan granites. Geologica Carpathica, **52**: 79–90.

Burrus, J. & Foucher, J.P. (1986): Contribution to the thermal regime of the Provencal basin based on flumed heat flow surveys and previous investigations. Tectonophysics, **128**: 303–34.

Cambel, B. & Jarkovský, J. (1985): The Rudňany ore field – Geochemical and metallogenetic characteristics. Bratislava: Veda, 363 p (in Slovak).

Cambel, B., Žukov, F., Savchenko, L. & Šmejkal, V. (1985): Isotopic composition of sulphur, carbon and oxygen in the minerals of siderite-barite-sulphidic ores in Rudňany. In Cambel, B. & Jarkovský, J. (eds): The Rudňany ore field – Geochemical and metallogenetic characteristics. Bratislava: Veda, 247–262 (in Slovak).

Cambel, B., Kráľ, J. & Burchart, J. (1990): Isotopic geochronology of crystalline complexes of the Western Carpathians. Bratislava: Veda, 183 p (in Slovak).

Čapo, J., Tomášiková, Z., Bachňák, M. & Mihalík, F. (1992): ČZS Dúbravský masív-220, magnezit. Open-file report, Bratislava, Geofond, archive No. 77903.

Chi, G. & Savard, M.M. (1997): Sources of basinal and Mississippi Valley-type mineralising brines: mixing of evaporated seawater and halite-dissolution brine. Chemical Geology, **143**: 121–125.

Chovan, M., Turan, J., Turanová, L. & Majzlan, J. (1996): Mineralogical and geochemical evaluation of carbonate, barite and ore mineralization of the Rudňany deposit. Department of Mineralogy and Petrology, Comenius University, Bratislava (in Slovak).

Cicmanová, S. (2002): Geoenvironmental assessment of magnesite deposit Jelšava – Dúbrava massif. Boletim Paranaense de Geociençias, **50**: 87–95.

Cosgrove, J.W. (1997): Hydraulic fractures and their implications regarding the state of stress in a sedimentary sequence during burial. In Sengupta, S. (ed.): Evolution of geological structures in micro- and macro-scales. London: Chapman & Hall, 11–25.

Csikósová, A., Novek, Z. & Kameníková, K. (2000): Position of the Slovak magnesite on world market. Mineralia Slovaca, **32**: 530–532.

Ďuďa, R. (1976): Ore occurrences and mineralogical-paragenetic relationships in the region of Košické Hámre – Košice – Hýľov. Mineralia Slovaca, **8**: 447–468 (in Slovak).

Ebner, F., Cerny, I., Eichhorn, R., Götzinger, M., Paar, W., Prochaska, W. & Weber, L. (1999): Mineral resources in the Eastern Alps and adjoining areas. Mitteilungen der Österreichischen Geologischen Gesselschaft, **92**: 157–184.

Eliáš, K. (1979): Contribution to elucidation of formation conditions of magnesite deposits by thermometric research. Západné Karpaty, Séria Mineralógia Petrografia Geochémia Metalogenéza, **6**: 7–32 (in Slovak).

Faryad, S.W. (1991): Metamorphism of the Early Paleozoic sedimentary rocks in Gemericum. Mineralia Slovaca, **23**, 315–324 (in Slovak).

Faryad, S.W. (1994): Mineralogy of Mn-rich rocks from greenschist facies sequences of the Gemericum, West Carpathians, Slovakia. Neues Jahrbuch Mineralogie Monatshefte, **10**: 464-480.

Faryad, S.W. (1995a): Petrology and phase relations of low-grade high-pressure metasediments from the Meliata unit, Western Carpathians. European Journal of Mineralogy, **7**: 71–87.

Faryad, S.W. (1995b): Phase petrology and P-T conditions of mafic blueschists from the Meliata unit, Western Carpathians. Journal of Metamorphic Geology, **13**: 701–714.

Faryad, S.W. & Dianiška, I. (1999): Degree of Alpine metamorphism in Early Palaeozoic rocks of the Gemericum. Mineralia Slovaca, **31**: 485–490 (in Slovak).

Faryad, S.W. & Henjes-Kunst, F. (1997): Petrologic and geochronologic constraints on the tectonometamorphic evolution of the Meliata unit blueschists, Western Carpathians, Slovakia. In Grecula, P., Hovorka, D. & Putiš, M. (eds): Geological evolution of the Western Carpathians. Bratislava: Geocomplex, 145–154.

Finger, F., Broska, I., Haunschmid, B., Hraško, Ľ., Kohút, M., Krenn, E., Petrík, I., Riegler, G. & Uher, P. (2003): Electron-microprobe dating of monazites from Western Carpathian basement granitoids: plutonic evidence for an important Permian rifting event subsequent to Variscan crustal anatexis. International Journal of Earth Sciences (Geologische Rundschau), **92**: 86–98.

Fontes, J.C. & Matray, J.M. (1993): Geochemistry and origin of formation brines from the Paris Basin, France. 1. Brines associated with Triassic salts. Chemical Geology, **109**: 140–175.

Fournier, R.O. & Truesdell, A.H. (1973): An empirical Na-K-Ca geothermometer for natural waters. Geochimica et Cosmochimica Acta, **37**: 1255–1275.

Friedman, I. & O'Neil, J.R. (1977): Compilation of stable isotope fractionation factors of geochemical interest. US Geological Survey Professional Paper, **440-KK**.

Foy, C.D., Chaney, R.L. & White, M.C. (1978): The physiology of metal toxicity in plants. Annual Review of Plant Physiology, **29**: 511–566.

Gánovský, J. (1995): Lubeník – reserve calculation of magnesite deposit, stand 1.1.1994. Bratislava: Geofond, 17 p (in Slovak).

Gehrig, M. (1980): Phasengleichgewichte und pVT-Daten ternären Mischungen aus Wasser, Kohlendioxid und Natriumchlorid bis 3 kbar und 550°C. PhD thesis, Univ. of Karlsruhe, Germany.

Germann, K., Lüders, V., Banks, D.A., Simon, K. & Hoefs, J. (2003): Late Hercynian polymetallic vein-type base-metal mineralization in the Iberian Pyrite Belt: fluid inclusion and stable-isotope geochemistry (S-O-H-Cl). Mineralium Deposita, **38**: 953–967.

Gleeson, S.A., Wilkinson, J.J., Stuart, F.M. & Banks, D.A. (2001): The origin and evolution of base metal mineralising brines and hydrothermal fluids, South Cornwall, UK. Geochimica et Cosmochimica Acta, **65**: 2067–2079.

Grecula, P. (1982): The Gemericum – segment of Palaeotethynian riftogeneous basin. Bratislava: Alfa, 263 p (in Slovak).

Grecula, P., Abonyi, A., Abonyiová, M., Antaš, J., Bartalský, B., Bartalský, J., Dianiška, I., Drnzík, E., Ďuďa, R., Gargulák, M., Gazdačko, Ľ., Hudáček, J., Kobulský, J., Lőrincz, L., Macko, J., Návesňák, D., Németh, Z., Novotný, L., Radvanec, M., Rojkovič, I., Rozložník, L., Rozložník, O., Varček, C. & Zlocha, J. (1995): Mineral deposits of the Slovak Ore Mountains. Bratislava: Geocomplex, 834 p.

Grecula, P., Radvanec, M. & Németh, Z. (2000): Magnesite and talc mineralization in Slovakia. Mineralia Slovaca, **32**: 533-542.

Halahyjová-Andrusovová, G. (1964): About origin of the Dobšiná ore deposits. Geologické Práce – Správy, **33**: 53–67 (in Slovak).

Hančuľák, J. (2001): Development of the dust deposition in the area of SMZ, Inc. Jelšava. Acta Montanistica Slovaca, **5**: 310–312.

Heijlen, W., Muchez, P. & Banks, D.A. (2001): Origin and evolution of high-salinity, Zn-Pb mineralising fluids in the Variscides of Belgium. Mineralium Deposita, **36**: 165–176.

Holloway, J.R. (1981): Compositions and volumes of supercritical fluids in the Earth's crust. In Hollister, L.S. & Crawford, M.L. (eds): Fluid inclusions: applications to petrology. Mineralogical Association of Canada Short Course Handbook, **6**: 13–38.

Hubbert, M.K. & Rubey, W.W. (1959): Role of fluid pressure in mechanics of overthrust faulting. Bulletin of the Geological Society of America, **70**: 115–166.

Hurai, V., Simon, K. & Bezák, V. (1997): Contrasting chemistry and H, O, C isotope composition of greenschist-facies, Hercynian and Alpine metamorphic fluids (Western Carpathians). Chemical Geology, **136**: 281–293.

Hurai, V., Gazdačko, Ľ., Ferenčíková, E., Majzlan, J. & Repčok, I. (1998): Origin of ore-forming fluids in the vein siderite deposits of Gretla, Jedľovec, and Rudňany (the Spišsko-Gemerské Rudohorie Mountains). Mineralia Slovaca, **30**: 423–430 (in Slovak).

Hurai, V., Harčová, E., Huraiová, M., Ozdín, D., Prochaska, W. & Wiegerová, V. (2002): Origin of siderite veins in the Western Carpathians I. P-T-X-δ^{13}C-δ^{18}O relations in ore-forming brines of the Rudňany deposits. Ore Geology Reviews, **21**: 67–101.

Hurai, V., Urban, M., Konečný, P., Thomas, R., Lexa, O., Schulmann, K. & Chovan, M. (2006): Cretaceous age of quartz-stibnite veins near Čučma (Spišsko-gemerské rudohorie Mts.). Mineralia Slovaca, **38**: 131–140.

Hurai, V., Prochaska, W., Lexa, O., Schulmann, K., Thomas, R. & Ivan, P. (2008a): High-density nitrogen inclusions in barite from a giant siderite vein: implications for Alpine evolution of the Variscan basement of Western Carpathians, Slovakia. Journal of Metamorphic Geology, **26**: 487–498.

Hurai, V., Lexa, O., Schulmann, K., Montigny, R., Prochaska, W., Frank, W., Konečný, P., Kráľ, J., Thomas, R. & Chovan, M. (2008b): Mobilization of ore fluids during Alpine metamorphism: evidence from hydrothermal veins in the Variscan basement of Western Carpathians, Slovakia. Geofluids, **8**: 181–207.

Huraiová, M., Vozárová, A., Repčok, I. (2002): Fluid inclusion and stable isotope constraints on the origin of magnesite at Burda, Ochtiná, Lubeník, and Ploské deposits (Slovakia, Western Carpathians). Geologica Carpathica Special Issue, **53**: 98–100.

Ilavský, J. (1957): Geology of ore deposits of the Spišsko-gemerské Rudohorie Mts. Geologické Práce – Zošit, **46**: 51–95.

Ilavský, J. (1979): Metallogenèse de l'Europe alpine central et du sud-est. Bratislava: GÚDŠ, 413 p.

Ilavský, J., Bajaník, Š., Štohl, J. & Vozár, J. (1975): Volcanism and metallogenesis of the Western Carpathians. Geologické Práce – Správy, **64**: 97–134 (in Slovak).

Ilavský, J., Malkovský, M. & Odehnal, L. (1977): The iron ore deposits of the Czechoslovak Socialist Republic. In Zitzmann, A. (ed.): The iron ore deposits of Europe and adjacent areas. Explanatory notes to the international map of the iron ore deposits of Europe 1:2 500 000, Vol. 1. Hannover: Bundesanstalt für Geowissenschaften und Rohstoffe, 111–124.

Ilavský, J., Turan, J. & Turanová, L. (1991): Metalogenesis of stratiform magnesite deposits in Western Carpathians. Západné Karpaty, Séria Mineralógia Petrografia Geochémia Metalogenéza, **14**: 93–155.

Iró, S. & Radvanec, M. (1997): Geochemical and mineralogical research on carbonate minerals from Nižná Slaná-Manó deposit (Gemericum, Western Carpathians). Acta Geologica et Geographica Universitatis Comenianae, **52**: 19–28.

Ivanov, M. (1953): Geological and paragenetic relationships in northern part of the Spišsko-gemerské rudohorie Mts., between Kluknava and Žakarovce. Geologický Sborník Slovenskej Akadémie Vied, **4**: 705–750.

Janák, M., Plašienka, D., Frey, M., Cosca, M., Schmidt, S.T., Lupták, B. & Méres, Š. (2001): Cretaceous evolution of a metamorphic core complex, the Veporic unit, Western Carpathians (Slovakia): P-T conditions and in situ ^{40}Ar/^{39}Ar UV laser probe dating of metapelites. Journal of Metamorphic Geology, **19**: 197–216.

Jankulár, M., Klimko, T., Jurkovič, Ľ., Lalinská, B., Šottník, P., Lintnerová, O. & Šutriepka, M. (2008): Examination of abandoned Sb deposits by mineralogical methods in Poproč (Slovakia). Chemické Listy, **102**: 380–382.

Jeřábek, P., Janák, M., Faryad, S.W., Finger, F. & Konečný, P. (2008): Polymetamoprhic evolution of pelitic schists and evidence for Permian low-pressure metamorphism in the Vepor Unit, West Carpathians. Journal of Metamorphic Geology, **26**: 465–485.

Kaličiaková, E., Pacindová, N., Repčiak, M., Seliga, J. & Volko, P. (1996): Poproč – haldy, skládky, odkaliská, VP – životné prostredie. Bratislava: GSSR, 76 p.

Kamenický, J. & Kamenický, L. (1955): Gemeric granites and ores of the Spiš-Gemer Ore Mountains. Geologické Práce – Zošit, **41**: 5–55 (in Slovak).

Kantor, J. (1957): Ar^{40}-K^{40} method of absolute age determination of rocks and its application to the Gemeric granite of Betliar. Geologické Práce – Zprávy, **11**: 188–199 (in Slovak).

Kantor, J. & Ďurkovičová, J. (1977): Sulfur isotopes in selected barite deposits of Western Carpathians. Unpublished report. Bratislava: Geofond, 244 p (in Slovak).

Kenis, I., Muchez, Ph., Verhaert, G., Boyce, A. & Sintubin, M. (2005): Fluid evolution during burial and Variscan deformation in the Lower Devonian rocks of the High-Ardenne slate belt

(Belgium): sources and causes of high-salinity and C-O-H-N fluids. Contributions to Mineralogy and Petrology, **150**: 102–118.

Kesler, S.E., Martini, A.M., Appold, M.S., Walter, L.M., Huston, T.J., Furman, F.C. (1996): Na-Cl-Br systematics of fluid inclusions from Mississippi Valley-type deposits, Appalachian Basin: Constraints on solute origin and migration paths. Geochimica et Cosmochimica Acta, **60**: 225–233.

Klimko, T., Lalinská, B., Chovan, M., Jurkovič, Ľ. & Jankulár, M. (2009): Mineralogy and geochemistry of secondary Fe/Sb mineral phases from tailing's material at abandoned Sb-deposits Dúbrava and Poproč (Slovakia). In: International symposium on mineralogy, environment and health, Paris 17.-18. 9. 2009 (abstr.).

Klinec, A., Planderová, E. & Miko, O. (1975): Lower Paleozoic age of the Hron complex in the Veporides. Geologické Práce – Správy, **63**: 95–104 (in Slovak).

Koděra, P. & Radvanec, M. (2002): Comparative mineralogical and fluid inclusion study of the Hnúšťa-Mútnik talc-magnesite and Miková-Jedľová magnesite deposit (Western Carpathians, Slovakia). Boletím Paranaense de Geociências, **50**: 131–150.

Koděra, M., Andrusovová-Vlčeková, G., Belešová, O., Briatková, D., Dávidová, Š., Fejdiová, V., Hurai, V., Chovan, M., Nelišerová, E. & Ženiš, P. (1986): Topographical mineralogy of Slovakia, Vol. 1. Bratislava: Veda, 577 p (in Slovak).

Koděra, M., Andrusovová-Vlčeková, G., Belešová, O., Briatková, D., Dávidová, Š., Fejdiová, V., Hurai, V., Chovan, M., Nelišerová, E. & Ženiš, P. (1990): Topographical mineralogy of Slovakia, Vol. 2. Bratislava: Veda, 607–1098 (in Slovak).

Kozur, H. & Mock, R. (1973): Zur Alter und zur tektonischen Stellung der Meliata-Serie des Slowakischen Karstes. Geologický Zborník Geologica Carpathica, **24**: 365–374.

Kozur, H., Mock, R. & Mostler, H. (1976): Stratigraphische Neueinstuffung der Karbonatgesteine der unteren Schichtfolge von Ochtiná (Slowakei) in das oberste Visé-Serpukhovian (Namur A). Mitteilungen der Geologie und Paläontologie, **6**: 1–29.

Kralik, M., Aharon, P., Schroll, E. & Zachmann, D. (1989): Carbon and oxygen isotope systematics of magnesites: a review. Monograph Series Mineralium Deposita, **28**: 197–223.

Kučerová, G., Lalinská, B., Klimko, T. (2009): Mineralogické a geochemické štúdium sekundárnych produktov oxidácie odkaliskového materiálu na opustenom ložisku Čučma. In Geochémia pri riešení aktuálnych problémov, Banská Štiavnica 29.-31. 5. 2009 (abstr.).

Kužvart, M. (1954): Report on provisional research on magnesite deposits of Slovakia. Věstník Ústředního Ústavu Geologického Praha, **29**: 178–185 (in Czech).

Kužvart, M. (1955): Geological and petrographical relationships of the talc deposits and their surroundings at Hnúšťa (Slovakia). Sborník Ústředního Ústavu Geologického Praha, **22**: 145–180 (in Czech).

Lalinská, B., Homolová, K., Milovská, S. & Piliarová, L. (2009): Porovnanie mineralogického a chemického zloženia Fe oxyhydroxidov z rôznych opustených Sb ložísk Slovenska. In: Geochémia pri riešení aktuálnych problémov, Banská Štiavnica 29.-31. 5. 2009 (abstr.).

Laube, N., Frimmel, H.E. & Hoernes, S. (1995): Oxygen and carbon isotopic study on the genesis of the Steirischer Erzberg siderite deposit (Austria). Mineralium Deposita, **30**: 285–293.

Leško, O. & Bobro, M. (1987): Development of the dust deposition in the plants of SMZ Jelšava and SMZ Lubeník. Rudy, **8**: 232–234.

Lexa, J., Bezák, V., Elečko, M., Mello, J., Polák, M., Potfaj, M., Vozár, J., Schnabel, G.W., Pálenský, P., Császár, G., Rylko, W. & Mackiv, B. (2000): Geological map of Western Carpathians and adjacent areas 1:500 000. Bratislava: Geological Survey of Slovakia.

Lexa, J., Bačo, P., Chovan, M., Petro, M., Rojkovič, I. & Tréger, M. (2004): Metallogenetic map of Slovakia. Bratislava: Ministry of Environment and Geological Survey of Slovakia.

Lexa, O., Schulmann, K. & Ježek, J. (2003): Cretaceous collision and indentation in the West Carpathians: View based on structural analysis and numerical modeling. Tectonics, **22**: 1066.

Lisý, E. (1971): Talc deposits of Slovakia. Mineralia Slovaca, **3**: 343–348 (in Slovak).

Maderspach, L (1880): Iron ore deposits of Hungary. Budapest: Kir. M. Természettudományi Társulat, 111 p (in Hungarian).

McCaffrey, M.A., Lazar, B. & Holland, H.D. (1987): The evaporation path of seawater and the coprecipitation of Br^- and K^+ with halite. Journal of Sedimentary Petrology, **57**: 928–937.

Mello, J., Reichwalder, P. & Vozárová, A. (1998): Bôrka Nappe: high-pressure relic from the subduction-accretion prism of the Meliata Ocean (Inner Western Carpathians, Slovakia). Slovak Geological Magazine, **4**: 261–273.

Michard, G. & Fouillac, C. (1981): Sodium/lithium ratio in water applied to geothermometry of geothermal reservoirs. Geothermics, **10**: 55–70.

Mihalík, F. & Tréger, M. (1995): The Ochtiná deposit – magnesite – prospecting, reclassification of reserves, stand 1995. Spišská Nová Ves: Geological Survey of Slovakia, 16 p (in Slovak).

Milovský, R., Hurai, V., Plašienka, D. & Biroň, A. (2003): Hydrotectonic regime at soles of overthrust sheets: textural and fluid inclusion evidence from basal cataclasites of the Muráň nappe (Western Carpathians, Slovakia). Geodinamica Acta, **16**: 1–20.

Mullis, J. (1987): Fluid inclusion studies during very low-grade metamorphism. In Frey, M. (ed.): Low temperature metamorphism. Glasgow: Blackie,162–199.

Németh, Z., Prochaska, W., Radvanec, M., Kováčik, M., Madaras, J., Koděra, P. & Hraško, L. (2004): Magnesite and talc origin in the sequence of geodynamic events in Veporicum, Inner Western Carpathians, Slovakia. Acta Petrologica Sinica, **20**: 837–854.

O'Neil, J.R., Clayton, R.N. & Meyeda, T.K. (1969): Oxygen isotope fractionation in divalent metal carbonates. Journal of Chemical Physics, **51**: 5547–5558.

Ohmoto, H. & Rye, R.O. (1979): Isotopes of sulfur and carbon. In Barnes, H.L. (ed.): Geochemistry of hydrothermal ore deposits. 2nd edition. New York: Wiley, 509–567.

Öztürk, H., & Frakes, L.A. (1995): Sedimentation and diagenesis of an Oligocene manganese deposit in a shallow subbasin of the Parathetys: Thrace basin, Turkey. Ore Geology Reviews, **10**: 117–132.

Papp, K. (1919): Die Eisenerz- und Kohlenvorräte des Ungarischen Reiches. Budapest: M. Kir. Földtani Intézet, 639 p.

Pecho, J. (1980): Structural-geological relationships in stibnite deposits of Spišsko-gemerské rudohorie Mts. In Ilavský, J. (ed.): Antimony ores of Czechoslovakia. Bratislava: GÚDŠ, 103–113 (in Slovak).

Planderová, E. (1982): First finding of Viséan microflora in Gemerides (Slovakia). Západné Karpaty, Séria Paleontológia, **8**: 111–126 (in Slovak).

Plašienka, D. (2002): Alpide tectonic progradation and its structural record in units of Western Carpathians. DrSc thesis, Bratislava, Slovakia (in Slovak).

Plašienka, D., Janák, M. Hacura, A. & Vrbatovič, P. (1989): First data on the illite crystallinity from metamorphosed rocks of the Veporicum. Mineralia Slovaca, **21**: 43–51 (in Slovak).

Plašienka, D., Grecula, P., Putiš, M., Kováč, M. & Hovorka, D. (1997): Evolution and structure of the Western Carpathians. In Grecula, P., Hovorka, D. & Putiš, M. (eds): Geological evolution of the Western Carpathians. Bratislava: Geocomplex, 1–24.

Plyasunova, N.V. & Shmulovich, K.I. (1993) Immiscibility in the ternary fluid systems H_2O-CO_2-$CaCl_2$ and H_2O-CO_2-NaCl at high temperatures and pressures. Archiwum Mineralogiczne, **49**: 170 (abstr.).

Powell, R., Condcliffe, D.M. & Condcliffe, E. (1984): Calcite-dolomite geothermometry in the system $CaCO_3$-$MgCO_3$-$FeCO_3$: An experimental study. Journal of Metamorphic Geology, **2**: 33–41.

Price, N.J. & Cosgrove, J.W. (1990): Analysis of geological structures. Cambridge: Cambridge Univ. Press, 494 p.

Prochaska, W. (1999): Die Bedeutung der chemischen Zusammensetzung von Einschlussfluiden und laugbaren Salzen für die Genese von hydrothermalen und sedimentären Karbonatgesteinen in den Ostalpen. Mitteilungen der Österreichischen Geologischen Gesselschaft, **90**: 175–183.

Prochaska, W. (2001): Magnesite mineralization of the Eastern Alps and the Carpathians. In Piestrzyński, A. (ed.): Mineral deposits at the beginning of the 21st century. Lisse: Balkema, 1017–1019.

Prochaska, W., Frank, W. & Bechtel, A. (1996): Pretertiary siderite mineralization in the Greywacke Zone of the Eastern Alps. In Grecula, P. (ed.): Variscan Metallogeny in the Alpine Orogenic Belt. Bratislava: Alfa, 165–174.

Radvanec, M. (1994): Petrology of gneiss-amphibolite complex of the Gemericum in the northern margin of the Rudňany ore field. Part I.: P-T-X conditions and metamorphic zones. Mineralia Slovaca, **26**: 223–238 (in Slovak).

Radvanec, M. & Prochaska, W. (2001): Successive replacement of Upper Carboniferous calcite to dolomite and magnesite in Dúbrava magnesite deposit (Western Carpathians, Slovakia). Mineralia Slovaca, **33**: 517–525.

Radvanec, M., Grecula, P. & Žák, K. (2004a): Siderite mineralization of the Gemericum superunit (Western Carpathians, Slovakia): review and a revised genetic model. Ore Geology Reviews, **24**: 267–298.

Radvanec, M., Koděra, P. & Prochaska, W. (2004b): Mineralogy, fluid inclusion and C, O, Sr isotope study of the Košice-Medvedia magnesite deposit, Western Carpathians, Slovakia. Acta Petrologica Sinica, **20**: 855–876.

Radvanec, M., Koděra, P. & Prochaska, W. (2004c): Mg replacement at the Gemerská Poloma talc-magnesite deposit, Western Carpathians, Slovakia. Acta Petrologica Sinica, **20**: 773–790.

Roedder, E. & Bodnar, R.J. (1980): Geologic pressure determination from fluid inclusion studies. Earth Planetary Science Annual Reviews, **8**: 263–301.

Rojkovič, I. (1985): Paragenesis and mineral succession. In Cambel, B. & Jarkovský, J. (eds): The Rudňany ore field – geochemical and metalogenetic characteristics. Bratislava: Veda, 183–193 (in Slovak).

Rojkovič, I. (2001): Early Paleozoic manganese ores in the Gemericum Superunit, Western Carpathians, Slovakia. Geolines, **13**: 34–41.

Rojkovič, I., Novotný, L. & Háber, M. (1993): Stratiform and vein U, Mo and Cu mineralization in the Novoveská Huta area, CSFR. Mineralium Deposita, **28**: 58–65.

Rojkovič, I., Puškelová, Ľ., Khun, M. & Medveď, J. (1995): U-REE-Au in veins and black shales of the Gemericum, Slovakia. In Pašava, J., Kříbek, B. & Žák, K. (eds): Mineral deposits: from their origin to their environmental impacts. Rotterdam, Brookfield: Balkema, 789–792.

Roy, S. (1992): Environments and processes of manganese deposition. Economic Geology, **87**: 1218–1236.

Rozložník, L. (1965): Analysis of structural and metallogenetic elements between Dobšiná and Mlynky villages. Geologické Práce – Zprávy, **28**: 103–112 (in Slovak).

Rozložník, L. & Slavkovský, J. (1980): Some structural properties of antimony ore deposits of the Spišsko-gemerské rudohorie Mts. In Ilavský, J. (ed.): Antimony ores of Czechoslovakia. Bratislava: GÚDŠ, 115–124 (in Slovak).

Rybárová, J. (1985) Thermometry on fluid inclusions in quartz and carbonates from selected deposits in the Slovenské rudohorie Mts. MSc thesis, Comenius University, Bratislava, Slovakia, 66 p (in Slovak).

Sandler, A., Nathan, Y., Eshet, Y. & Raab, M. (2001): Diagenesis of trioctahedral clays. Miocene to Pleistocene in a sedimentary-magmatic sequence in the Dead Sea Rift, Israel. Clay Mineralogy, **36**: 29–47.

Sassi, F.P. & Vozárová, A. (1987): The pressure-temperature character of the Hercynian metamorphism in the Gemericum (West Carpathians, Czechoslovakia). Rendiconti della Societá Italiana di Mineralogica e Petrologica, **42**: 73–81.

Schroll, E., Papesch, W. & Dolezel, P. (1986): Beitrag der C- und O-Isotopenanalyse zur Genese ostalpiner Sideritvorkommen. Mitteilungen der Österreichischen Geologischen Gesselschaft, **78**: 181–191.

Schulmann, K., Montigny, R., Lexa, O., Faryad, S.W, & Jeřábek, P. (2005): Geochronological constraints of Mesozoic and Tertiary reworking of Paleozoic basement units in SW Carpathians. Geolines, **19**: 103–104.

Slávik, J. (1967): Mineral raw materials of Slovakia. Bratislava: SVTL, 510 p (in Slovak).

Snopko, L. (1971): Priebeh bridličnatosti v paleozoiku Spišsko-gemerského Rudohoria. Geologické Práce – Zprávy, **57**: 207–213.

Šottník, P. & Jurkovič, Ľ. (2009): Contamination of stream sediments and soils from areas affected by Sb mining in Slovakia. In International symposium on mineralogy, environment and health, Paris 17.-18. 9. 2009 (abstr.).

Šottník, P., Šucha, V., Lintnerová, O. & Šutriepka, M. (2007): Ťažba nerastných surovín a jej dopad na životné prostredie (unpublished manuscript). ESC, Comenius University, Bratislava, 77 p.

Span, R. & Wagner, W. (1996): A new equation of state for carbon dioxide covering the fluid region from the triple-point temperature to 1100 K at pressures up to 800 MPa. Journal of Physical Chemistry Reference Data, **25**: 1509–1596.

Span, R., Lemmon, E.W., Jacobsen, R.T., Wagner, W. & Yokozeki, A. (2000): A reference equation of state for the thermodynamic properties of nitrogen for temperatures from 63.151 to 1000 K and pressures to 2200 MPa. Journal of Physical Chemistry Reference Data, **29**: 1361–433.

Sterner, S.M. & Pitzer, K.S. (1994): An equation of state for carbon dioxide valid from zero to extreme pressures. Contributions to Mineralogy and Petrology, **117**: 362–374.

Šucha, V. & Eberl, D.D. (1992): Burial metamorphism of Permian sediments in the Northern Gemeric and Hronic units, West Carpathians. Mineralia Slovaca, **24**: 399–405 (in Slovak).

Suchár, A. (1960): Final report and calculation of reserves – Mútnik – magnesite. Bratislava: Geofond (in Slovak).

SVENSEN, H., JAMTVEIT, B., YARDLEY, B., ENGVIK, A.K., AUSTRHEIM, H. & BROMAN, C. (1999): Lead and bromine enrichment in eclogite-facies fluids; extreme fractionation during lower-crustal hydration. Geology, **27**: 467–470.

TOMEK, Č. (1993): Deep structure beneath the central and inner West Carpathians. Tectonophysics, **226**: 417–431.

TRDLIČKA, Z. (1959): Contribution to mineralogy of Slovak magnesites. Geol Práce – Zošit, **56**: 165–200 (in Czech).

TRDLIČKA, Z. & KUPKA, F. (1964): Determination of formation temperature of metasomatic magnesites of the Spišsko-gemerské rudohorie Mts., using decrepitation method. Geologický Sborník Slovenskej Akadémie Vied, **15**: 95–100 (in Czech).

TRÉGER, M. & BALÁŽ, J. (2001): Economic assessment of magnesite and talc deposits in the Slovak Republic. Mineralia Slovaca, **33**: 527–534.

TRÉGER, M., MALACHOVSKÝ, P., MESARČÍK, I., KILÍK, J. & MIHÁĽ, F. (2004): Position of Betliar Formation in Gemericum geological structure. Mineralia Slovaca, **36**: 51–60 (in Slovak).

TURAN, J. & VANČOVÁ, L. (1976): Occurrences of magnesite in evaporites of the Western Carpathians. Západné Karpaty, Séria Mineralógia Petrografia Geochémia Metalogenéza, **2**: 95-149 (in Slovak).

TURAN, J. & VANČOVÁ, L. (1979): Strukturen und Texturen der Lagerstätten-Ausfüllung von Magnesitlagerstätten im Karbon der Westkarpaten. Geologický Zborník Geologica Carpathica, **30**: 207–226.

TURANOVÁ, L., TURAN, J. & MORTEANI, G. (1996): Isotopic evidences and REE contents of the Slovak magnesite deposits (Western Carpathians). In Grecula, P. (ed.): Variscan metallogeny in the Alpine orogenic belt. Bratislava: Alfa, 293–306.

UEXKÜLL, O., SKERFVING, S., DOYLE, R. & BRAUNGART, M. (2005): Antimony in brake pads - a carcinogenic component? Journal of Cleaner Production, **13**: 19–31.

ULRICH, F. (1928): Occurrence of rutile in siderite veins near Rožňava and its position in vein paragenesis. Rozpravy České Akademie Věd a Umění Praha, **8**: 1–19 (in Czech).

URBAN, M., THOMAS, R., HURAI, V., KONEČNÝ, P. & CHOVAN, M. (2006): Superdense CO_2 inclusions in Cretaceous quartz-stibnite veins hosted in low-grade Variscan basement of the Western Carpathians, Slovakia. Mineralium Deposita, **40**: 867–873.

VARČEK, C. (1955): To the question of origin and abundance of albite in siderite veins in the surroundings of Rožňava. Geologické Práce – Zprávy, **4**: 86–92 (in Slovak).

VARČEK, C. (1957): Overview of paragenetic relationships in ore deposits of the Gemericum. Geologické Práce – Zošit, **46**: 107-131 (in Slovak).

VARČEK, C. (1962): Evolution of the hydrothermal mineralization of the Spišsko-gemerské rudohorie Mts. in time and space. Geologické Práce – Zošit, **61**: 101–111 (in Slovak).

VARČEK, C. (1967): Überblick der Metallogenese der Westkarpaten. Geologický Sborník Geologica Carpathica, **18**: 3–9.

VARČEK, C. (1968): Ore deposits of the West Carpathians. In 23th International Geological Congress, Guide to Excursion 24 AC. Praha: Ústřední Ústav Geologický, 48 p.

VARČEK, C. (1973): Paragenetic and geochemical relations in hydrothermal deposits of the Spišsko-gemerské rudohorie Mountains. In Bartalský, J. (ed.): Geologicko-ložisková štúdia Spišsko-gemerského rudohoria, Book VII. Bratislava: Geofond (in Slovak).

VARČEK, C. (1985): Metalogenetic characteristics of the Spišsko-gemerské rudohorie Mountains and the position of the Rudňany ore field. In Cambel, B. & Jarkovský, J. (eds): The Rudňany ore field – Geochemical and metallogenetic characteristics. Bratislava: Veda, 61–77 (in Slovak).

VARČEK, C. & REGÁSEK, F. (1962): Ore mineralization in Mesozoic of Slovakia. Geologické Práce – Zošit, **62**: 287–300 (in Slovak).

VARGA, I. (1970): Some regularities of origin and development of geological environment of metasomatic carbonate deposits of the Spišsko-gemerské Rudohorie Mts. Mineralia Slovaca, **2**: 85–92 (in Slovak).

VARGA, I. (1992): Possible resources of the mineral raw materials of Slovakia – magnesite, prospecting, stand 31.12.1991. Geological Survey, Spišská Nová Ves, 177 p (in Slovak).

VERMA, S., SANTOYO, E. (1997): New improved equations for K/Na, Na/Li and SiO_2 geothermometers by outlier detection and rejection. Journal of Volcanology and Geothermal Research, **79**: 9–23.

VITÁLIS, I. (1914): Geological and ore geological aspects of Hungarian magnesite occurrences. Bányászati és Kohászati Lapok, **47(1)**: 409–419, 624 (in Hungarian).

VOZÁROVÁ, A. (1993): Thermodynamic conditions of metamorphism of the crystalline rocks in northern part of the Branisko Mts. Geologica Carpathica, **44**: 219–231.

VOZÁROVÁ, A. & VOZÁR, J. (1988): Late Palaeozoic in West Carpathians. Bratislava: GÚDŠ, 314 p.

VOZÁROVÁ, A. & VOZÁR, J. (1992): Tornaicum and Meliaticum in borehole Brusník BRU-1, southern Slovakia. Acta Geologica Hungarica, **35**: 97–116.

VOZÁROVÁ, A. & VOZÁR, J. (1996): Terranes of West Carpathians – North Pannonian domain. Slovak Geological Magazine, **1**: 65–85.

VOZÁROVÁ, A., ĎURKOVIČOVÁ, J. & REPČOK, I. (1995): Data on chemical and isotope composition of Carboniferous and Mesozoic carbonates of Inner Western Carpathians. Slovak Geological Magazine, **1**: 127–152.

WHIELDON, J., MORGAN, P., WILLIAMSON, K.H., EVANS, T.R. & SWANBERG, C.A. (1994): Heat flow in the Kenya rift zone. Tectonophysics, **236**: 131–149.

YARDLEY, B.W.D. & GRAHAM, J.T. (2002): The origins of salinity in metamorphic fluids. Geofluids, **2**: 249–256.

ZHENG, Y.-F. (1999): Oxygen isotope fractionation in carbonate and sulfate minerals. Geochemical Journal, **33**: 109–126.

ZHENG, Y.-F. & HOEFS, J. (1993): Carbon and oxygen isotope covariations in hydrothermal calcites. Theoretical modelling on mixing processes and application to Pb-Zn deposits in the Harz Mountains, Germany. Mineralium Deposita, **28**: 79–89.

ŽÁK, K., RADVANEC, M., GRECULA, P., BARTALSKÝ, B. (1991): Sr, S, C, O-isotopes and metamorphic-hydrothermal model of vein mineralisation in the Gemericum. Mineralia Slovaca, **23**: 95–108 (in Slovak).

ŽÁK, K., RADVANEC, M. & GRECULA, P. (2005): Siderite mineralization of the Gemericum superunit (Western Carpathians, Slovakia): review and a revised genetic model [Ore Geology Reviews 24, 267-298] – a replay. Ore Geology Reviews, **26**: 173–180.

ZHENG, Y.-F. (1999): Oxygen isotope fractionation in carbonate and sulfate minerals. Geochemical Journal, **33**: 109–126.

ZHENG, Y.-F. & HOEFS, J. (1993): Carbon and oxygen isotope covariations in hydrothermal calcites. Theoretical modelling on mixing processes and application to Pb-Zn deposits in the Harz Mountains, Germany. Mineralium Deposita, **28**: 79–89.

ZORKOVSKÝ, B. (1955): On the question of the magnesite origin. Geologický Sborník Slovenskej Akadémie Vied, **6**: 131–145 (in Slovak).

Appendix – Itinerary for IMA2010 SK2 Field trip

Saturday, August 28, 2010 (Day 1, 261 km)

07.00–11.00	Travel from Budapest to Hnúšťa via Salgótarján, Lučenec, Rimavská Sobota (190 km)
11.00–12.00	Field stop 1: Hnúšťa–Mútnik, magnesite–talc deposit, dumps, processing plants.
12.15–13.15	Lunch break at Hnúšťa
13.15–14.15	Travel from Hnúšťa to Jelšava (34 km)
14.15–15.15	Field stop 2: Jelšava, magnesite deposit, open pit operations and processing plants
15.15–16.00	Travel to Ochtiná (14 km)
16.00–17.00	Field stop 3: Ochtiná aragonite cave
17.00–17.30	Travel to Rožňava (25 km)
17.30–18.00	Accomodation in Hotel Kras
19.00–	Dinner

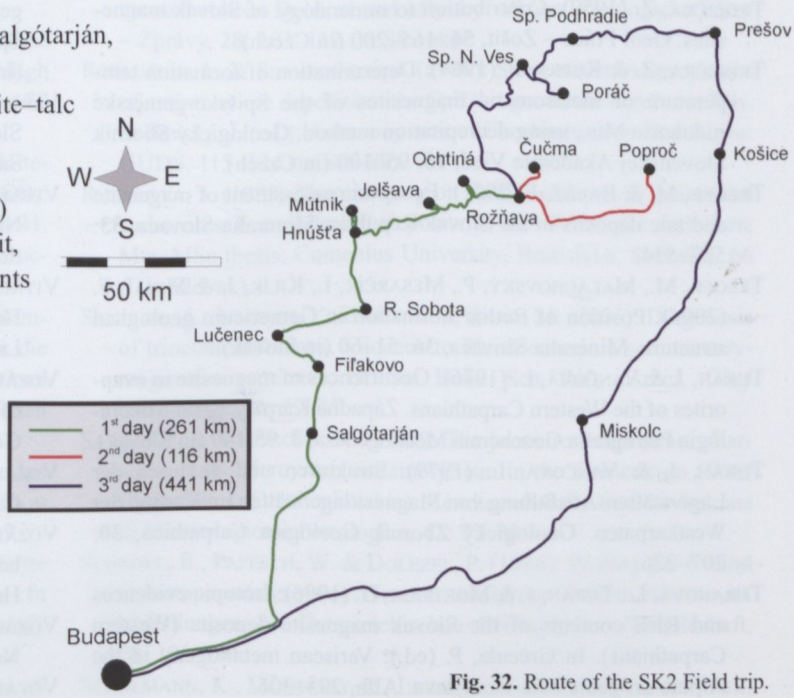

Fig. 32. Route of the SK2 Field trip.

Monday, August 29, 2010 (Day 2, 116 km)

07.00–08.00	Breakfast
08.00–08.30	Travel to Čučma (6 km)
08.30–09.30	Field stop 4: Čučma, mineralogy of abandoned dumps and tailings of stibnite deposits
09:30–10.30	Field stop 5: Čučma, mineralogy of stratiform Mn ores
10.30–11.30	Travel to Poproč (58 km)
11.30–12.30	Field stop 6: Poproč, dumps of Anna and Agneska adits, environmental aspects and remediation
12.30–14.30	Travel to Krásnohorské Podhradie, including lunch break
14.30–16.00	Krásna Hôrka castle and mausoleum of the Count Andrássy family
16.00–16.15	Travel to Rožňava-Nadabula
16.15–17.00	Field stop 7: Nadabula, dumps of Bernardi and Stefan veins, mineral assemblage of siderite veins
17.00–17.15	Return to Hotel Kras in Rožňava
18.00–	Dinner

Monday, August 30, 2010 (Day 3, 441 km)

07.00–08.00	Breakfast
08.00–10.00	Travel to Rudňany via Dobšiná and Spišská Nová Ves (78 km)
10.00–11.30	Field stop 8: Rudňany – Poráč, open pit exploitation of siderite-barite ore, processing plants at Rudňany
11.30–12.00	Travel to Spišské Podhradie (27 km)
12.00–12.15	Field stop 9: Sivá Brada, mineral springs and recent travertine precipitation
12.15–13.00	Lunch at Spišské Podhradie, travel around Spiš Castle
13.00–14.30	Travel to Košice via Prešov (78 km)
14.30–16.30	Mineral collection of East Slovakian Museum in Košice
16.30–20.30	Travel to Budapest via Miskolc (258 km)